National Academy of Sciences of Ukraine
A.N. Podgorny Institute for Mechanical Engineering Problems

B.A. TROSHENKIN

RENEWABLE ENERGY

IN 2 PARTS

PART II

THERMODYNAMICS OF THE LITHOSPHERE. GEOTHERMAL POWER PLANTS

Translated from the Russian
By
V.A. OBRISAN

Kharkov
Fort Publishers
2004

UDC 523.9+524.6+551.14:550.83+621.311.22:551.23+621.484/.484
LBC 31.55
T-76

Reviewers:
A.L. Shubenko, Doc. Sc. (Eng.), Prof., Head of Department for Optimization of Processes in and Design of Turbomachines at IPMash NAS of Ukraine;
V.P. Shaporev, Doc. Sc. (Eng.), Prof., Head of Chair for Chemical Engineering and Industrial Ecology at the National Technological University "KhPI".
Recommended for printing by the Scientific Council of the A.N. Podgorny Institute for Problems in Mechanical Engineering (Protocol No. 4 of 9 July 2003).

Troshenkin B.A.

T-76 Renewable Energy. In 2 parts. — Part II — Thermodynamics of the Lithosphere. Geothermal Power Plants. — National Academy of Sciences of Ukraine. A.N. Podgorny Institute for Mechanical Engineering Problems. — Kharkov: Fort Publishers, 2005. — 148 pp.
ISBN 966-02-3053-2
ISBN 966-02-3055-9 (Part 2)
ISBN 966-8599-06-3

Since the moment of its emergence, the development of the Solar system, and in particular of the Earth, has been strictly governed by the laws of thermodynamics. These laws govern the behaviour of ocean waters, the Earth's crust, and Nature. Based on i-thermodynamics, the monograph exposes the effect of ocean and atmospheric currents on Earth's rotational speed, explains ancient floods and glaciations, and establishes the atmosphere's chemical composition during the period of formation of coal, oil and gas deposits. The sites of ocean thermal energy conversion plants, which would not affect Earth's climate, have been identified. The most effective methods of recovering natural energy have been substantiated. In turn, μ-thermodynamics has made it possible to assess the rate of formation of Earth's crust and associated therewith periods of volcano eruptions and earthquakes. As a rule, seismic zones correspond to geothermal heat sources. An analysis of the cycles of power plants utilizing Earth's heat has been presented. The connection of underground reactions with oil and gas formation processes has been established.

The monograph is intended for experts in Earth-related power and physics problems as well as for those readers in geophysics who have a solid background in this area. It can also benefit students of higher education institutions.

UDC 523.9+524.6+551.14:550.83+621.311.22:551.23+621.484/.484
LBC 31.55

ISBN 966-02-3053-2
ISBN 966-02-3055-9 (Part 2)
ISBN 966-8599-06-3

PREFACE

Let us continue exploring the amazing world of Nature.

As we have found, solar energy drives the processes occurring in the atmosphere and Ocean. The World Ocean receives the bulk of solar radiation falling on Earth. Estimates have proved the commercial value of this energy, making it possible to substantiate the construction of ocean thermal energy conversion (OTEC) plants. It has been suggested to allocate OTEC plants in the equatorial zone, which obviously will not disturb the environmental equilibrium on Earth.

Our next objective is to develop the second-ranking energy source — the heat in Earth's interior. This requires solving roughly the same problems as in the first case, viz. identifying the sites of subsurface heat sources; proving their commercial value; selecting power plants of adequate capacity and substantiating the environmental safety of the accepted technology of generating electric power.

To solve these problems, it is advisable to know the regularities of heat generation in Earth's interior.

In our quest for heat sources, let us go underground to several kilometres. To interpret the intricate distribution of rock forming minerals that we witness, one should know the separate stages of Earth's development.

Obviously, the first step in our studies should be investigating the regularities of rotation of the molten mass of matter wherefrom Earth originated later. It is the initial angular momentum imparted to Protoearth in the course of its origination that had a dramatic impact on the planet's stratification and formation of continents during its cooling.

Our immediate objective therefore is to find the rotational speed of Protoearth and the liquid Earth.

In solving this problem, we will consider the transition of Earth's matter from the stellar state to a planetary one, and further from a liquid state to a crystalline one.

Thus, being preoccupied with purely practical issues involving power engineering, we are compelled to explore the depths of cosmogenic hypotheses [1 – 9]. Nevertheless, this should not confuse us much since the course of our studies will be checked against a reliable "compass" — the energy conversion laws.

First, let us address only those models of cosmic and terrestrial phenomena whose development in an isolated state involves growth of entropy S. In these systems, a small deviation from the equilibrium state corresponds to a negative value of entropy variation, i.e.

$$\Delta_i S < 0,$$

this being linked to the fact that, at equilibrium, entropy achieves its maximum value. Hence, negative values of $\Delta_i S$ serve as a criterion of stability of an isolated system.

Recall that, in investigating spontaneous effects using the methods of equilibrium *i*-thermodynamics, we had to account for growth of entropy in actual cycles by introducing the internal efficiency η_{ie} of circulation circuits into calculation relationships. In so doing, the circulations in each circuit were considered as a local phenomenon having no dynamic affect on the environment.

Meanwhile, the development of natural processes is ensured, as a rule, by the combined effect of a multitude of circulation cells coordinating their motion with one another and interacting with the environment. The hydrodynamic structures thus evolving are far from equilibrium. Stability of non-equilibrium stationary states is known to be achieved when the derivative of the second variation of entropy with respect to time is positive, i.e.

$$\frac{d}{d\tau}\frac{\delta^2 S}{2} > 0.$$

The constraint imposed on the systems is satisfied in the range of the maximum rate of generation and dissipation of energy. Dissipation is known to belong to the category of irreversible processes. However, as distinct from such physical phenomena as diffusion or heat transfer, where simple redistribution of entropy and its slight growth occurs, in "dissipative" systems entropy is produced. Production of entropy is the local rate of its occurrence.

Introducing the value $\delta^2 S$ into estimates, we nevertheless still remain within the domain of the principles of *i*-thermodynamics. Each of the effects being considered (gravitational, rotational and compressional) corresponds to its own hydrodynamic structure differing by a certain distribution of flows in space and the flow rate. These differences are imposed by the character of energy influx into the planet mantle from the outside, the Sun (except for Jupiter, where there is an influx from the subsurface). The intense liberation of energy in the nuclei of galaxies and in the interior of stars involves superimposing of the gravitational effect on the rotational and compressional ones, this being accompanied by emergence of peculiar gas-dynamic structures within their outer shells. We will be familiarised with the features of these structures when modelling the processes of flow distribution on experimental test benches.

As you have already noticed, we have succeeded in disclosing the key regularities of the rotational effect acting on planets only after tests have been con-

ducted on a comparatively complex evaporation installation. One can gain an understanding of its design though by using the principles of symmetry.

Experimental test benches for modelling the hydrodynamic situation on the Sun are rather sophisticated, but their design will manifest the elements of symmetry more distinctly. The test results will make it possible to formulate topological constraints imposed on systems emerging in space after explosion of celestial objects. Explosion herein is meant to be the behaviour of dissipative structures in a clearly defined transient process.

Stationary processes are known to differ by slight variations of their parameters. But as these variations accumulate, conditions are created for violent reconstruction of dynamic structures. The spontaneous effects we have studied also relate to non-stationary (or transient) processes, but their system transitions from one state to another are smoother than during explosion.

Part II of the book is focused to investigating namely transient processes because the current face of the Earth was formed largely under their influence. Information on transient processes serves as a basis for estimating the angular momentum of both the Protoearth and the liquid Earth.

We would like to stress once again that the available angular momentum has defined the sequence of formation of continents and the regularities of stratification of Earth's substance.

Further, when studying cosmic objects, we will certainly come across a wide variety of chemical, nuclear and subnuclear reactions as well as different phase transitions.

Here one should take into account that presently there is little knowledge about the mechanism of subatomic reactions occurring in the interior of the most massive celestial bodies at superhigh temperatures and pressures. Therefore, we are compelled to judge their intensity only by the character of distribution of the mass of matter ejected into space during an explosion.

We can consider more definitely the conversion of elements and their compounds on Earth and, in part, on the Sun. In this case, the criterion of reality of processes in closed systems at constant T and P are negative values of ΔGi. The isobaric-isothermal potential ΔGi has found wide application because it accounts for changes in both enthalpy and entropy of a system. In this case, the stability of a state is written as follows

$$\delta^2 Gi > 0.$$

Since the specific values of ΔGi are nothing else but the chemical potential, this implies that, in our studies, we are now moving into a domain governed by equilibrium μ-thermodynamics.

However, we are interested no less in non-equilibrium processes complicated by chemical reactions. This area of physical chemistry, known as kinetics, is completely dominated so far by empirical methods of investigation, which have little in common with thermodynamics techniques.

In the majority of cases, however, the rate of phase and chemical transformations underground depends on changes in the chemical potential of a concrete open system. To prove this thesis, we will have to use the results of testing evaporators and reactors of different types. In so doing, high-pressure reactors will be preferable in the latter case. The same investigations will allow specifying the thermodynamic criteria of stability of the systems considered.

Finally, we have established a good tradition of comparing processes occurring on Earth with similar ones on the nearest planets. This logic is straightforward, viz. the solar system originated as a unique entity during one global event, and therefore the energy conversion laws should hold for any planet. If the energy component of a process fails to hold on one of the planets, this implies that the given process is also impossible on other ones.

The constraints introduced significantly constrict the area of our scientific investigation, making it possible to focus our efforts on the most likely natural processes. As a result, one can draw a physically substantiated scheme of Earth's present structure, and identify the type of reactions occurring in its interior. This clears the way for solving the energy problems that face us.

At the same time, we will have to solve several ecological problems because power plants are located in zones of Earth's most intense seismic activity.

The problem of formation of oil and gas fields touched upon in the afterword looks somewhat isolated. But since formation of these fields is an integral part of the natural cycle of processes discussed herein, we had to mention it to some extent.

Part I of this book was published last year, and received a favourable response from the scientific community in many countries. Unfortunately, no comments on Part I were received, therefore discussion materials are absent in Part II of the book.

In conducting numerous experiments, the author collaborated with many specialists whose names are given in joint publications, inventor's certificates and patents. The author expresses his acknowledgments to these persons.

Special acknowledgments are addressed to Cand. Sci. (Eng.) V.B. Troshenkin who compiled paragraphs 3.3.1–3.3.3 of this book.

The author also acknowledges the efforts of reviewers and editors.

CHAPTER 1

TRANSITION OF EARTH'S MATTER FROM A STELLAR STATE TO A PLANETARY ONE

First, we will cite the opinion of leading experts in this field of knowledge. V.A. Ambartsumian assumed that, when studying the evolution of an object, it is important to start by analysing the properties of a given object derived by generalising observation data rather than proceeding from *a priori* assumptions.

Thus, observing the expansion and disintegration of stellar associations, V.A. Ambartsumian established the fact of star scattering from certain star formation centres. Hence, he inferred that stars are formed from small-size high-density bodies. In particular, the protostellar substance of the nuclei of gigantic galaxies produces huge fluxes of high-energy particles capable of ejecting significant masses over great distances. Being ejected from the nucleus, the substance mass is transformed to conglomerates of stars, interstellar gas and clouds of high-energy particles.

There is an intimate link between the process of initial nucleus splitting and formation of spiral-shaped arms. Here, it is appropriate to cite one of V.A. Ambartsumian's statements: "Facts have been proving that emergence of nebulae from stars is a widespread phenomenon. Conversely, we are not yet aware of at least one case when a dense object would emerge from diffusive matter, though such transitions, admissible in old cosmogony theories, are admitted even in many cosmogony theories widespread to date" [1 and 2].

A.Ye. Fersman's view of the course of Earth's evolution was as follows: "Here we prefer remaining in the realm of facts and observations. To understand the history of Earth and its chemistry, we cannot depart far from the current moment. In Earth's life one can distinguish, so to say, three epochs, viz. the young age — stellar one — when its life was part of Sun's in conditions of peculiar stellar processes with temperatures of millions of degrees, rarefied gases and radiation phenomena. The grown-up age of its independent life is still cosmic but it exists in conditions of searching for new forms of equilibrium

and formation of mantles and the core. Finally, its senile age — the epoch of geological development — has set in. For us, this epoch is the only clear and comparatively short one, continuing for about two billion years. In some way or other, Earth, in its current state, is a physico-chemical system that has emerged through an extended stellar, planetary and geological process" [2].

Let us cite several other statements to this effect. Carbon chemistry data, specifically the correspondence of Sun's chemical composition (except for hydrogen and helium) to that of Earth's and meteorites, allowed A.P. Vinogradov to suggest that the Solar system bodies were formed of matter ejected by the Protosun alone [2 and 3]. To some extent, V.A. Ambartsumian's hypothesis has something in common with S. Hawking's ideas. He assumed that our Sun is a second or third-generation star that emerged from a cloud of rotating gas containing fragments of earlier stars [4].

In both cases, we are observing scattering of matter and energy dissipation in cosmic space, which, in mathematical terms, implies growth of configuration and thermal entropy. This allows accepting V.A. Ambartsumian's hypothesis as our working assumption.

Note that since the times of I. Kant and P. Laplace, the concept of solar system formation from a cloud of cold or hot dust is still being developed [5, 6, and 26]. However, in spite of the extended period of its formation, well-known models have failed so far to explain clearly the origins of the energy source that ensures rotation of the gas-and-dust cloud. The issue of the power of this source remains vague. Nevertheless, separate elements of the hypotheses suggested [7–9, and 15] can apparently be used for describing the process of transformation of clouds of matter ejected from the nuclei of galaxies into stars and planets.

In starting our studies, we will focus on answering the following questions:

– What is the structure of flows in the shells of nuclei of galaxies and stars?

– What is the cause of explosions of celestial bodies?

– Why is the mass of matter ejected to cosmos distributed in space in the form of spiral-shaped arms and planetary systems?

– What is the cause of fragmentation of spiral arms into stars and planets? and

– What forces cause the major share of the angular momentum to concentrate in the ejected mass, with only its minor one kept in the mass of substance remaining in the nucleus?

Having answered these questions, we will proceed to the next part of our studies, namely, calculating the angular momentum of Protoearth.

1.1. DISTRIBUTION AND CIRCULATION OF FLOWS IN THE SHELL OF THE GALAXY PROTONUCLEUS AND ON THE SUN

Certain clarity in assessing the process of splitting of a parent celestial body into parts can be achieved by comparative analysis. Such analysis is applied to the consequences of discarding of shells by galaxy and protostar nuclei. No doubt the shapes of spiral galaxies and the arrangement of planets in the solar system, which are observed in the sky, reflect in detailed discrete form the pattern of circulation of flows that have developed in the shells of parent celestial bodies prior to their explosion.

One can assume that the nuclei of the processes of "swirling" of the arms of galaxies and planetary systems can be traced in the dynamic structures of the flows that have vanished. Having interpreted their ancestral features makes it possible to evaluate the magnitude and direction of the angular momentum received by Protoearth at the time of its separation from the Protosun.

When spontaneous effects were investigated, we gained insight into the regularities of circulation of flows in gas and liquid shells of planets. As we know, the gravitational effect ensured energy transport in the radial direction; the rotational effect did the same thing in the meridional one, and the compressional effect did this in the latitudinal direction [10]. Obviously, the same processes occur in nuclei and stars, involving circulation of gas-plasma flows with a higher and lower temperature relative to a certain averaged temperature of the bulk of shells.

In analysing natural circulation, we should account for the differences in processes occurring, for example, on Earth and the Sun. Thus, evaporation should be replaced with ionisation, i.e. transition of matter at high temperatures from the gaseous state to the plasma one; and condensation with re-ionisation. Here this implies the reverse transition of matter at lower temperatures from the plasma state to the gaseous one.

Let us trace the transformation of these effects in conditions prevailing in the shells of nuclei of galaxies and stars.

1.1.1. Assumed structure of flows in the shell of the Galaxy protonucleus

The Galaxy is a complex stellar system comprising hundreds of billions of stars as well as dust and gas. The bulk of stars and gas, and nearly all the dust, are concentrated close to the main plane of the Galaxy, which is its plane of symmetry, and comprises the Milky Way. A significant number of stars and a

known amount of gas form a near-spherical component surrounding a relatively compact nucleus (Fig. 1).

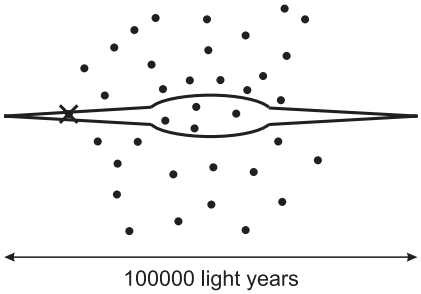

Fig. 1. Schematic side viewof the Galaxy. The thin Galaxy disk and the central concentrated (nucleus) are shown. The cross indicates the Sun's position, and black circles are spherical clusters.

The nucleus of the Galaxy, being embedded in comparatively dense masses of interstellar matter, is challenging for optical observation. Radio astronomical observations, however, indicate nucleus activity, and a presence therein of large masses of matter and energy sources.

The Galaxy demonstrates an irregularity in the distribution of stars, gas and dust. Thus, one can observe merging of stars into clearly defined structural units, viz. star clusters and associations, and of gas and dust into dark and light nebulae.

Studies in the distribution of nebulae and, especially, of star associations have detected a spiral-shaped structure in the arrangement of objects comprising the Milky Way (Fig. 2).

Hence, our Galaxy belongs to the class of spiral galaxies, a typical representative of which, for example, is galaxy M51 (Fig. 3).

The Galaxy rotates about its minor axis of symmetry. The laws of rotation of galaxies coincide in many respects, namely, the nucleus rotates practically as a solid, whereas the angular velocity of the outer parts of the Galaxy first drops rapidly in moving away from the centre, and then, after increasing slightly, gradually decreases.

The period of rotation of the Galaxy at the Sun's position is about 200 million years. A detailed overview of galaxies is given, for example, in publications [5 and 11–15].

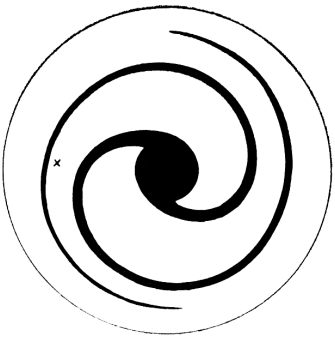

Fig. 2. Schematic plan view of the Galaxy. The spiral-shaped structure is evident. The cross indicates the Sun's position.

Galaxy observation data allow drawing some tentative conclusions on the character of circulation of flows in the protonucleus shell. Thus, if the length of the spiral arms in Fig. 2 is decreased slightly, one obtains the rotating flows ("ropes") that have transferred "cold" masses of matter from the poles to the equator in the protonucleus shell. Coriolis forces cause their deviation from the meridional direction.

Fig. 3. Spiral galaxy M51 of the Sc kind with a satellite galaxy

The marked coincidence of the shape and direction of protonucleus ropes, and of Galaxy spiral arms confirms V.A. Ambartsumian's hypotheses. This also points to the high probability of a spiral-shaped arrangement of planets at the initial moment after the Protosun had rejected its shell. Further, we will try to obtain useful information by analysing solar gas dynamics.

1.1.2. Solar gas dynamics

The planet Earth is attracted by the Sun and receives its radiation. Due to advances in astrophysics, we know that, under conditions existing in the Sun's interior, matter therein is in plasma form, and obeys the ideal gas state equation. Gravitational forces ensure spherical symmetry of the gas mass. Here we will explore only the features of gas dynamic structures existing in the Sun's shell. Detailed information on the structure and type of reactions occurring in its interior is given in monographs and reference books [16–26].

The Sun is unique because it is the closest star to Earth, and the only one whose surface allows for in-depth analysis. The current model of the gas dynamic structure in the Sun's shell assumes separation of flows into separate cells, which combine, in turn, into assemblies similar in shape to bee honeycombs.

In the thick gas layer, the convection zone, in turn, is separated into layers whose thickness is close to that of a uniform atmosphere (at this distance, the density changes by a factor of $e \approx 2.7$). Large cells are formed in the base of the convection zone where the temperature is high, and hence, the thickness of the uniform atmosphere is great. The lateral dimensions of these cells are about one-half of the star's radius. In the next layer, the dimensions of the cells are smaller and, finally, in the upper layer their dimensions are equal to several

hundred kilometres. The Sun's surface exhibits the traces of all these cells, viz. small ones make up granules; average ones make up supergranules, or a chromosphere grid, and the largest cells form gigantic structures.

The rate of convective motion in the interior of stars is small, and equals dozens of meters per second. With increase in altitude, the rate increases and becomes especially high under the photosphere (1–2 km/s) where the radiation emitted from the upper layer of the cells increases the temperature difference.

The authors of the model assume that, in the presence of an intense magnetic field, convection stagnates in the upper or middle layer; the heat flux drops, and dark spots appear on the star's surface [26]. If the spots originate on the opposite side of the Sun, the following is usually observed. The spots appear on the Eastern side of the Sun, travel across the solar disk for 12 to 14 days (Fig. 4), and then they become invisible for nearly the same time interval.

The spots' paths — oblique lines — are the result of tilting of the Sun's axis relative to the ecliptic (Earth's orbital plane). Generally, these paths are parallel to the Sun's equator, and to each other. The spots' paths change during the year owing to changes in the mutual positions of the Sun and Earth.

Round-shaped spots, in moving over a sphere, approach its edge and become oval-shaped instead of remaining round ones; and then they contract to nearly a line. This phenomenon is a result of the perspective view. The sites of spot formation are located in the deep unobservable layers of the Sun. The rotational speed of spot formation sites remains invariable over the 11-year cycle, though the latitudes of the spots change regularly within 5° to 35°. Therefore, it is assumed that the sites lie on the nucleus of the Sun, which rotates as a solid. Hence, the established poleward decrease in angular speed is a surface phenomenon relating only to the uppermost layers. In the lower latitudes, the spots rotate at higher speeds, and in the higher latitudes, their rotation is slower.

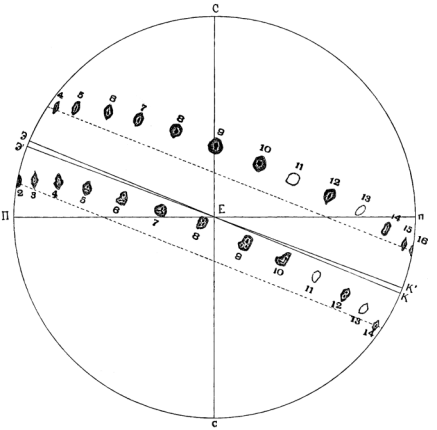

Fig. 4. Trajectory of two Sunspots established by Scheiner on March 2 to 16, 1627 [16]

The dimensions of the spots vary within wide limits. In some

cases, groups of small spots appear, and in other cases huge ones appear that exceed Earth's diameter by 15–20 times. The shift in the spectrum lines of the spots caused by the Doppler effect indicates that the substance in the spots moves, viz. there is efflux at lower levels and influx at higher ones. The motion velocity is up to 3 km/s. Analysis of spots' spectra and the photosphere also indicates that the spots are colder than the photosphere by 1 000 to 2 000 °C, making the spots appear darker against its background. Several researchers observed occurrence of vortices in the Sun's shell [16].

Many investigations deal with granulation — the fine structure of the solar photosphere. The grainy structure of the Sun's surface comprises a system of continuously emerging and disappearing bright granules separated by narrow dark spaces (Fig. 5). The average size of granules is approximately 700 km, and their average life is about 8 minutes.

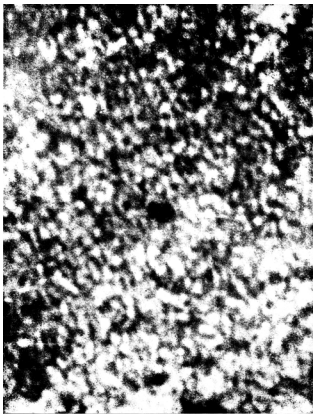

Fig. 5. The photosphere (photo by Gansky Ya.P. [16])

The granules are brighter than the intergranular spaces by 20–30 %, corresponding to an average temperature difference of 300 K. The speed of irregular motions of the granules is 2–4 km/s. In several cases, oscillatory (lateral) motion with a speed of about 30 km/s has been detected. Presently, convection flows are assumed to be the causes of granulation whose emergence depends on the temperature gradient alone. The Sun's atmosphere consists mainly of hydrogen, which is ionised slightly in its outer layers. However, when the mass of gas consisting of hydrogen descends to hotter areas, the intensity of its ionising increases, this requiring a certain amount of energy. Analysis of circulation flows is based on the assumption that, in the zone where hydrogen is ionised, the ascending and descending convective flows meet.

During several long-term observations, researchers succeeded in ascertaining that the Sun's diameter is subject to slight variations. At the same time, they found that the Sun's diameter is relatively small when it is most active, and vice versa [17].

The quantitative characteristics of this phenomenon are as follows: every 160 minutes the Sun expands, and then contracts. During such pulsations, the solar radius increases or decreases on the average by 10 km. The Sun as if "breathes", making the brightness of the solar disk change in step [23 and 24].

The Sun rotates in the same direction as Earth does, viz. the Eastern edge approaches us, and the Western one moves away. Points with the heliographic latitude of 17° perform one rotation relative to Earth in 27.275 days (the synodic period). The linear speed of rotation on the Sun's equator is 2 km/s.

As a star, the Sun is a typical yellow dwarf. The Sun's spectral class is G2V, and its age is approximately $5 \cdot 10^9$ years.

The convective model that we have just investigated fails to expose the causes of Sun's rotation. The situation is no better with explaining the causes of granule pulsation and formation of spots on the surface of our star. The claim that these phenomena occur because of magnetic field "blocking" implies that a certain entity (Maxwell's demon) is introduced into the system and controls the process observed. The known model also fails to account for Sun's "breathing".

Obviously, the Sun's gas dynamics is vague in many respects. These phenomena should be explored prior to proceeding with our studies.

Recollect that, in our previous investigation, it was proved that any celestial body possessing a gas-fluid or gas-plasma shell rotates due to energy exchange with outer space.

The Sun itself generates energy and discharges it to outer space. The Sun's surface is continuously renewed on the equator due to both natural circulation and rotation. At the same time, renewal on the poles is effected mainly by natural circulation. Hence, the surface layers on the star's poles should be cooler than those on the equator. This causes a rotational effect when the flows of "hot" plasma move poleward from the equator, to be replaced with "cold" flows from the poles. In so doing, the angular momentum appearing above the "hot" flows is imparted to the Sun to rotate it, and therefrom to the "cold" flows. As mentioned earlier, the dark spots on the Sun are nothing else but efflux of "cold" plasma flows to the surface near the equator. Essentially, the structure of flows on the Sun resembles that observed on Jupiter. If the gas plasma environment on the poles presumably has a higher temperature, as this was supposed in work [21], then, according to the rotational effect assumptions, the Sun would start rotating from North to South (or vice versa), and one of the meridians would become the equator.

It is also obvious that a combined process occurs in the zones of passage of "cooled" flows from the poles to the equator. Highly-ionised plasma flows that ascend from the Sun's interior encounter low-ionised ("cooled") flows passing from the poles to the equator. In colliding, they produce a compressional effect. The increased pressure of the gas mass splits the meridional flows into several ones whose exit near the equator can be detected by groups of small spots.

Following the same principle, it is reasonable to assume that compressional effects could occur in the nuclei of galaxies. In this case, ultra-high gas pressures developing during the most intense explosions could destroy the symmetric construction of galaxies to form stellar "clouds" similar to Magellanic Clouds.

It remains to clarify the nature of pulsations of granules and the "breathing" of stars. This can be achieved only by superimposing the structures of flows acting in their shells due to various effects.

First, let us consider in detail the spontaneous effects.

1.2. THERMODYNAMICS OF REGULAR FLOWS

In our quest to perceive the world, we in some way use our notions on symmetry and asymmetry of the geometric shapes of objects surrounding us, and on their arrangement in space.

Once symmetry was called "world harmony". In his quest for world harmony, J. Kepler derived the laws of planetary motion. After this, the ideas of symmetry of space and time, developed for the macro world, pervaded crystallography and chemistry when describing the structures of crystals and chemical compounds. However, dramatic success was achieved during creation of the quantum presentation of the micro world, in particular, the structure of particles comprising the atom. It turned out that the laws of conservation of energy, impulse and angular momentum are essentially consequences of the general principles of symmetry [27–35].

Recently, this effective method of investigation has reverted to its "*alma mater*" — the macro world — where it is employed productively in analysing so-called "dissipative" structures. These structures emerge in open systems that are far from the state of thermodynamic equilibrium. As the authors of works [36–39] believe, these formations are maintained in ordered pattern due to continuous dissipation of energy.

Based on the current level of scientific knowledge, in this section we will attempt to disclose the principle of formation of flows in the shells of stars and nuclei of galaxies.

The structures of flows in the atmosphere and ocean studied earlier are undoubtedly dissipative ones. For ease of calculation, we assumed that the circulation circuits emerging in aqueous and air media are closed systems that exchange only heat with the environment. Actually, real systems cannot be considered truly closed ones. The correlation between the velocities of particles in the flows is disturbed by their interaction with stationary layers of water and

air. Obviously, we are dealing with open systems maintained as symmetric formations by the outer solar energy flux. It is these hydrodynamic structures that are able to transfer energy from Earth's equator to the poles on a wider scale than common heat transfer can.

Strictly speaking, defining these structures as dissipative ones reflects but one property of the system, viz. the capacity to dissipate kinetic energy continuously and convert it to heat energy. It is obvious, however, that natural hydrodynamic formations act as systems capable of spontaneous regeneration of kinetic energy being lost. Therefore it would be more appropriate to call these structures "creational-dissipative" ones (In Latin. *creatio* — creation; *dissipatio* — dissipation). The name suggested, however, is general in essence, but we prefer emphasizing the individual properties of objects being classified. Therefore, it would be practical to retain in the name the type of force field interacting with the heat flux, which was introduced earlier. Thus, further we will use the following terminology: "gravitational-..., rotational-..., compressional-dissipative" structures. Using this approach, the name will directly point to the path of circulating flows, and the possible intensity of processes expected.

We will highlight some differences in the techniques of analysing processes of obtaining kinetic energy and expending it later by individual circulation cells. If in the former case the intensity of the force field, in which a certain thermodynamic effect is manifested, was of prime concern, whilst the dimensions and the shape of the channels, and contacting therein phases, were not vital, the situation in the latter case is reversed. Here, namely the geometric characteristics of hydrodynamic structures and the phase relations determine the amount of energy losses. This occurs because the laws of friction are not invariant with respect to changes in the spatial scale of systems or, stated otherwise, to the similarity transformation. The affect of spatial factors on energy dissipation increases yet more during the combined action of circulation cells. Now we will proceed to investigate this phenomenon.

1.2.1. Gravitational-dissipative structures

We will take the so-called Benard cells [40] as an analog of gravitational-dissipative structures emerging in a mountain lake (Fig. 1, Part I).

The picture in Fig. 6, magnified by about 25 times, demonstrates the hexagonal convective structure in a layer of silicon oil 1 mm thick during uniform heating on the bottom, and ambient air action on the top. If the upper surface is free, flow is created mainly by irregular surface tension rather than by buoyancy. Light reflected from aluminium flakes demonstrates fluid upwelling in

the centre of each cell and its downwelling on the edges. The exposure time is 10 s, whereas the time of fluid motion across the cell from the centre to the edge is 2 s. (Photo by V.G. Velarde, M. Yuste, and J. Salan.)

When getting into the flow zone, Benard cells acquire an elongated form [17].

The external appearance of the cells indicates that, in effecting one or other process, nature strives to observe its basic principle — the principle of least expenditure of space and energy. Such economy is achieved by arrangement of flows in a certain order. Hexagonal structures are known to possess two kinds of symmetry, viz. translational (displacement) and rotational of the sixth order.

Imagine that the heat influx from Earth's interior to the mountain lake has increased abruptly. Observing the behaviour of flows, in short time we will see that the number of circulation cells is increasing concurrently with thermal load growth. Finally, the entire water body will be involved in circulation. Newly emerging circulation circuits will be accommodated comparatively uniformly in the lake water to create a hydrodynamic structure similar, in the ideal case, to that shown in Fig. 6.

Further growth of the temperature differential will disturb the coordinated movement of separate parts of the flows. A layer of steam that reduces heat transfer intensity will be formed close to the lake bottom. The system will transfer to a pulsating regime involving chaotic ejections of significant volumes of steam in different parts of the lake. The disturbance of "orderliness" implies that the system is losing those kinds of symmetry that were allowed by the current conditions of its interaction with the environment.

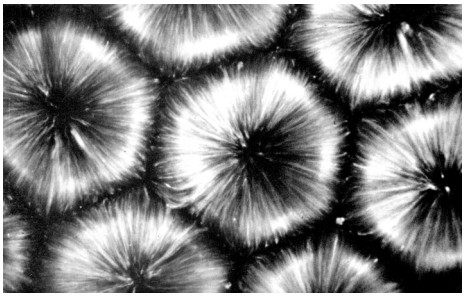

Fig. 6. Convection created by surface tension (Benard convection)

Now we will discuss the energy issue of the problem considered.

The equilibrium state of an isolated system is known to be its most likely one. In this case, stability is characterised by a negative change in entropy at small deviations from stability because entropy achieves its maximum value in equilibrium conditions. At the same time, equilibrium structures exist owing to conservative forces acting within the system.

Recall that the common trend in non-equilibrium systems is conversion of all kinds of energy into heat. This conversion brings the system to the most likely state.

The criterion of stability of a strongly non-equilibrium state formulated by P. Glansdorff and I. Prigogine implies that the derivative of the second variation of entropy with respect to time should be positive. Evidently, a non-equilibrium system becomes progressively stable and ordered at the maximum rate of dissipation of kinetic energy, which emerges, in turn, due to spatial transfer of an external heat flow.

Here we are facing a very peculiar interpretation of the law of energy degradation: entropy is considered a forbearer of a newly emerging order rather than a measure of continuous slipping of systems to a chaotic state.

Let us recur to the gravitational effect described in Part I of the book. More or less valid results of calculating the process of natural circulation were obtained only for an evaporator having specific geometric dimensions. Obviously, the internal efficiency h_{oe} of an individual circulation circuit accounts for the energy dissipation level in the uptake channel, whereas the total amount of kinetic energy obtained determines its expenditure on friction in the downtake channel. Hence, fairly accurate entropy values were found for the system analysed.

The spatial characteristics of local circulation circuits in the mountain lake obviously differ from the geometric parameters of commercial apparatus. Therefore, when calculating the flow resistances of channels, ad h_{oe} empirical formulae should be derived. Because field measurements are involved in the process, the entropy values obtained for local systems turn out to be approximate ones. However, these values allow conceiving the physical background of the process.

We will try to meet these challenges by using adopted methods of generalising experimental data.

Now we will describe the space-time structures emerging in a mountain lake in mathematical terms. Assume that an impermeable hood was placed over the lake. It would allow collecting and measuring the amount of vapour produced. We will denote the volume of vapour produced in time τ with symbol $V\tau$, and the total volume obtained at the end of the process by V_{max}. Further, we assume that the temperature difference on the lake bottom changes periodically. A graph will be used to trace the vaporisation rate. For this, we plot the ratio $V\tau/V_{max}$ on the Y-axis, and time τ on the X-axis. The result is a family of *S*-shaped curves (Fig.7).

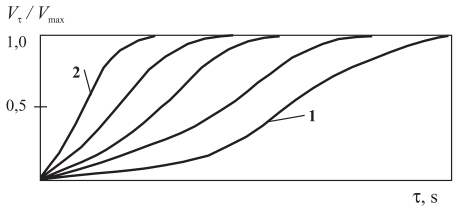

1 is water temperature ≈ 40°C; 2 is water temperature ≈ 85°C.

Fig. 7. Kinetics of vaporisation vs. temperature difference on a mountain lake bottom

Each temperature difference corresponds to a certain number of circulation cells. At a small temperature difference between the bottom and water, the number of circulation cells is small. In this case, the water will be heated only in zones of action of circulation cells, and vaporisation above the lake will be negligible. This corresponds to arrangement of *S*-shaped curves close to the X-axis. With increase in temperature difference, the entire amount of water in the lake will heat to the boiling temperature; the number of circulation cells will increase to a certain maximum, and the *S*-shaped curves will rise to the Y-axis.

All the curves are characterised by an inflection point, whence it is obvious that the vaporisation rate at the initial stage of the process increases to reach a maximum, and, upon occurrence of a pulsation regime at the end of the process, it drops.

In some cases, phase transitions are considered to be chemical reactions. Such an approach allows estimating the probability of equilibrium processes using a unified technique [41]. Further comparison shows that not only thermodynamic relationships, but the kinetic characteristics of processes as well can be evaluated using the same equations.

In our case, evaporation obeys the generalised equation of chemical kinetics of heterogeneous processes whose molecular-statistical derivation was made by B.V. Yerofeev [42]:

$$V_\tau / V_{max} = 1 - e^{-k\tau^n}, \qquad (I.1)$$

where k is a constant of the vaporisation process rate defined by the current temperature conditions in the lake; and n is a constant depending on the vapour and fluid properties.

Since the *S*-shaped curves are essentially two mating exponents, the values of k and n change in the inflection point. The character of variation of these values is found [43 and 44] by taking twice the logarithm of equation (I.1).

The formal kinetics equation given above allows for correct generalising of experimental data, though fails to disclose the energy aspect of the process. Moreover, equation (I.1) allows treating the inflection point of *S*-shaped curves as achieving of stability by the creational-dissipative structure. In this case, the second-order terms in the expression for deviation of entropy from its maximum value should be accounted for.

In approaching the inflection point, our system becomes progressively stable and ordered. In so doing, dissipation of kinetic energy increases over time to reach its maximum in the system. This assumption can be readily verified because, as in the evaporator case, we have the characteristics of one of the typical individual circulation cells (though even approximate ones), whereas the number of cells can be calculated by observing the lake surface. In so doing, one can confirm numerically that the rate of production of entropy in a system will drop when the system being considered deviates from ideal symmetry similar to that of Benard cells.

Now, by applying similar analysis to rotational-dissipative structures, we will obtain valuable additional information.

1.2.2. Rotational-dissipative structures

Developing the theory of formation of vortices and their interaction is one of the key problems in hydrodynamics. The background of this problem and details of numerous experiments are given in fundamental monographs [45–47].

Outstanding milestones of the past were the works of G. Taylor [48] and A.N. Kolmogorov [49] as well as the materials of several conferences [46].

Turbulence can be described by an hierarchy of vortices, or turbulence cells, which exist simultaneously in many different length scales. To date, several models of the process have been developed, which nevertheless are being refined.

We already know that "cold" flows, in moving from the poles of planets to the equator ("ropes"), rotate about their axes. Therefore, they can be considered vortices. For example, the Red Spot on Jupiter rotates once about its axis in six days, whereas the planet itself does so in approximately 10 hours. The spot moves about the planet's axis slower than its surrounding southern tropical zone. The spot lags by one complete planet's revolution in approximately 30 years.

Studying data on spiral galaxies, we can gain an insight into the system of vortices that move similarly over a spherical surface.

We will consider galaxies that demonstrate a regular spiral-shaped pattern. G. de Vaucouleurs offered a classification of these galaxies [26]. As seen

in Fig. 8, families of spiral galaxies are denoted by letters *A*, *B*, and *AB*. Here, *SA* designates a normal spiral galaxy; *SB* is a barred spiral galaxy; and *SAB* are intermediate forms. Besides families, varieties are accounted for as follows: ring — *r*, spiral — *s*, and mixed — *rs*.

Note that the spiral construction possesses rotational symmetry whose order corresponds to the number of galaxy arms.

The patterns shown suggest the structure of flows that once existed in the shells of protonuclei of galaxies. Evidently, at weak liberation of energy in the interior of protonuclei, two rotating "ropes" were sufficient for transferring heat from the equatorial zones to the poles. However, with increasing power of the intranucleus energy source, the number of circulation circuits increases. Naturally, the object's rotational speed also increases. Due to an explosion, the multirope rotational-dissipative structure, in separating from the celestial body, transforms into a multi-arm spiral galaxy rotating in cosmic space.

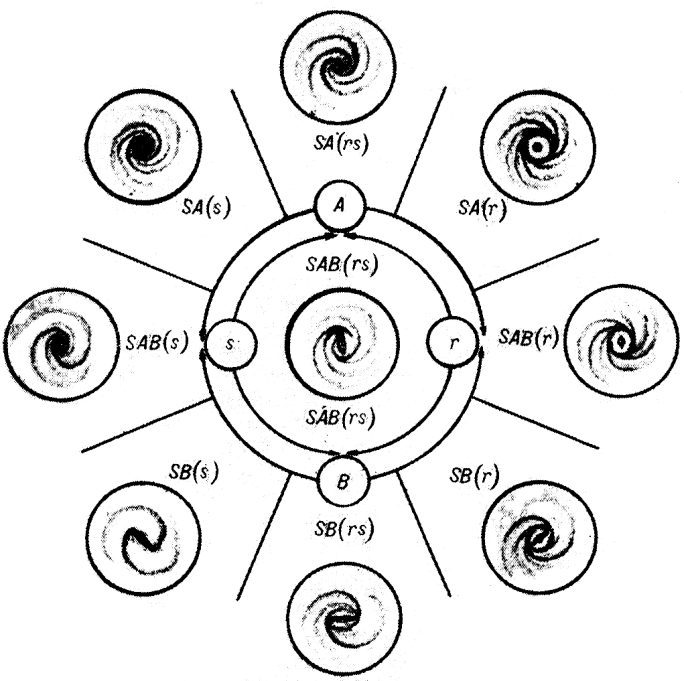

Fig. 8. G. de Vaucouleurs' classification of spiral galaxies

The pattern of the central part of the galaxies depends on the hydrodynamic situation that had developed in the interior of the protonuclei. After analysing experimental data, we will deal with this problem.

1.2.3. Evaporator with a pulsating distribution device

To interpret the behaviour of solar granules, it is necessary to establish the regularities of distribution of two opposing flows, viz. the highly ionised flow ascending to the surface, and the low ionised one descending to the depths of our star. The most similar regime of interaction of vertical flows can be observed in evaporators with a streaming down film.

Evaporators are intended for concentrating heat-sensitive solutions and dispersions, desalinating water, and separating liquids. A construction of an evaporator with a streaming down film is shown in Fig. 9. A pilot apparatus consists of 7 tubes dia. 38 × 2.5 mm and length 4 m. A common hydraulic lock comprising two shells 4 and 5 installed concentrically in chamber 7 are used to

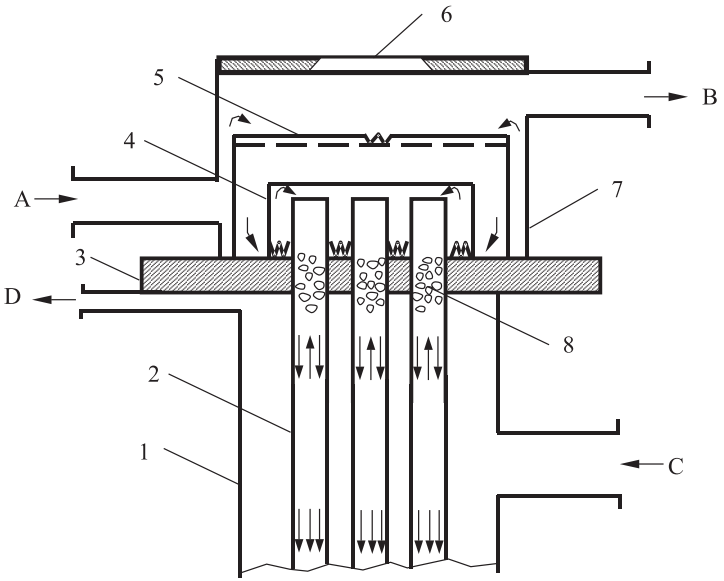

1 — heating chamber; 2 — evaporation tube; 3 — tube plate; 4 — cylindrical partition with lower slots; 5 — cylindrical partition with upper slots; 6 — inspection hole; 7 — distribution device casing; 8 — position of foam plugs. Unions: A — solution inlet; B — secondary vapour outlet; C — primary vapour inlet; D — gas discharge

Fig. 9. Evaporator with a streaming down film

distribute the fluid across the apparatus section. To ensure formation of streaming down films, four tangential channels are cut in the protruding part of each tube 2. Inspection port 6 allows observing the character of film flow inside tubes 2.

During evaporator operation, the fluid flows via union A into distribution chamber 7, spreads over its perimeter and overflows through the toothed edges of shell 5. Then the flow approaches tubes 2 by flowing through the lower slots in cylindrical partition 4. After this, the fluid again rises to the edges of tubes 2. In entering the tubes through the tangential slots, the fluid starts swirling to spread evenly over the inner surface and streams down. Heating steam is fed to heating chamber 1 via union C. Due to heat transfer through the walls of the tubes, the streaming down solution film partially evaporates. The secondary vapour thus formed rises into chamber 7, and via union B flows to the condensing system. The lower part of the apparatus accommodates a separator (not shown in the diagram), wherein the bulk of extracted secondary vapour is cleared of droplets.

As a rule, primary vapour contains a certain amount of air. As vapour condenses, air accumulates under tube plate 3 wherefrom it is evacuated to the atmosphere via union D.

The pilot evaporator has been tested at several chemical production and petrochemical facilities. Specifically, heat and mass transfer was investigated when films of glycerol, styrene, and alkyl borate solutions streamed down [50].

Observations have shown that, close to the upper edges of tubes 2, foam plugs 8 are formed during evaporation. The plugs pulsate continuously and periodically eject excess fluid from tube to tube, thereby equalising the resistance of channels to vapour flow. (The plug formation phenomenon disappears at high product viscosity.)

Hence, the granulation being studied is nothing else than gas dynamic structures occurring spontaneously in the Sun's surface layer. This ensures allocation of two opposing flows. A characteristic feature of these formations is intensive pulsation of a foamy mass of substance in points of flow collision. We believe that their most appropriate name is "pulsating-dissipative" structures.

So far, our investigations have dealt with reallocation of opposing radial flows close to the free surface of the Sun. However, we are also interested in reallocation of flows in the interior of our star as well. The point is that the plasma sphere rotates because the meridional flows transfer excess energy from the equatorial zones to the poles. The cooled flows, in returning from the poles to the equator, would have to "drop" immediately into the downtake channels first encountered.

However, nothing similar is observed on the Sun. Moreover, judging by the spots, flows of "cooled" plasma exit close to the equator. Most likely, the principle of allocation of flows in the deep layers is about the same as in the surface ones. According to this assumption, there is a spherical mass of low-ionised plasma in the centre of each underlying convective cell. During simultaneous rising of these masses, highly ionised plasma flows ascend, whereas the plasma currents from the poles descend within the spaces between these flows. During simultaneous descending of spherical compactions, high-temperature plasma flows are cut off, and the meridional low-temperature flows can move to the equator. From this follows the observed "breathing" of the Sun.

We shall validate the assumption suggested by example of fluid distribution across the section of a multitube evaporator with a streaming down film.

Distribution devices were investigated on an hydrodynamic stand with a 120-tube model of an evaporator. The diameter of heating tubes used was 38×2.5 mm. The intensity of tube refluxing across the apparatus section was determined by measuring fluid flow rates in ten reference tubes arranged over the apparatus diameter.

The required degree of order of flows in film evaporators is achieved at equality of rates of fluid streaming down in all heat transfer tubes. The design of the evaporating chamber dictates observance of symmetry elements in descending flows. The maximum possible arrangement of the heat exchange surfaces per unit volume of the apparatus makes the space be divided with tubes so that their full symmetry is observed in a rhombic grid. The evaporation tubes are arranged in the chamber space in orderly rows to occupy the nodes of this grid in the tube plate. The grid consists of a system of equal rhombs oriented in parallel and mutually adjoined with their whole sides. The rhombs uniformly fill in the tube plate plane without spaces and superpositions. The basic property of the grid is that its any two nodes can be mutually aligned by means of translation (Figs. 10 and 11c).

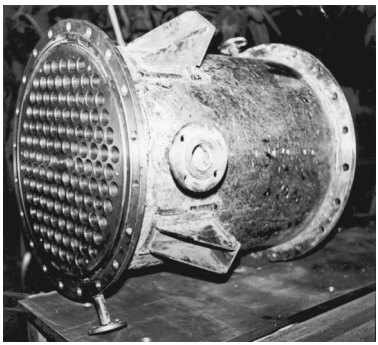

Fig. 10. Evaporator heating chamber with a streaming down film

Regularity of spatial arrangement of the tubes ensures minimal metal consumption required for manufacturing, and required apparatus robustness at optimal interaction of the structure with flowing therein flows of heat carrier and evaporated product.

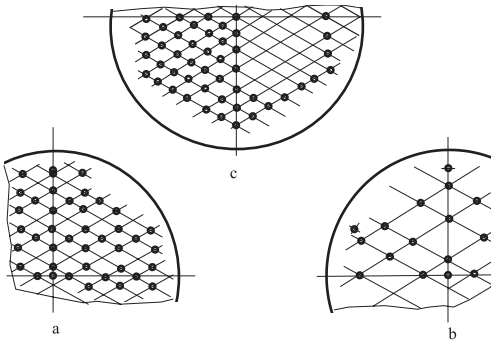

a – middle; b – upper; c – lower (the perforation matches the arrangement of tubes in the heating chamber).

Fig. 11. Perforated plates

The evaporators consist of a relatively small number of standard elements having a cylindrical, conical, spherical, elliptic and flat shape. One or other type of apparatus can be obtained by combining these elements, and changing their mutual arrangement and scale. If the number of equivalent methods of arranging the structural elements in the apparatus is taken to be R, the configuration entropy of the system will be

$$S = k \ln R,$$

where k is a proportionality factor.

By introducing order, symmetry of elements always acts to reduce the number of possible options. In this respect, rhombic arrangement of tubes in the evaporation chamber yields a certain minimal value of R_0 and its respective minimal value S_0:

$$S_0 = k \ln R_0,$$

Value S_0 characterises the minimal expenditures required for manufacturing the apparatus. Any deviation from the established law of tube arrangement increases R and, hence, results in growth of entropy.

If we consider entropy as a measure of loss of public material wealth, then, for this specific case of manufacturing evaporators, an equation of the economic state can be derived. In its form, it would not differ from the equation of state of ideal gas. In this case, optimal economic expenditures are secured at minimum entropy value [63].

Similarly, an increase or decrease in thickness of the streaming down film in one or several heat transfer tubes would involve a disturbance of hydrodynamic symmetry and growth of the configuration entropy of flows, and hence,

to an increase in material resources required for conducting the process. With such strict requirements to the symmetry of the evaporation chamber and the hydrodynamic flows, it is obviously necessary to analyse the elements of symmetry of distribution devices.

It has been established that uniformity of tubes reflux improves with increasing number of fluid inlets to the apparatus, and an increase in symmetry of these inlets relative to the apparatus axis. This method, however, makes the structure involved, so the experiments were confined to two options, viz. fluid inlet from the top along a vertical axis, or with two mutually opposing peripheral inlets arranged horizontally.

Axial symmetry of inserts designed as a bell with three mounting ribs ensures generation of films in each tube, though not across the apparatus section (Fig. 12).

Applying symmetry laws to arrangement of holes in perforated plates allows distributing the fluid across the apparatus section, but does not guarantee generation of a film in each tube (Figs. 11 and 13).

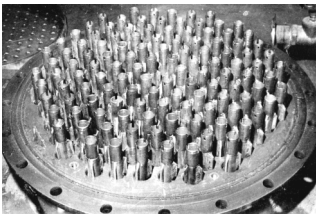

Fig. 12. Distribution device with inserts in evaporation tubes

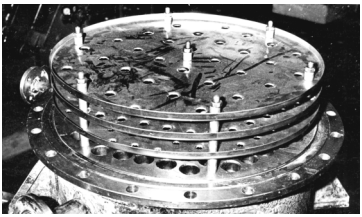

Fig. 13. Distribution device with three perforated plates

Finally, both types of distribution devices require a fluid flow rate that exceeds an economically sound value by an order. Under such conditions, only increasing the number of axes of symmetry of throttling elements, and the symmetry of perforation of plates relative to tubes' layout coordinates yields the necessary results. Seeking to meet both requirements, we arrive, on the one hand, at a perforated plate whose holes coordinates match those of tube arrangement in the tube plate, and on the other hand to a throttling element designed as a ball imbedded to one-third of its diameter into the heat exchange tube. A sphere is known to have an infinite number of axes of symmetry of infinite order. However, this turned out to be insufficient. Besides geometric symmetry of elements in three dimensions, symmetry in the fourth dimension was required. In other terms, the balls had to oscillate between the tube plate and the constraining perforated plate. The rising of balls (caused by rarefaction in

the distribution chamber) and their dropping (under the force of gravity) are symmetric in time (Fig. 14) [51–59].

The basic element of the device are hollow balls (throttling elements) 4 located in the upper ends of heat transfer tubes 2 secured in tube plate 3. The tubes are located in evaporation chamber 11 supplied with vapour via union 1. Perforated plate 5 is arranged above the balls. Distribution chamber 6 is fitted with pulsator 8 with valves 7, unions 10 for supplying the solution, and unions 9 for outlet of secondary vapour.

The initial solution, when being fed to the lower part of the distribution chamber at the time when the throttling elements drop, spreads uniformly over the entire tube plate. When the pulsator piston rises, rarefaction is created in the distribution chamber relative to the pressure in the evaporation tubes, and the throttling elements rise. Since each throttling element is designed as a hollow ball, and in rising the ball centre moves over a path close to the tube axis, this displacement creates an annular opening of equal thickness. A certain amount of fluid flows through this opening. When the piston drops, valves 7 open and the vapour that had entered when the balls had risen from the tubes to the distribution chamber is directed to the separator. The balls return to their place, and are positioned strictly along the centre of the tubes under the force of gravity. After this, the cycle is repeated. In moving up and down, the balls rotate chaotically about their centre of gravity.

The film streaming down in the pulsation regime is evaporated and then separated from secondary vapour in the separator.

A seven to ten-fold decrease in density of pulsating reflux (as compared to that in known distributors [60]) allows for considerable electric power saving in spite of its certain consumption by the pulsator. The device does not become clogged.

When the apparatus diameter is increased to several meters, the perforated plate is fitted with adjustment screws installed above each throttling element [61]. At the same time, the piston pulsator in the secondary vapour outlet union is replaced with a three-way pneumatic valve for alternate connection of the distribution chamber with the vapour space of the given apparatus and the installation vacuum system. A pulsator with a rotating rotor fitted with an electric motor and variable-speed gear can replace the three-way valve as a pulse generator [62].

The device allows to exclude asymmetry due to feeding the solution to the distribution chamber in one point, and achieve full geometrical symmetry of streaming down flows in separate tubes and across the apparatus section.

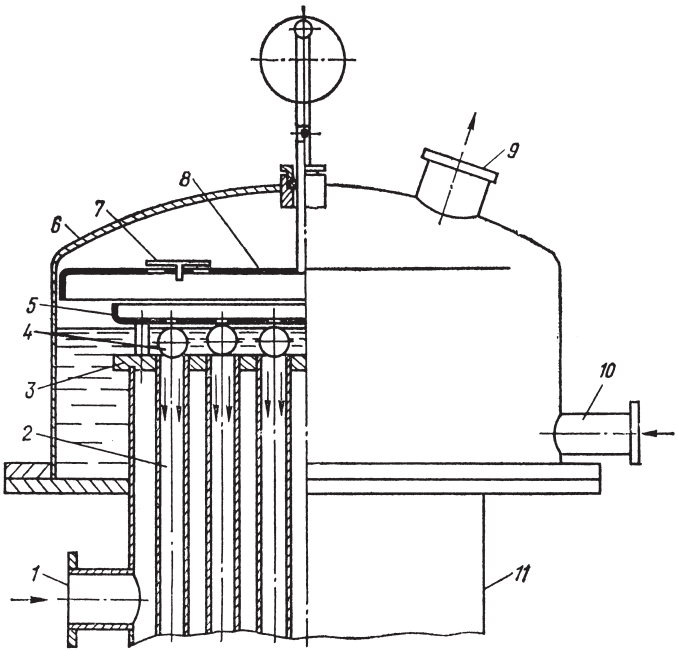

a

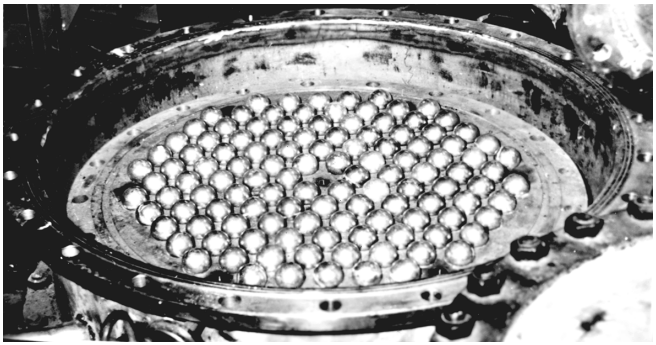

b

Fig. 14. Pulsating distribution device with balls (a), and its inner view (b)

In designing the pulsating distributor, a minimal number of elements was used, and their complete symmetry was observed. Any improvement of the device will lead either to disturbance of elements symmetry, or to an increase in their number. In both cases, this involves a growth of configuration entropy and, as a result, big expenditures of materials and power for its manufacture and operation. In addition, the quality of the heat-sensitive product degrades.

Hence, being guided by the laws of symmetry, one can solve concrete problems of distribution of fluid and gas flow in apparatuses on a well-grounded basis, and ensure the best possible practical results.

A decrease in flow velocity at the initial stage of the process, and flow intermittence during the following one involving changes in the direction of the field of velocities, are the necessary and sufficient conditions for distribution of a fluid in a gravitational field. The results of testing a pulsating distribution device are given below.

The ultimate goal of experiments with a 120-tube model of an evaporating apparatus with a pulsating distribution device was obtaining a mathematical dependence of the quality of distribution ξ vs. flow rate $\overline{G}$ per one tube, the rise of balls H, the oscillation frequency f, and the piston stroke L.

Here, ξ is the root-mean-square deviation of the fluid flow rate in the evaporator being investigated. The values of ξ are calculated with account of the number of tubes enclosed with reference tubes across the apparatus section.

Unfortunately, a theoretical solution of this problem is impossible because of the extreme complexity of hydrodynamic processes occurring in the distribution device. Hence, one method remains at our disposal — experimental definition of the distribution quality depending on the above factors.

Mathematically, the statement of this problem is as follows: it is necessary to obtain a certain representation of the response function. Since the kind of sought for functional dependence is unknown, it is convenient to present it in the form of a polynomial. Expansion of a function into a power series is equivalent to representing it as a Taylor series.

Taking into account the specific features of conducting the experiment, and the total body of experimental data, the functional dependence $\xi = f(\overline{G}, H, f, L)$ is assumed to be linear. By approximation of experimental data, the following equation was obtained

$$\xi = 1.95 \cdot 10^{-4} + 0.025\overline{G} + 6.4 \cdot 10^{-3}H - 2.28 \cdot 10^{-5}f - 4.17 \cdot 10^{-3}L.$$

This equation is valid for the following values of arguments:

$$1.4 \cdot 10^{-3}\ \text{kg/s} \le \overline{G} \le 13.2 \cdot 10^{-3}\ \text{kg/s};$$

$$2 \cdot 10^{-3}\ \text{m} \le H \le 1.2 \cdot 10^{-3}\ \text{m};\ 0.6\ \text{Hz} \le f \le 2.0\ \text{Hz};$$

$$3.5 \cdot 10^{-2}\ \text{m} \le L \le 5 \cdot 10^{-2}\ \text{m}.$$

The technique of conducting the experiments and generalising the data obtained is presented in greater detail in work [50].

Thus, we have succeeded in establishing experimentally that an optimal distribution of fluid and gas flows across the section of a multitube film evaporator, and in the tubes, can be achieved by employing pulsating throttling elements.

The elements are designed as balls that periodically cut off vertical flows from horizontal ones. Evidently, the same principle underlies the redistribution of radial and meridional flows in the shells of stars, where spherical plasma compactions spontaneously occurring in circulation cells play the role of throttling elements.

The observed process of periodical expansion and contraction of the Sun seemingly reflects the mechanism of alternate activation of the gravitational and rotational effects.

The pulsation-dissipative structures discussed here hold a special position in the hierarchy of creational-dissipative structures because they coordinate the interaction of opposing flows that carry energy out of Sun's interior and redistribute it in the surface layers.

In our studies of Sun's gas dynamics, one yet unsolved problem remains, namely, it is not quite clear how the flows of low-ionised plasma (ropes) that move from the poles to the equator rotate about their axis. The results of testing evaporators with natural circulation will help clarify the features of rotation of meridional flows.

1.2.4. Evaporator with tangential flow injection to the separator

We will highlight some features of a vortex flow that were detected when testing evaporators with natural circulation [64 and 65].

As shown in Fig.15, when a two-phase flow is injected at a tangent to the inner wall of separator 3, the fluid acquires rotational motion. At this, two clearly defined flow areas are observed: a central one with a hollow vortex rope 5, and a weakly rotating part of fluid 4 adjoining the wall. On the hollow core of the vortex surface, there are dilations and contractions caused by inertial waves.

With increasing heat load, the velocity of the two-phase flow injected into the separator also increases. Upon achieving a certain critical velocity, the flow, being constrained in the downtake channel, closes and a fountain 1—1.5 m high

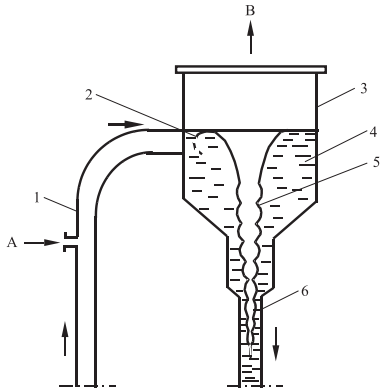

1 – uptake channel; 2 – tangential flow injection; 3 – separator;4 – layer of weakly rotating fluid; 5 – vortex; 6 – downtake channel;

Unions: A – air inlet; B – air outlet.

Fig. 15. Diagram of the circulation circuit of an evaporator

appears above the vortex. The fountain appears only at a certain combination of technological and design parameters of the circulation circuit.

This phenomenon can be observed, for instance, when the diameters of the separator are within 4–6 m, and the velocity of tangential injection of the vapour-and-fluid mixture is within 25–30 m/s. At the same time, the velocity of the steady-state translational movement of the flow in the downtake channel in this regime is within 1.5–2.5 m/s.

A different process pattern is observed when testing a cold stand. In this case, circulation was provided by pumping air into the uptake channel. There was no fountain, but the fluid level close to the vortex increased slightly (Fig. 16, b).

Both established features will be needed to evaluate the conditions of formation of galaxies and planetary systems as well as of Earth itself.

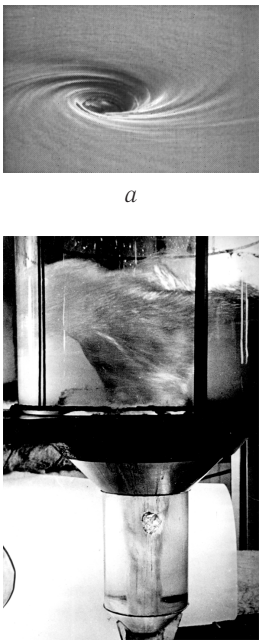

a

b

a) plane view; b) lateral view.

Fig. 16. Fluid vortex in the lower part of the separator (cold model)

1.3. CAUSES OF EXPLOSION OF CELESTIAL BODIES

A priori, it can be asserted that the quiet period of development of the protonuclei of galaxies and protostars occurred in conditions of a balance

between influx of energy into their mass in the course of inner reactions, and efflux of this energy to outer space through their outer surface.

The light of distant stars that were formed from the protonuclei of galaxies demonstrates that reactions similar to those in the solar system occur within their interior. This implies that explosions of nuclei occur due to impediments involving evacuation of generated energy to outer space rather than owing to lack of "fuel" within their interior.

Here it should be noted that the volume of a celestial body is proportional to its cubed current radius, whereas the outer surface is proportional only to the squared radius. Due to this, with increase in size and mass of a celestial body, the amount of energy produced surpasses that which it can discharge to outer space through its surface. Therefore, as a rule, massive bodies rotate at higher speeds and explode more frequently.

The natural cause of this trigger effect can be accumulation of reaction products in the outer shell during evolution of a celestial body. In this case, energy exchange with outer space is impaired and involves object overheating and explosion. It is reasonable to assume that shell shedding and its transformation to stars reflects the system's tendency to develop its surface of energy exchange with outer space, i.e. to acquire a more stable state.

At the same time, the diminished nucleus balances influx of energy from its interior with energy efflux to outer space. A reduction in the amount of energy generated in the interior per unit area of outer surface allows the body to reduce its axial rotational speed, and enter the stage of its undisturbed development.

1.4. DISTRIBUTION OF ANGULAR MOMENTUM AND SUBSTANCE MASS DURING EXPLOSION OF A CELESTIAL BODY

In this section, by example of formation of the Solar system and galaxies, we will demonstrate the validity of V.A. Ambartsumian's hypothesis. The best corroboration of this would be proving that the distribution of the angular momentum and mass of substance during explosion of the Protosun should have been just the same as observed presently in our planetary system. The same relates to galaxies.

The Sun, as we already know, rotates slowly, and its angular momentum is relatively small. The greater share of the angular momentum, as appears to be, is "contained" in the orbital motion of planets — primarily in the motion of the hugest one — Jupiter, in spite of the fact that the mass of the planets is less than 1 % of the Sun's.

The dynamic situation that occurs during an explosion was simulated by the instantaneous changing of parameters of the process that occurs in an evaporator with a turbine-driven circulation pump (Figs. 9 and 10; Part I). First we checked the system behaviour during a rapid increase in temperature of the circulating medium. For this, during evaporator operation, the pressure of primary vapour in heating chamber 6 was increased abruptly. The increasing heat influx to the water flow raised the available turbine's temperature difference from 4 °C to 40 °C within 20 to 30 s. As a result, the turbine-driven pump rotational speed increased from 500 to 2 600 rpm.

Hence we can conclude that, at the instance of explosion, the celestial body increases its axial rotation speed many-fold. As a result, the shell mass acquires kinetic energy in an amount sufficient for its breaking away from the central part of the object. Masses of substance, ejected at high speed to outer space, do not experience for long any friction with surrounding space in their orbital motion about the parent body. This allows them to conserve their angular momentum acquired during the explosion.

The remaining mass of substance behaves otherwise. When the medium temperature drops at the end of the explosion, the parent body sharply reduces its generation of mechanical energy. In this case, friction of flows in the nucleus will retard its rotation in short time. The situation is similar to that of the behaviour of gyroscopes of different design, for example, a top. As is well known, a "sleeping" top is a solid body rotating about its axis of symmetry, with a bearing point located lower than its centre of gravity. After being started, a balanced top rotates for quite a long time. But if the top is made with a hollow filled with a fluid, it will lose its stability after several axial rotations. The cause of this is significant mechanical energy loss inside the top due to friction between the fluid layers.

All this means that during explosion of the Protosun the major share of the angular momentum (98 %) was acquired by planets formed of masses of substance, whereas the Sun retained but its slight part.

The same situation seemingly also occurred during explosion of the Galaxy Protonucleus. Its spiral arms should possess a significantly greater angular momentum than the nucleus does.

Let us proceed to discuss the results of testing an evaporator with a turbine-driven pump. In the second series of experiments, we simulated the conditions of shedding the shell mass in outer space. For this, the amount of water in separator 2 was decreased abruptly to the minimum possible level, allowing nevertheless to maintain circulation. The installation immediately entered the pulsation regime. The flow of superheated fluid entered the turbine by separate

portions. When the flow passed the nozzles, the turbine rotational speed increased sharply, and in the idle regime it dropped. Thus, when the solution was superheated by 20 °C, the rotational speed of the turbine periodically increased to 1 200 rpm, and then dropped to 400 rpm.

Evidently, with an insufficient amount of water in the circuit, the angular momentum appears and disappears over certain time intervals to maintain installation operation in a certain transient regime.

Earlier we found that rotation of celestial bodies, including Earth, is caused by exchange of momentum between the gas-fluid or gas-plasma shell, where the momentum appears, and the nucleus. If the mass of substance belonging to the shell is shed to outer space during an explosion, the natural pump that discharged this mass from the poles to the equator stops its normal functioning.

Hence, an explosive loss of mass reduces the rotational speed of a celestial body, and transfers it to the pulsating regime of rotation.

So far, in building a model of formation of galaxies and planetary systems, we relied on the results of testing an individual circulation circuit. But we already know that huge groups of circulation cells of both gravitational and rotational type acted in the shells of the protonucleus of the Galaxy and the Protosun. It was their combined action that defined the law of distribution of the angular momentum among masses of matter ejected to outer space.

Let us start our discourse by stating that the supply of primary substance to the reaction zone was provided by the gas and hydrodynamic structure that was composed of a complex of circulation cells occurring in the shell of a celestial body. Hence, the rates of subnuclear and nuclear reactions that developed during explosions also obey Yerofeev's law (here we assume that the activation energy is small). This implies that the maximum value of the reaction rate corresponds to the systems' achieving such gas and hydrodynamic stability, which is reflected by the Glansdorff-Prigogine criterion. Needless to say, the rate of increase and decrease of rotational speed of an exploding celestial body will strictly follow the above regularity of reactions proceeding in its interior.

The same regularity should be observed in the distribution of velocities of stellar associations ejected to outer space, which form the arms of spiral galaxies, as well as in the differentiation of orbital speeds of rotation of planets about the Sun. However, to use the regularities established, it is necessary, at least, to define the principle of formation of stellar associations and planetary systems.

Let us consider the inertial waves that occur in vortices and, in particular, in rotating ropes — those "cold" flows that move from the poles to the equator. The waves in these ropes have the same inertial origin as the waves in vor-

tex-type ropes in circulation evaporators do. With increase in rotational speed, during an explosion the ropes develop into spiral arms that obviously enter the resonance regime. This enhances the effect of inertial waves and facilitates, ultimately, separation of flows in the narrowest locations.

The disintegration of ropes that break away from the rotating spherical surface obviously follows the most likely scenario, i.e. observing the golden section principle. The golden section (harmonic division) is such division of section a when its bigger part x is the mean geometric of entire section a and its smaller part $a-x$, i.e. $a:x = x:(a-x)$ [66].

Having retained their "ancestral features", the stars in the arms of the galaxies arranged as separate clusters so that the ratio of the periods of rotation of adjacent clusters formed a spectrum based on the golden section principle. In this case, we have simply applied the features of the Solar system structure to the law of formation of spiral galaxies.

Surprisingly, the arrangement of perihelions and aphelions of planets along a logarithmic spiral, as K.P. Butusov has proved, is also linked to harmonic numbers that confirm the rule underlying the golden section [67 and 68]. It is also possible that the Titius-Bode rule currently used to estimate the distance between planets [69] reflects the regularity established by K.P. Butusov.

Let us continue to discuss the features of distribution of momentum during an explosion. A certain share of the angular momentum is picked up by the belts of asteroids and comets. These belts are a relic of the "breathing" system of the Protosun. The system, as we have clarified, was composed of a group of spherical compactions of substance which once were located as cut-off valves in the uptake channels of gravitational-dissipative structures. Being located at a certain level, the spherical compactions, in descending, created something similar to "diaphragms" that separate spaces with increased pressure from those with a lower one. One might assume that the Protosun had several such diaphragms that disintegrated later into belts of asteroids.

Asteroids have survived to date because the majority of them move within a wide range between the orbits of Mars and Jupiter.

J. Oort discovered another belt made up of comets. He found that the planetary system is surrounded by a multitude of rock-ice bodies. By analogy with this, one can assume that the rings observed in several spiral galaxies are remnants of pulsating-dissipative structures that once ensured "breathing" of protonuclei.

Let us revert to discussing the arrangement of planets around the Sun. Obviously, changes in centrifugal forces that developed during an explosion also followed the *S*-shaped curve. Close to the point of inflection of this curve,

where the Protosun achieved its maximum rotational speed, a planet with a minimum current orbiting time had to break off. This planet, as will be demonstrated further, was Mercury.

Ejection of "diaphragms" to outer space possibly caused a disturbance of the resonance regime of separation of ropes, which further caused the appearance of planets with a small mass in the system. Thus, if one moves from the periphery of the solar system to its centre, beyond the belt of Oort comets we will find the small planet Pluto; and beyond the belt of asteroids we will find Mars, which also has a small mass. Continuing to move towards the Sun, we would have to find a belt of asteroids also before Mercury (Fig. 17). The dis-

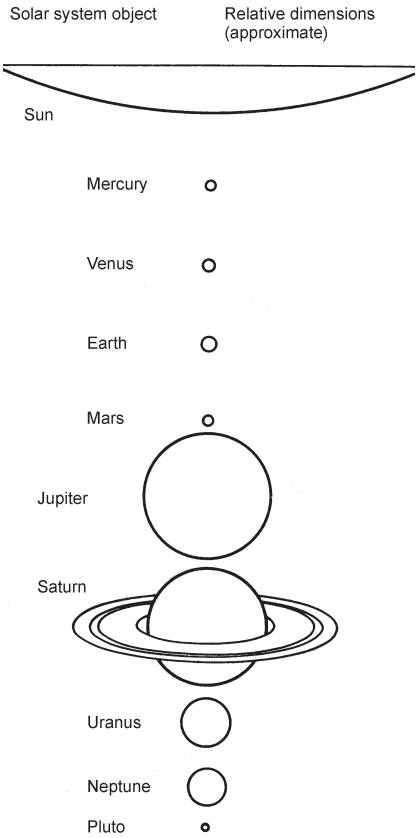

Fig.17. Relative dimensions of planets and the Sun

tance between Mercury and Venus is greater than that between Venus and Earth for good reason. But it seems that hardly anything has remained of this belt. Nevertheless, individual representatives of this "family" should have been observed recently when they crossed Sun's disk.

The above statements should be extended by adding that, after being self-compacted, the masses of substance ejected to outer space were the nuclei that attracted dust and gas particles, which occurred in their orbit of motion. Judging by the many kilometre-wide craters that have been preserved on the surfaces of the terrestrial group planets, many asteroids also "had no objection" to share their destiny with them.

Further we will expand our notions on energy conversions occurring during explosions.

1.5. NON-EQUILIBRIUM THERMODYNAMICS OF TRANSIENT PROCESSES

Certainly, we are interested in quantitative relations that confirm the regularities observed. In our quest for these relationships, we will as usual rely on entropy values.

Let us make it clear that entropy changes can occur in the following cases [70]:

1) Owing to changes in configuration entropy (for example, due to an increase in the number of particles or molecular disordering when substance scatters in a large volume);

2) Owing to changes in thermal energy (for example, due to thermal disordering when heat dissipates in a large volume or when potential energy dissipates similar to heat).

During a cosmic explosion, both the configuration and thermal entropy of a system increase. This fact creates an impression that the process should certainly end in formation of a cloud of dust and gases from the celestial body.

In principle, by analogy with thermal efficiency η_t, nothing prevents us from introducing the configuration efficiency η_c into our calculations. By intent, value η_c should reflect the degree of conservation of symmetry of gas dynamic formations during an explosion. With account of the general trend of natural processes moving to chaos, one can assume that only $1-2$ % of the ejected substance mass can be accommodated in outer space as stars and planets. The entire remaining substance, it seems, should scatter around the nucleus in the form of dust and gases. Moreover, the assumption suggested relates only to objects with sufficiently intense gravitational and rotational fields

that ensure stable circulation of flows. Evidently, stereotype reasoning is inciting us to assign the value $1-2$ % to η_c.

Actually, cosmos demonstrates a clearly reverse pattern. Here we can see sharply defined spiral arms of galaxies made up of stars that concentrate the bulk of ejected mass, whereas the content of interstellar dust and gases in these stars remains within $1-2$ % [14]. Hence, configuration entropy undergoes much smaller changes during an explosion than thermal entropy does. This is a manifestation of a remarkable feature of the systems considered. It implies that the elements of their symmetry, which existed in the shells of protonuclei, are preserved in galactic formations presented to us after billions of years.

The revealed feature of formation of galaxies and planetary systems is entirely predictable because reactions in cosmic objects proceed stagewise. In part, the reason of this is that creational-dissipative structures are capable of carrying the primary substances to the reaction zone and discharging therefrom the products formed only over a finite time interval that appears, as we have established, in Yerofeev's equation.

As a result, at the first stage, when subnuclear reactions proceed, the system is not capable of generating an amount of kinetic energy that would be sufficient for complete scattering of the shell substance. This substance should experience still a second stellar stage of its development involving nuclear reactions, and then, after having shed the stellar shells, proceed to the subsequent planetary stage where, as we know, chemical reactions prevail.

After each explosion, deformation forces split the system into separate parts and increase the distance between them. However, in so doing, they retain the common geometric features residing in the parent structure. One gets an impression that the laws of transition of non-equilibrium systems from one state to another are invariant with respect to similarity transformations.

Let us consider the basic principles of these transformations. Having specified, say, two similar figures, for example, a big and a small triangle of identical shape, we can consider any of them as a result of deformation or transformation of the other one, i.e. either imply that the small triangle was stretched uniformly to the bigger one or, conversely, that the big triangle was compressed uniformly to the smaller one. We can even consider more radical transformations. Let us highlight one of them.

Thus, B. Riemann suggested transformations allowing for extension, compression, bending and even twisting. Figures that can be obtained from one another by applying such transformations are known as homeomorphic or topologically equivalent ones. As a rule, one seeks to characterise equivalent

figures using certain defining properties. If such properties are found in two figures, then such figures are topologically equivalent in just the same way, for example, as two triangles are congruent when two sides and the angle between them in one triangle are equal to the respective elements in the other one [71].

The key task of topology is to establish when two figures are topologically equivalent. However, this can be challenging if we compare the figures only visually, as we are doing now at the current stage of our studies. To increase the validity of comparison results, a separate branch of mathematics known as differential topology has been developed [72]. However, to apply its methods, it is necessary to identify a priori the creational-dissipative structures not only on the Sun, but also on the nearest stars, as well as in the nuclei of galaxies. Besides, it is necessary to perform a respective statistical treatment of the observed types of spiral galaxies and planetary systems discovered to date. Only after this, topology and differential geometry methods can be applied to confirm strictly the affinity of the figures considered.

At the same time, based on classical concepts [73 and 74], it is necessary to develop a special terminology for Riemann transformations, which would be related to the stability of shapes of deformed objects. For the time being, we can use the techniques of non-equilibrium thermodynamics, assuming that, for each separate time interval, the system achieves stability characterised by the Glansdorff-Prigogine criterion. The sum of these intervals comprises the total time of transition of substances from one stage of their development to another one. For the sake of fairness, it is necessary to note that the level of deformation is determined by the adopted criterion of stability of a closed system, if the exploding object and the surrounding space are included therein. The noted ambivalence of phenomena observed during transformation of creational-dissipative structures is inherent evidently to the majority of open natural systems.

The theoretical and experimental substantiations presented here give us a relatively complete idea on the regularities and essential links that were present in cosmic transient processes. Therefore, an approximate estimate of the initial angular momentum of Earth made in the following section acquires, as we believe, a definite validity.

1.6. ESTIMATING THE ANGULAR MOMENTUM OF PROTOEARTH

First we will place certain landmarks along the course of our computational process. These landmarks will be the observation data available. Thus, it has been established that stars of spectral classes O, B, and A rotate very rap-

idly. As a rule, their equatorial speed exceeds 100 km/s. As mentioned earlier, the equatorial speed of Sun — a typical class G star — is only about 2 km/s [13].

Obviously, the solar system planets were formed of one intense "cooled" flow (rope) that moved in Protosun's shell from one of the poles to the equator.

It seems that the situation in Protosun's shell was similar to that observed currently on Jupiter.

This planet maintains its rotation mainly due to one rope located in its southern hemisphere. The efflux of the "cold" flow near to the equator is registered by the so-called Big Red Spot (BRS). The BRS has an oval-shaped form with the length of 40 000 km and width of about 14 000 km. Jupiter's diameter is within 143 000 km; its mass exceeds that of Earth by 317.8 times, and the period of rotation is 0.41 Earth's days.

In turn, the period of rotation of the BRS about Jupiter's axis differs from that of the planet itself. The spot drifts in the surrounding southern tropical zone. The BRS lags behind it by one revolution in about 30 years. The BRS itself rotates about its own axis, making a full rotation in six Earth's days. Recall that the bulk of energy influx to Jupiter's shell is from its core [68].

To all appearances, the circulation of flows on Jupiter can be taken as an analog of circulation that once existed in Protosun's shell.

In Part I of the book, we have mentioned that cooled flows of liquid hydrogen, entrained by the planet, as if roll over denser underlying layers. Such a flow regime makes the ropes rotate about their axes in a direction opposite to that of the planet's rotation.

Obviously, the same regularity was observed in the Protosun's shell as well. Hence it follows that the protoplanet spiral that separated during the explosion rotated in a direction opposite to that of the majority of planets. To date, only Venus and Uranus have retained the direction of relic rotation.

During their development, the remaining planets changed the direction of their initial rotation to the opposite one. This did not present a big challenge in the presence of a gas-liquid shell and mountains.

Here it is worth mentioning that the direction of rotation of asteroids about their axes cannot serve as a landmark for us because the rotation of masses of plasma, from which these celestial bodies were formed, had no clearly defined direction.

Earlier we concluded that Mars, at the initial stage of its history, had a gas-liquid shell. Now, with account of the above statements, we can conclude that Pluto also had a shell consisting of gases and liquids.

To start a rough estimate, let us consider one more value, namely, the rate of loss of matter during an explosion. Here we should take into account that ef-

fluence of plasma, which is under ultrahigh pressures and at temperatures of millions of degrees, can be observed only in cosmic conditions. All that remains to be done is to identify a benchmark for comparison. Taking into account the rate of discharge of substance into outer space on Wolf-Rayet stars — very bright blue objects — we will limit the value being considered to [13]

$$v = 1000 \text{ km/s}.$$

Note that the second orbital velocity required for an object to escape from Sun's surface is 618 km/s.

Let us estimate the rotational speed of the "cold" rope about Protosun's axis. Obviously, in separating from the Protosun, the rope disintegrated into pieces, while retaining its angular momentum. Hence, the orbital speed of planets should approximately coincide with the rotational speed of the parent rope.

The orbital speeds of planets are taken from reference data, e.g. [12 and 26].

Evidently, during the explosion the rotational speed of the Protosun increased from 4.7 km/s to 47.7 km/s. The bulk of the planet mass segregated in the range of circumferential speeds within 5.4–13.06 km/s. The Earth travelled to the orbit of Sun's satellite with the speed of 29.27 km/s. Here we have neglected the slight variance in the rotational speed of the Protosun and its rope due to drift of the latter. By comparing these speeds with the rotational speeds of the most active stars, we can see that the parent celestial body that originated our planetary system relates to the class of "yellow dwarfs", as the Sun does. In essence, one cannot expect anything else from a star orbited to the periphery of the Galaxy. One can also ascertain that the rotational speed of the rope of the protonucleus Galaxy that initiated the spiral arm where the Sun is currently located, was also relatively small — 250 km/s in all. It appears that, at the beginning of the explosion, the protonucleus of the Galaxy rotated but slightly faster than the stars of classes O, B, and A did.

Having no opportunity within the framework of this study to go to the crux of the problem of fragmentation and expansion of creational-dissipative structures to the dimensions of the present Solar system, we, nevertheless, will highlight the key issues in analysing the explosion of the Protosun.

The most likely process during an explosion is evidently the process of layerwise advancing of nuclear reactions into the interior. During the transient process, the celestial body shell transforms into a "layered cake", wherein each underlying layer expulses the overlying plasma layers. Since the density of the layers drops towards the surface, the overlying layers acquire an extremely high velocity.

For example, during shooting, gunpowder gases eject the shell from the gun barrel with a velocity of 2.81 km/s. But if a light gas — hydrogen — is pumped between the gunpowder charge and the shell, the gunpowder gases will first compress the hydrogen layer ("pad"). Then, being compressed to higher pressures, hydrogen expands to impart the second orbital velocity 10–11 km/s to the shell [75 and 76].

Following this scheme, the upper layers of the Protosun shell that did not participate in the depth reactions were discharged to outer space.

Further, with increasing pressure in the Protosun nucleus, an explosion initiates synthesis of new elements. Here it can be assumed that a definite part of each newly synthesised element had acquired a velocity during the reaction that was sufficient for entrance to outer space. This part of the substance entrained a certain angular momentum. Judging by the results of testing a reactive turbine, the same amount of angular momentum was imparted to the Protosun to increase its rotational speed.

The remaining part of the newly generated element penetrated into the depth and participated in the next stage of nuclear reactions. This sequence of events resulted in differentiation of escape velocities of future satellite planets.

Thus, being compressed with the shock wave, the hydrogen plasma expulsed Protopluto and its satellite from the upper layers of the shell to the most distant orbit. This was followed by the masses of the future giant planets whose working media were mixtures of highly ionised gases — hydrogen and helium. In so doing, the ratio of these components changed from one planet to the other one.

The most massive part of future Jupiter was ejected by a plasma flow that later became the atmosphere of young Mars. Apparently, this was a mixture of ionised hydrogen and water vapour, or more precisely, oxygen whose synthesis was initiated after the hydrogen-helium shell had been shed.

The same flow, but with a greater content of ionised oxygen, orbited Sun's satellite — Protomars. Subsequently, this flow was acquired by Earth in the form of a water vapour cloud.

In turn, the compressed "pad" of ionised carbon and oxygen launched Protoearth to space, and then enveloped Protovenus that occupied its orbit. Protovenus occupied its position assisted by a flow of ionised light metals and oxygen that settled later on Mercury as oxides.

And finally, Protomercury used a combination of ionised gases based on heavy elements and oxygen as a working medium.

Evidently, at the early stage of development of the solar system, the concentration of heavy metals increased from its periphery to the centre, which partially affected the distribution in density of substance of planets formed.

Here we must lay special emphasis on the significance of the word "partially" because we are considering the disintegration of a "cooled" rope that moved rather superficially in Protosun's shell. Most likely, the rope consisted of products of reactions that were acquired by the Protosun from the protogalaxy. Therefore, the elements that were synthesised directly by the Protosun could have covered the surface of the planets formed only with a thin layer.

Hence, the law of harmonic numbers observed in the distribution of distances of the planets and the Sun is dictated by the place of one or other element, synthesised during the explosion, in D.I. Mendeleev's periodical system of elements.

It looks like we have acquired sufficient data for an approximate estimate.

Logically, it is best to start the calculations by estimating the speed of separation of Mercury from the Protosun. By this point, the bulk of Protosun's shell was shed to outer space.

Since Mercury had already acquired the orbital speed of 47.7 km/s, it follows that the speed of its radial ejection to outer space was

$$v_{\text{M}} = 618 - 47.7 = 570.3 \text{ km/s},$$

where the known value 618 km/s is the second orbital speed on the Sun.

Further we assume that the ratio of the outflow velocity of ionised hydrogen that ejected Pluto to outer space, and that of ionised light metals and oxygen that orbited Mercury, was the same as we had observed in the gun barrel during outflow of gunpowder gases and hydrogen.

In this case, the speed of Pluto's separation will be

$$v_{\text{P}} = 3 \times 570.3 - 4.7 = 1706.2 \text{ km/s}.$$

But the Protosun was more massive than the Sun is. We assume that it's mass exceeded that of the Sun by 30 %.

Then, for Protopluto to separate, the following velocity was needed

$$v_{\text{P-p}} = 1.3 \times 1706.2 \approx 2218 \text{ km/s}.$$

Obviously, the initial speed of the explosive flow was twice greater than the gas outflow velocity in Wolf-Rayet stars.

Let us proceed with Earth's separation. At this point, about a tenth of the Protosun's shell was still in place. Hence, the speed of Earth's separation will be

$$v_{\text{E}} = (618 - 29.27) \times 1.03 \approx 606.4 \text{ km/s}.$$

For comparison, we will provide some data. At Earth's current position, the velocity of 41.74–42.45 km/s is required to overcome Sun's gravity.

Taking into account that its orbital speed varies within 29.27–30.26 km/s, we find that it has to acquire the speed of only 12.47–12.8 km/s to separate completely from the Sun [77].

No doubt the Earth acquired an additional angular momentum during the explosion. We will use Jupiter's data to evaluate it. We know that the planet's equatorial speed is 12.7 km/s, whereas the peripheral layers of the BRS rotate with the speed of $5.15 \cdot 10^{-2}$ km/s. In other words, Jupiter's rotational speed exceeds the rotational speed of the BRS about its axis by 246 times.

Let us apply this relationship to the outflow velocity of ejecting gases and the equatorial velocity of Earth's rotation $v_{eq.E}$. Hence we obtain

$$v_{eq.E} = \frac{606.4}{246} \approx 2.5 \text{ km/s}.$$

Hence, Protoearth's equatorial rotational speed was relatively low — only 2.5 km/s.

Nevertheless, when an iron core was formed in the mass, and the remaining substance accreted thereon, the speed of the planet being formed had to increase because the initial angular momentum changed but slightly.

Hence, liquid Earth was a rapidly revolving ellipsoid. This defined Earth's structure when its substance changed from the liquid state to the crystalline one.

CONCLUSIONS

Let us summarise our studies.

Thus, the inner processes that cause pulsation and rotation of celestial bodies can be accounted for logically within the framework of the theory of dissipative structures.

The dynamic structures occurring in the shells of celestial bodies ensure supply of primary components to the zone of depth reactions, and discharge of reaction products and energy to their outer surface. The compactions and rarefactions observed in the flows create conditions for quantisation of matter during an explosion.

During transition from the continuous to the discrete state, the flows that acted in the shells of galaxies' nuclei disintegrate into separate masses of matter wherefrom stellar clusters are subsequently formed.

The spiral arms of galaxies are traces of extinct structures of rotational-dissipative structures that ensured rotation of protonuclei; and the rings are traces of pulsation-dissipative ones that were responsible for their "breathing". Moreover, the "breathing" of protonuclei and protostars involved their periodic compression and expansion.

The rotation and pulsation of celestial bodies enabled them to find the most optimal conditions for exchanging energy with surrounding cosmic space.

The formation of our solar system followed the same principle during the explosion of the Protosun.

The results of testing film and circulation evaporators whose circuits have been accepted as analogs of creational-dissipative structures allowed to confirm that the main angular momentum, after explosion of the Protosun, had to concentrate in the planets (as indeed was the case).

The emergence of a belt of asteroids and comets (a relic of the Protosun's "breathing" system) had no critical impact on Earth's formation.

Disintegration of creational-dissipative structures during the explosion follows the most likely scenario — the one governed by the "golden section" principle.

The star (Protosun), which exploded in the distant past, possessed one intense "cooled" flow (rope) that moved in its shell from the south pole to the equator. The rope rotated about its axis similar to that how the flow on Jupiter rotates currently.

The planets were formed when the rope disintegrated during the explosion of the celestial body. The elements synthesised during explosion of the

Protosun created flows that ejected the masses of future planets to space. The law of harmonic numbers, which is observed in the distribution of distances between planets, is dictated by explosion of specific elements found in D.I. Mendeleev's periodical system of elements.

The Protoearth, orbited to Sun's orbit, rotated about its axis with the equatorial speed of about 2.5 km/s.

When Earth's substance condensed, its rotational speed increased many-fold. The liquid Earth had the shape of a rapidly rotating ellipsoid.

CHAPTER 2

EARTH'S TRANSITION FROM THE LIQUID STATE TO THE CRYSTALLINE ONE

Modern ideas on the planet's state distinguish the lithosphere — an outer zone including the crust and the upper part of the mantle to the depth of about 70 km. The lithosphere is split into some ten big plates. The rigid lithosphere is underlain with a layer of increased yield — the asthenosphere. Owing to the low viscosity of the asthenosphere, the lithosphere plates float in an "asthenospheric ocean".

As the model developers claim, the shell-type structure of Earth originated by differentiation of its substance under gravitational field action in conditions of interior heating. The continental crust, consisting of two main layers — the granite and basalt ones, is located under the cover of metamorphic and sedimentary rocks having a variable thickness. The ocean crust has a basalt composition, and the entire mantle consists of ultrabasites. The key components of basalt and granites are aluminium, silicon, magnesium, calcium, and iron oxides. Besides, as compared to basalts, granites show an increased content of potassium oxides.

The external core (30 % of Earth's mass) is in a liquid state representing a mixture of sulphur (12 %) and iron (88 %). The internal core (1.7 % of Earth's mass) is solid and consists of an iron-nickel alloy (20 % Ni and 80 % Fe). Earth is assumed to receive the bulk of heat energy in its interior due to radioactive fission of uranium, thorium, and potassium. Planet heating could also be enhanced by heat accumulated during formation of the planet as well as liberated during subsequent gravitational differentiation of matter into a silica-base mantle and an iron core (Fig. 18).

Due to gravitational differentiation of matter in Earth's interior, and its degassing, the hydrosphere and atmosphere also originated [78–85].

Let us investigate the known model of Earth's structure for its correspondence to thermodynamic constraints established in our studies. In particular,

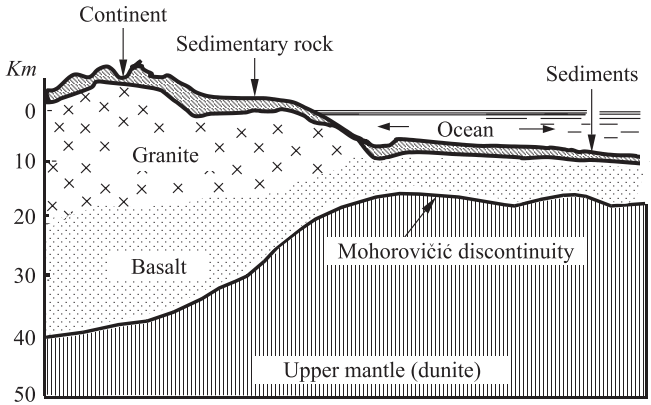

Fig. 18. Schematic section through the continental and oceanic Earth's crust

we will check whether opposing motion of iron flows, on the one hand, and water with aluminium and silicon oxides, on the other hand, was possible prior to the planet's solidification.

2.1. FORMATION OF THE LITHOSPHERE AND HYDROSPHERE

Thus, affected by the gravitational field, iron tends to descend to the centre of the heated Earth, whereas lighter oxides and water tend to rise to its surface. Recall that the mass of water in the World Ocean accounts for only 0.02 % of Earth's mass, whilst the mass of iron alloys concentrated in the core exceeds 30 % of its mass. The rising water currents could hardly avoid the fatal encounter with intense liquid iron flows rushing to Earth's centre. Obviously, contact between these flows would have been unavoidable.

Let us check what this process would involve. Under isobaric-isothermal conditions, the possibility of chemical and phase transformations in a closed system* is defined by the equation

$$\Delta Gi^0 = \Delta H^0 - T\Delta S^0. \qquad \text{(II.1)}$$

Fig. 19 gives the estimated values of ΔGi^0 for two types of reactions [86]

$$3Fe + 4H_2O\,(\text{water}) = Fe_3O_4 + 4H_2\uparrow, \qquad \text{(II.2)}$$

$$3Fe + 4H_2O\,(\text{vapour}) = Fe_3O_4 + 4H_2\uparrow. \qquad \text{(II.3)}$$

* The system consists of two mutually open subsystems.

The same reference gives data on interaction of aluminium and silicon with water and water vapour.

In our estimates, we have used the tabulated values of ΔH^0 and ΔS^0 given in reference literature [87]. Negative values of the isobaric-isothermal potential point to high probability of the reactions considered, in particular, the reaction of iron with water.

Hence, the current model of ocean formation by "rendering" water from Earth's interior fails to match the format of our further studies, and we are forced to abandon it. In this case, it remains to assume that water came to Earth's surface from its atmosphere. This idea, however, is not new because it prevailed among national scientists as far back as the early XX century [16].

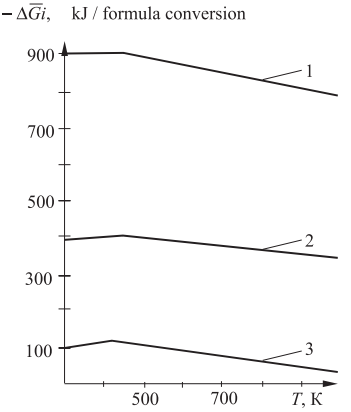

1 – Al; 2 – Si; 3 – Fe.

Fig. 19. Averaged Gibbs' energy vs. temperature during interaction with water and water vapour

This assumption can be corroborated by comparing Earth's protoatmosphere with that of the nearest planets, for example, Jupiter and Saturn. These planets are hydrogen-helium ones. Jupiter's solid core accounts for 3–4 % of the planet's mass, and Saturn's core accounts for 26–28 % of its total mass.

Now we have to explain how, according to the known theory, such huge liquid masses of planets could have "rendered" from negligibly small cores. The process discussed relates to the category of practically unlikely ones. This implies that clouds of gases, and possibly, the substance of protonuclei originated initially in the form of masses of matter that separated during explosion of a protostar. It is assumed that, during formation of planets, the core was first formed from condensate, followed by accretion of gases onto the solid surface that was formed [88 and 89].

It is clear that, if the cores of Jupiter and Saturn were able to retain such gas shells near their surfaces, it would have been easy for the gravitational field of our planet to attract a layer of water vapour whose mass, moreover, was not greater than 0.02 % of its total mass.

Further, the known theory fails to explain why continents originated on Earth. The planet's external appearance, however, can serve as a basis for interpreting its entire history.

Let us again address energy conversions that accompanied Earth's formation. Undoubtedly, the influx of radiation energy from the nearest star and

its efflux to outer space were the key causes of occurrence of intense flows in liquid Earth' shell. The formation of continents alone, whose shapes represent the solidified structure of ancient flows, justifies this assumption. At the same time, we cannot be assured that such intense flows could have originated in an environment made up of alumina, silica and iron, whose viscosity in the molten state was several orders higher than that of water [90 and 91]. It is unlikely that the amount of mechanical energy generated by Earth as a thermal engine would suffice to move high-viscosity flows over thousands of kilometres from the equator to the poles, and vice versa.

Most likely, the viscosity of liquid Earth components differed but slightly from that of water. If we assume its two or three-fold excess, this value will coincide with that of the ferro-silica-aluminium alloy (FSA) viscosity [92–94].

Thus, we have found that Earth, at a certain stage of its evolution, consisted mainly of an iron, aluminium, and silicon alloy. To all appearances, our conclusion is not so farfetched. Indeed, if even in the initial conditions we had granted iron the right of not interacting with water, it would be inappropriate to deprive aluminium and silicon of such an option.

The temperature of a liquid FSA is within 1,600–1,700 °C. It is unlikely for liquid water to exist in Earth's upper layers at atmospheric pressure and such high temperatures. Even if the entire mass of oceanic water were evaporated, the layer of vapour formed would rise to hundreds of kilometres, and the pressure exerted on Earth's surface would increase to dozens of atmospheres. Under these conditions, FSA alloy vapours, in spite of the separating layer of deoxidation gases, would interact with water vapour to cause rainfalls on Earth with droplets of aluminium, silicon, and iron oxides.

Hence, flows of pulp, consisting of the FSA alloy and its oxides, circulated over prolonged periods in Earth's surface layers. However, the chemical affinity of aluminium and silicon to oxygen is substantially higher than that of iron (Fig. 19). Therefore, the bulk of iron oxides was deoxidised by aluminium and silicon to pure iron. It is these alloys and, in part, their oxides that served as the basic material for alluviation of continents.

However, for an extended period, the red-hot bed of the World Ocean remained empty until the temperature and atmospheric pressure drop caused water vapour to condense. The first water flows moved to the cooling ocean bed from Earth's poles. The process of ocean formation alone continued for about 500 million years [95]. The ancient ocean covered both low and elevated areas of Earth, including continents, with an even layer. Afterwards, however, mountain ranges started developing as aluminium, iron and silicon began reacting with water. The continents gradually shed the water. This process is continuing

even nowadays, though the reaction front has descended to the depth of several dozens of kilometres.

The ratio of the number of volcanoes on land and in the ocean backs up the theory being developed here. It seems quite logical to assert that the probability of a reaction of the FSA alloy with water in Earth's interior under the ocean is significantly higher than under the continents for the simple reason that, in the former case, the distance from the water to the reaction zone is significantly less than in the latter case. Indeed, there are more than 10 000 volcanoes in the ocean, whereas on land only 817 of them are active and located, as a rule, on islands or peninsulas, i.e. close to seas and oceans [96].

The reaction of aluminium, silicon, and iron with water yields oxides of these elements and hydrogen. It is silica, alumina and iron that account for the bulk of the lithosphere.

Thus, V.I. Vernadsky assumed that, to the depth of 25 km and more, aluminium silicates and silicates are undoubtedly the prevailing minerals that constitute Earth's crust.

The properties of the substance of this part of the planet, except for oxygen, are determined above all by the properties of two elements — silicon (Si) and aluminium (Al). On average, these elements account for over one-third of the mass of Earth's crust that contains 26.0 % of Si and 7.45 % of Al by weight to a total of 33.45 %.

As to their abundance in Earth's crust, the following five metals are the leading ones: Fe, Ca, Na, Mg, and K. Their total content, by weight, in Earth's crust (down to 20 km) is 14.55 %. All other metals fail to contribute even 0.4 % by weight of its substance. Iron stands separate from these five elements because, in its case, one can observe a substantial number of atoms having no links with oxygen. The remaining part, being an analog of alumina, holds a special position in silica-alumina crystalline chemical structures (in the core) [97].

In his last works, Vernadsky made the following statement: "With depth, oxygen disappears rapidly, and the amount of hydrogen apparently grows. At the same time, the temperature and pressure also grow. All this can result in conservation of hydrogen compounds at these depths. There are indications of a general process that is a function of depth, namely, CO_2 is replaced with hydrocarbons. It is methane's exclusive link to life forms that raises doubt because this light gas possesses properties resembling those of hydrogen" [98].

Nearly the same conclusion can be drawn if we compare the chemical composition of atmospheres and distribution of substance mass among the Solar system planets. Thus, it is evident that the bulk of matter discharged to outer space is concentrated in the giant planets Jupiter, Saturn, Uranus, and

Neptune. In turn, the thick atmospheres and shells of these planets consist mainly of hydrogen and helium. Hence, a deoxidation environment prevailed in the shell of the Protosun. Therefore, it can be inferred that the majority of the terrestrial group planets are composed of pure elements and their hydrides.

It is also obvious that the bulk of oxygen was synthesised during the final stage of the explosion when the pressure in the nucleus of the Protosun increased dramatically. This made oxides of different elements appear in the upper layers and atmospheres of the terrestrial group planets.

Based on the knowledge gained, we will proceed to elaborate the model of Earth's structure in greater detail.

2.2. FORMATION OF CONTINENTS

In the known theory of Earth's structure, there is practically no section dealing with the lithosphere crystallising sequence. We will take the liberty to make up for this deficiency.

The version of the train of events that is suggested is based on the regularities of redistribution of heat in Earth's shell due to the rotational effect [10] that were discovered earlier. According to this effect, molten high-temperature FSA flows moved from the equator to the poles and evaporated partially. Since, at the same time, FSA alloy vapours interacted with water vapour, a significant amount of mechanical energy imparted to Earth was generated. In turn, Earth converted this energy to an angular momentum, and then transferred it to "cooled" FSA alloy flows to move them from the poles to the equator.

Excess energy was transferred continuously from the equatorial zone of the molten planet to the poles by intake of the mass of liquid alloy from the beds of the Atlantic and Pacific Oceans. Then this cooled mass was discharged to the equator to the sites of future continents. Expending minimum energy, Earth acted as a turbine pump to move the flows over the shortest distances in both the Northern and Southern Hemispheres. The same relates to the Eastern and Western Hemispheres. Stated otherwise, a circulation circuit, strictly isolated from other ones, operated in each quarter of Earth's spherical surface at that stage, as it does so presently. As a result, no less than four continents — two in each hemisphere — had to appear during uniform cooling of the planet.

First, using the external features of continents, we will attempt to interpret the dynamics of their formation. The tip of each continent faces the South Pole, and the expanding part faces the North one. The wedges are extended in the meridional direction to ensure minimal resistance to the flow of "cooled" currents (see Fig. 20). Evidently, a spacious bowl of the molten ocean bed was

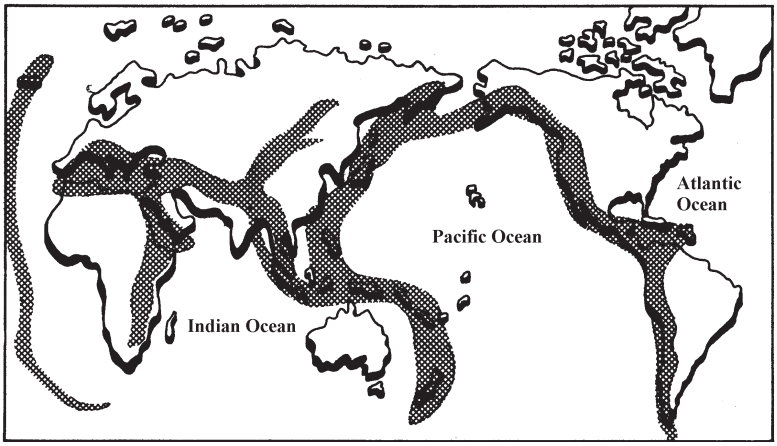

Fig. 20. Outlines of continents. The grid has been applied to areas with significant reserves of geothermal energy, which coincide mainly with regions of volcanic activity and orogeny.

formed first on the North Pole, and an archipelago was created on the South one. The capabilities of these two formations acting as pumps differed; therefore, the southern "cold" flows prevailed over the northern ones. At the same time, the bed of the Arctic Ocean continuously changed the latitude of the site of molten mass ejection to the equator. Consequently, the solidified edges of the nearest continents created a chain around the molten ocean bowl. The bases of the wedges of northern continents were formed in such a manner.

At the same time, the Antarctic shores, where the energy efflux to outer space was much more intense than in the North, succeeded in pumping the cooling mass to the tip of each wedge. With increasing resistance of any continent formed to the flow currents, the site of molten pulp ejection to the equator moved latitudewise to the tip of the newly-born continent.

Southern, more intense flows, pressed the cooling mass of future continents away from the equator to the North. This is the cause of the bulk of land masses observed in the Northern Hemisphere. Careful consideration of southern continents shows that their wedge-type form has no full symmetry in the meridional direction. The impression is that, during formation of Africa and Australia, the Coriolis force deflected "cold" southern flows westward, and hence, the direction of Earth's rotation coincided with the current one. At the same time, the geometry of the coastline and the inclination of South America's surface indicate that Earth rotated in the opposite direction. Probably

Earth had changed the direction of its rotation as early as the period of formation of continents.

At the final stage of terrestrial formation, Australia, New Zealand, the Island of Madagascar, the islands of the Arctic Ocean and, probably, Greenland were formed. At this point, due to lack of the liquid phase, Earth transferred to the pulsating regime of rotation. As we already know, in such cases circulating flows are discharged to the equator in separate portions. The biggest of these was obviously spent on Australia that emerged out of non-existence.

The regularities discovered do not allow for any other arrangement of continents apart from along the meridians. The sole forces capable of twisting the continents are the compression effect ones. This effect, as we already know, occurs in mountains during retarding of high-speed moist flows. In the Cordilleras and the Himalayas, baric forces act along tangents to Earth's sections arranged, in turn, parallel to the equatorial section, i.e. in the latitude direction. In essence, these forces ensure Earth's rotation.

However, during formation of continents, there were no mountains yet, making it possible for the continents to be embedded rigidly in the crystallising lithosphere. Islands are quite another case. At that time, the asthenosphere was located close to Earth's surface, and small formations of crystallised substance could move over it by the thrust of intense flows. In this case, it would be quite logical to suppose that the Island of Madagascar and New Zealand are most likely fragments of isthmuses that existed between Antarctica and Africa, and Australia, respectively, which were subsequently degraded and displaced eastward by the flows.

The cause of degradation of the isthmuses could have been a drop in Earth's rotational speed. This made the planet lose its gyroscopic effect to change, in turn, the spatial position of its axis of rotation. During this period, rather intense inertial forces emerged, which acted in the meridional direction. However, the displacement of islands caused by these forces could not have exceeded the level of spatial oscillation of Earth's poles.

Here it is appropriate to note that, if the cooling Earth changed its rotational speed or rotational direction, this could have occurred only due to external action on the Solar system, which is an unlikely event.

Greenland's history poorly fits that of Earth's described here. Greenland's mountainous landscape resembles but little Canada's flatlands located nearby. Of course, it is necessary to account for the mineralogical affinity of these two formations [99]. Hydrodynamic regularities indicate, however, that this giant island could have emerged simultaneously with Antarctica. One can assume that it was Greenland (located strictly on the North Pole) that worked as a

pump to discharge the molten mass towards Alaska and Scandinavia during the early stages of liquid planet crystallising. Afterwards, however, the island's small dimensions, as compared to those of Antarctica, prevented it to secure its legitimate position, and the angular momentum, in interacting with the flows, made it drift to the North American coast. The matching of Greenland's coastal outline with the profile of the Arctic Ocean basin supports this assumption.

Let us consider the mechanism of formation of Antarctica and Greenland. Experimental data on vortex flows indicate that, in descending swirling flows, in constrained conditions, a stream of liquid can be ejected upwards at rather high pressure. Obviously, with increase in Earth's rotational speed, part of the circulating matter at its poles was pressed upwards from the descending flows. Afterwards, Antarctica and Greenland were formed from this cooling matter.

Earlier we mentioned that the energy drain on the South Pole was higher than that on the North Pole. As a result, the Southern Hemisphere of the liquid planet rotated somewhat faster than the Northern Hemisphere did. During the crystallising period, this should have caused a torsion effect to appear. The effect consists in barely noticeable helical swirling of cooling meridional Earth "strands", including continents, about Earth's axis of rotation.

Indeed, it is evident that the central meridian of South America is slightly displaced eastwards in latitude relative to the central meridian of North America. The same can be seen in Australia in regard to Asia. P. Fourmarier [84] was the first investigator to point out the *S*-shaped axial lines of continents.

Africa's position fails to obey this rule. We will recur to this issue after having discussed the character of underground reactions that promoted displacement of this continent over Earth's surface.

Certainly, we are interested in how the intricate outlines of Europe — the cradle of Western civilisation — were formed. The centres of oriental culture — China and Japan — deserve no less merit. Their coastal outlines have to be accounted for as well.

In our reasoning, we in no way can assume that the process of substance crystallising during the period of alluviation of continents was the sole one. In fact, this process prevailed only on the poles, whereas the opposite phenomenon was observed closer to the equator, viz. here the alluviated continents "waned".

In penetrating the mass of clouds, solar radiation and the heat of Earth's interior continued to melt the solidified mass in zones of collision of northern and southern flows. Subject to pressure of adjacent rock, the dislocations thus formed moved eastwards, rotating about their axes and decreasing in size at the same time. In so doing, the shapes of the dislocations remained invariable.

This is manifested by the profile of the coastlines in the eastern part of the Mediterranean Sea, the Black and Caspian Seas [85] as well as of Lake Baikal whose depression is the last of dislocations that had moved from Europe to Eastern Asia (Fig. 21).

Probably, the layer of later sediments within the vast space from the Mediterranean Sea to the Sea of Japan covers dislocations of ancient rock types similar in form.

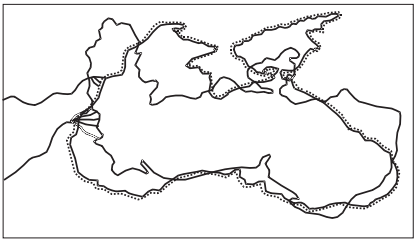

Caspian Sea;

Black Sea.

Fig. 21. Superposition of the outlines of the Black and Caspian Seas with rotation of one of them through 90°

In the Western hemisphere, the Sun succeeded in melting the basins of the Gulf of Mexico and the Caribbean Sea. Similarly, the basins of the Sea of Okhotsk, the Sea of Japan, and the East and South China Seas appeared close to Asia's coastline. The flows of molten mass emerging in these basins also kept pace in this "destructive" activity. For instance, Europe could have been shaped as an almost undivided continent resembling compact Alaska in shape. However, after Greenland had joined Canada's eastern coast, the hydrodynamic situation in the Western Hemisphere changed dramatically. Southern high-temperature flows advanced from the Caribbean Sea region along the path of the current Gulf Stream, and, in so doing, eroded the almost completely formed continent they encountered. As a result, Europe acquired a wedge-shaped form directed with its not altogether sharp tip towards the flows that had a "destructive" effect on the continent.

Likewise, the flows moving from the South China Sea eroded and smoothed out the coasts of China and Japan. Eventually, however, Earth's cooling culminated in final fixing of the shapes of the continents as we see them nowadays.

Having established the dynamics of formation of continents, we will proceed to study their inner structure. At the same time, we will consider the structure of Earth as a whole.

2.3. STRATIFICATION OF ELEMENTS IN EARTH'S INTERIOR

Seismic studies have shown that the continents are embedded in adjacent rock to the depth of 30—40 kilometres. Apparently, in growing, continental blocks slowly descended into the highly viscous part of the cooling melt. At the

same time, the easy-flowing part, in forming flows, continued to replenish the upper layers of the continents. Segregation of a liquid mass into fusible and refractory parts implies that, concurrently with "building" continents, circulation of flows ensured fractionation of the primary alloy. As a result, heavy silicon alloys settled under the ocean to form basalt rock, whereas lighter silicon alloys concentrated under the present-day sedimentary layer of continents to form granites. For the same reason, deposits of bauxites, and calcium and magnesium ores were arranged in the upper layers of continents.

Let us trace this process by example of segregation of the FSA alloy.

2.3.1. Segregation of the ferro-silica-aluminium (FSA) alloy

In experimental investigations, we have to establish how the gravitational and centrifugal fields affected the allocation of elements inside Earth. In the ideal case, the composition of the FSA alloy should match the one that existed during the period of Earth's crystallising. But since this condition cannot be met in full, we will take alloys obtained from coal for our experiments.

The inorganic part of power plant coal is known to consist mainly of iron, aluminium and silicon oxides with inclusions of rare and dispersed elements [100–102].

Presently, local TPPs are supplied with coal whose inorganic part accounts for 25–30 %. It is known, however, that only 1–2 % of inorganic compounds belong to trees alone that formed coal deposits, whereas all the remaining ones relate to sedimentary deposits. Hence, 400–500 million years ago when Earth was covered with tropical forests, the bulk of its surface layers was composed of silica, alumina and iron.

The technology of melting FSA from coaly rock and coal concentration waste is described in papers [103–106]. The required level of Si and Al content in the alloy is achieved at the alloy mixture temperature in ore-smelting furnaces within 1,900–2,500 °C. The amount of carbon in the alloy mixture is within 25–35 %. The reaction of deoxidation of alloys from oxides involves liberation of intermediate gaseous products, in particular, aluminium and silicon suboxides. The bulk of these suboxides is trapped and recycled by the opposing flow of the cold alloy mixture fed to the furnace.

The standard FSA produced presently for metallurgical and machine-building enterprises contains the following elements, by mass %: 15–25 Al; 55–60 Si; and 15–30 Fe. The alloy has inclusions of P, S, Ca, Mg, Na, K, and several other microelements.

Segregation of FSA into separate elements in a centrifugal field was studied by example of segregation of this alloy during granulation. The alloy

FS55A25 was subject to granulation (the alloy composition was as follows, by mass %: 55 — Si; 22.5–27.5 — Al; 0.03 — S; 0.07 — P; 0.4 — Mn; 0.4 — Cr; and the rest was Fe)*. The alloy density was 3.94 kg/dm^3. The functional diagram of the installation is shown in Fig. 22a.

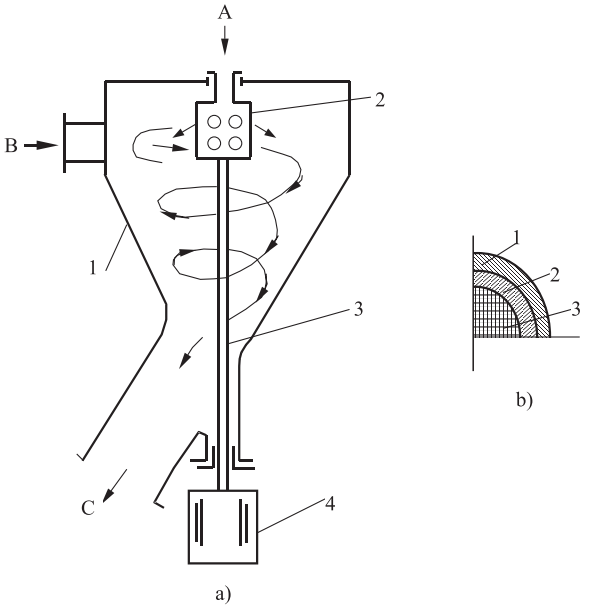

Fig. 22.
a) Granulator schematic diagram
1 – granulator casing; 2 – perforated sleeve; 3 – shaft; 4 – electric motor.
Unions: A – molten alloy feed; B – inert gas or water feed; C – discharge of gas and granulated product.

b) Granule cross-section
1 – aluminium; 2 – silicon; 3 – iron.

During operation of the stand, the alloy melted in an induction furnace is poured via union A into perforated sleeve 2. Electric motor 4 rotates shaft 3, and the alloy droplets are ejected from the sleeve perforations to be entrained by a flow of inert gas (or water) fed into casing 1 via tangential union B. The droplets are cooled and crystallised in a rotating gas flow. The granules thus formed are discharged with gas via union C.

* The R&D Institute of Metallurgy (NIIM, Cheliabinsk, Russian Federation) performed granulation in cooperation with IPMash NAS of Ukraine (Kharkiv).

Granulation was conducted with the following parameters: shaft rotational speed — 1,000–1,400 rpm; speed of injecting the inert gas into the granulator casing — 20–30 m/s; and inert gas temperature — 18–20 °C. The size of the granules was controlled by changing the shaft rotational speed and the speed of injecting gas to the granulator. Depending on the preset regime, the installation produced either spherical granules with a diameter of 1–2 mm or spindle-shaped ones of the same diameter in the largest cross-section, with a length of 4–5 mm.

Fig. 22 b shows a granule cross-section. Clearly, iron is located in the sphere centre, silicon is above, and aluminium is on the surface. It is important to note that, at the FSA melting temperature, aluminium has a density of about 2.2 kg/dm^3; silicon — 2.3 kg/dm^3, and iron — 7.8 kg/dm^3 [92–94].

If we follow the conventional theory of decantation, the centrifugal forces in the rotating droplet should have repelled heavy iron to the periphery; forced silicon to the intermediate layer, and retained aluminium in the particle centre. However, the granule cross-section shows that the elements' behaviour is "illegal".

Though crystallisation of the FSA alloy requires a fraction of a second, nevertheless this time interval, as evident, was sufficient for aluminium to segregate on the granule's surface. The issue becomes clear by comparing the temperatures of crystallisation of elements. Liquid iron is known to crystallise at the temperature of about 1,539 °C; silicon does so at 1,415 °C, and aluminium at 660 °C [92–94]. Hence, segregation of the FSA alloy occurred in strict compliance with the temperatures of crystallisation of its constituent elements.

We will call the newly discovered effect centrifugal segregation by crystallisation temperatures (CSCT). It is appropriate to note that a sufficiently intense force field is required for CSCT to be manifested. For instance, induction heating of the FSA alloy in quartz tubes to the melting temperature; maintaining it for some time in the liquid state, and subsequent crystallising by natural cooling failed to yield the desired result. The gravitational field succeeded merely in effecting a weak segregation of the crystallising alloy.

As we have ascertained earlier, the angular momentum of liquid Earth was quite significant. This fact predetermined the structure of our planet.

2.3.2 Centrifugal segregation of liquid Earth

Following the regularity established when segregating the FSA, we conclude that Earth's centre should contain alloys of iron with refractory metals. These are as follows: tungsten, rhenium, osmium, tantalum, and molybde-

num. The temperature of crystallisation of these elements at atmospheric pressure is within:

$$2610 < t < 3410\ ^{\circ}C.$$

The central region of the core should be surrounded with alloys of iron with iridium, niobium, ruthenium, hafnium, rhodium, vanadium, and chromium. For these elements [107 and 108]:

$$1875 < t < 2442\ ^{\circ}C.$$

The crystallisation temperatures of carbides of the metals mentioned fall into about the same range [108 and 109], allowing them to be part of Earth's core composition as well. Strange as it may seem, the carbides of light metals — aluminium, boron and beryllium as well as silicon, are arranged in the outer shell of the solid core. At atmospheric pressure, the crystallisation temperature of these solid solutions is within the range

$$2150 < t < 2830\ ^{\circ}C.$$

Thus, it seems that carbides will accompany the basic elements as far as to the asthenosphere.

The liquid shell of the solid core consists evidently of an alloy of iron with nickel (1,453 °C), cobalt (1,493 °C), and titanium (1,668 °C). Iron carbide (1,650 °C)* is also found here.

The total content of alloys, including carbides, in the mass of the iron core should be relatively low. Undoubtedly, the significant pressure in Earth's interior will change the crystalline lattice of alloys and increase their melting temperature [110]. However, the ratios between the crystallisation temperatures will be retained, therefore, the layered structure considered will remain invariable.

Having completed the arrangement of iron and its alloys, we will proceed with decantation of the following most abundant elements — silicon, magnesium, calcium, and aluminium. The bulk of Earth's mantle as far as the asthenosphere is composed, most likely, of silicon (1,415 °C) and its alloys, it being assumed that magnesium alloys prevail among all other ones.

At the early stage of formation of Earth's layered structure, prior to the period of condensation of water vapour from the atmosphere, these components comprised the bulk of the lithosphere. The lighter alloy of silicon and potassium was among the components of the base of continents. Intense flows carried the fusible elements and their alloys into their surface layers. Thus, the zone overlying the base was occupied by calcium (842–852 °C); the next one above was aluminium (660 °C), and still higher was magnesium (650 °C).

* Hereinafter, the temperatures of crystallisation of pure elements will be placed in paretheses.

Judging by their crystallisation temperatures, such compounds as nitrides and sulphides should be arranged more or less uniformly in Earth's interior, playing the role of inclusions in the layers of basic elements [108].

Of course, we are very interested in the behaviour of free carbon in this situation. The point is that carbon, possessing a high crystallisation temperature (3,500 °C), should have been one of the first elements to appear in Earth's core. However, on the other hand, its low density (1.75 kg/dm^3) [111] inevitably would have caused its displacement by surrounding heavier elements to the surface layers. Since large deposits of pure "surfaced" carbon, except for minor diamond and graphite ones, are absent in the lithosphere, the rate of crystallising of components of Earth's layers can be assumed to have surpassed the rate of carbon decantation. In this case, carbon that was not included in the composition of carbides had to be "sealed up" in Earth's interior, and its content should have increased in moving to the centre. As the underground reactions proceeded, carbon was concentrated in limestone and dolomite deposits, and later, as life developed on Earth, it became concentrated in coal and oil fields.

Here we took note of crystallisation and stratification of only those elements whose content in Earth's rock exceeds 2–3 % [112]. A self-explanatory exclusion was made for carbon alone.

The arrangement of rare and dispersed elements in the layered structure has its own features. The point is that these elements, in dissolving in metals and metalloids, form rather stable chemical compounds [113 and 114]. The electromagnetic forces occurring at the atomic and molecular levels hindered decantation of these elements in Earth's centrifugal field. By virtue of the same reason, a part of iron occurred in the lithosphere.

The prevailing role in the current arrangement of compounds of rare and dispersed elements in Earth's crust belongs to volcanoes, glaciers, and water and airflows that circulated in the lithosphere during the later stages of the planet's development, as well as to animate nature.

However, there remains one extremely remarkable element, which is present in 95 % of compounds that are vital for humans. The element of concern is hydrogen.

There are sufficient grounds to assume that the lower layers of the asthenosphere are a boundary between oxygen and non-oxygen silicon compounds, to which FSA also belongs. It is in this thin layer that the key reaction of interaction of water with silicon alloys takes place. 1.4 to 1.6 m^3 of hydrogen are liberated per each kilogram of expended silicon. The bulk of hydrogen, in the pure state or in combination with carbon or sulphur, diffuses to Earth's surface [95 and 115]. A minor part, however, penetrates to Earth's centre. The

point is that protons are capable of being incorporated rather readily into the crystalline lattice of metals and metalloids to form therewith solid solutions or gaseous hydrides. As a rule, in dislocations, atomic hydrogen recombines to molecular hydrogen, which, in turn, also possesses a high penetrating capacity [116–121]. Accordingly, it can be assumed that hydrogen will be observed everywhere from the reaction zone to Earth's core, though its highest concentration should be in close proximity to the asthenosphere.

However, we cannot rule out the option that the liquid part of the core consists of hydrides formed with participation of relic hydrogen that travelled to Earth directly from the Protosun shell.

Evidently, our studies, based on purely thermodynamic premises, ultimately confirm the surprising insight of Vernadsky V.I. with regard to distribution of substances in Earth's interior.

Now we will highlight several fragments of atmosphere's history.

Formation of the ocean involved changes in the atmosphere's composition. Continuous rainfalls, accompanied with lightning discharges, started over the entire planet. Lightning caused electrolysis of water vapour. Water also decomposed into oxygen and hydrogen in the upper layers of the atmosphere under the influence of Sun's ultraviolet radiation. The hydrogen thus formed ascended, as a lighter gas, and then escaped into outer space. As a result, the air gradually accumulated oxygen. In this way, long before photosynthesis of plants started, the atmosphere accumulated about 25 % of the oxygen existing nowadays [122].

With the appearance of first organisms, animate nature became actively involved in controlling the content of oxygen and carbon dioxide in the planet's shell [123].

Thus, we have succeeded mainly in discovering the regularities of arrangement of elements in Earth's interior. The sequence of further events was determined by how rapidly the ocean water that downwelled due to natural circulation reached a certain layer of elements. Here one should note that, in oxidising, rock-forming alloys reacted with water rather than oxygen dissolved therein or the oxygen contained in air [122].

Formation of mineral deposits having a commercial value started with formation of deposits of magnesium, magnesite, and dolomite oxides, and other magnesium-based minerals. With further advancing of the reaction front to Earth's deep, deposits of bauxites, nephelines, clay and kaolin appeared. In the Cretaceous period, this was followed by emergence of deposits of limestone, marble, chalk, and gypsum. In evaluating ore formation, it is crucial to account for thermodynamic relations established for natural systems [124–127].

In this case, however, we are interested in the amount of heat liberated by underground reactions rather than in the distribution of minerals. Accordingly, further we will focus on the reactions of interaction of ferro-silica-aluminium with water. As mentioned earlier, the FSA alloy was the key rock forming material.

We will take the reaction of activated aluminium with water as a reference for comparison. Besides estimating the total amount of liberated heat, we have to find the rate of the above reaction. This will allow to estimate the periods and intensity of earthquakes, making it possible, in turn, to ensure safe operation of geothermal power plants.

Further, in considering chemical processes, we will follow the assumptions that have been defined clearly up to this point. Specifically, the total liberation or absorption of energy, for a particular chemical reaction, is affected more or less essentially by the transition of reacting substances from one aggregate state to another because all such transitions involve absorption or liberation of heat [128].

Analysis of volcanic gases shows that water vapour accounts for up to 80 % of their composition [82]. Hence, the bulk of heat of underground reactions is expended on evaporating water. The phase transition of one of the reacting components undoubtedly limits the growth of the system temperature, which, in turn, imposes a certain limit on reaction rate growth.

Obviously, in our further studies, we should proceed with investigating the evaporation process.

CONCLUSIONS

Let us summarise our studies in this section.

The mass of the iron core accounts for 30 % of Earth's mass, and only for 0.02 % of that of the World Ocean.

An estimate of the probability of iron reacting with water has shown that the core and ocean could have been formed concurrently only if water had condensed from a cloud of water vapour surrounding the molten planet. Hence, Earth's ocean was formed following the same principle as that related to oceans of liquid hydrogen on Jupiter and Saturn.

On molten Earth, similar to present-day conditions, flows circulated to transfer heat from the equatorial zones to the poles. These flows were a moving pulp mass consisting of alloys of metals and metalloids, with inclusions of their oxides. Continents, which appeared during the period of Earth's crystallising, bear an imprint of the solidified structure of ancient flows. The majority of continents have a wedge-shaped form extending along the meridians. The pointing of the wedge tips southward and their *S*-shaped form indicates that the flows acting within Earth's shell ensured energy discharge to outer space on the South Pole on a greater scale than on the North one. The meridional arrangement of continents has remained invariable during Earth's entire history.

Concurrently with shaping continents, the circulation of flows ensured fractionation of primary alloys, making the compounds of the lightest elements concentrate in the continents. Experimentally it has been established that segregation of the key rock-forming alloy of iron, aluminium, and silicon (ferro-silica-aluminium, or FSA) occurred by action of Earth's centrifugal field, involving crystallisation of its components.

Likewise, the entire cooling planet segregated at the temperatures of crystallisation of elements and their alloys. As a result, refractory metals and their alloys occupied the centre, and the fusible ones ascended and formed Earth's mantle.

The most likely process occurring in the planet's interior is the reaction of interaction of the FSA alloy with water. Analysis of volcanic gases has shown that the bulk of heated liberated by the reaction assumed is expended on steam generation.

CHAPTER 3

PHASE AND CHEMICAL TRANSFORMATIONS IN EARTH'S INTERIOR

Now we have come to face one of the key objectives of our investigation — estimate the capacity of underground heat sources and determine their rate of energy liberation.

However, before proceeding with these estimates, it is necessary to identify the defining methods and techniques available to thermodynamics, and demonstrate how these methods can be used to estimate the intensity of heat transfer during phase and chemical transformations.

As an example of phase transformations, we will take the process observed in evaporators with an ascending film.

3.1. HEAT TRANSFER IN AN EVAPORATOR WITH AN ASCENDING FILM

As a rule, the temperature difference is taken as an independent variable for describing heat transfer during boiling and condensation. In this connection, there is a distinct contradiction between the heat transfer intensity observed and the method of generalising experimental data.

Thus, it is known that the density of a heat flux, at any kinds of heat transfer, is proportional to the established difference of temperatures. During boiling and condensation, the temperature differences between the phases can be arbitrarily however small, but in the majority of cases the heat transfer intensity can exceed many-fold that observed in convective heat transfer.

One of the drawbacks of known methods of evaporator, condenser and steam generator design is introduction of unknown quantities such as temperature difference and specific heat load into the dependencies for heat transfer coefficients.

One can ascertain this when analysing, for example, the Nuselt equation for condensation of saturated vapour of any substance when the condensate film streams down the walls of vertical tubes [129 and 130]*

$$\alpha = 1.15\sqrt[4]{\frac{r \cdot \rho^2 \cdot \lambda^3 \cdot g}{\mu \cdot H \cdot \Delta t}} \ [\mathrm{W/(m^2 \cdot {}^\circ C)}], \qquad \text{(III.1)}$$

where α is mean calorific efficiency;

r is heat of condensation, J/kg;

ρ is condensate density, kg/m^3;

λ is condensate thermal conductivity, W/(m • °C);

μ is condensate dynamic viscosity, kg/(m • s);

H is vertical tube height, m;

Δt is temperature difference, °C; and

g is gravitational acceleration, m/s^2.

The prerequisites for deriving formula (III.1) are as follows: the flow of condensate film is laminar; the forces of inertia occurring in the film are negligible as compared to the forces of viscosity and weight; the force of gravity of a unit volume of condensate is balanced by the force of viscosity imparted by the adjacent films of fluid; convective heat transfer in the film as well as heat conductance along it are small as compared to heat conductance across the film; condensate-vapour friction is absent; the temperature of the external surface of the film is equal to the temperature of saturated vapour; and the density and condensate heat conductance, and viscosity coefficients are not temperature-dependent.

From equation (III.1) it follows that the mean calorific efficiency decreases with increase in height H of evaporator heat transfer tubes and the temperature difference. Accurate estimates account for the wavelike film flow regime and temperature-dependent changes in the physical properties of the condensate.

Accounting for the latter two corrections fails to eliminate the key drawback of the formula, namely, value Δt remains unknown. Besides, the relationship given above holds for stationary vapour, or low-velocity vapour flow. In the heating chambers of standard evaporators, the vapour flow velocity both in the longitudinal and the transverse directions through the tube bundle to the centre is rather high. In this case, the vapour flow has a dynamic impact on the condensate film.

* Should the reader be out of reach of Part I of this book, the author gives here the designations of the physical quantities.

In long-tube evaporators, the vapour temperature (in the saturated state) drops from the zone of vapour inflow in the upper part of apparatuses to the point of condensate discharge close to the bottom tube plate by about 2–3 °C. The tube bundle also has a certain temperature drop across the apparatus. Estimates have to account for this factor.

A similar situation of uncertainty existed when known formulas were used for estimating heat transfer during boiling. Since the volume of vapour generated during boiling is hundreds of times greater than that of vaporising liquid, intensive turbulisation in the wall boundary layer occurred during vapour extraction from the heat transfer surface. This is accounted for by introducing experimental values of specific heat load q to the estimation dependencies of calorific efficiency α. In particular, a widespread dependence has an exponential form [131]

$$\alpha = cq^{2/3}, \qquad \text{(III.2)}$$

where c is a proportionality coefficient whose value depends on the kind of fluid and pressure as well as on surface conditions to some extent.

The technique of estimating heat transfer described above is clearly contradictory because, if value q is known, then there is practically no need to calculate α to select the heat transfer surface.

These contradictions are eliminated when the processes of boiling and condensation are considered based on the laws of thermodynamics. For example, let us consider the sequence of design of evaporators with a rising (or ascending) film. The apparatus are designed so that the condensing flow moves downwards in the tube space, as this is the case for evaporators with a streaming down film, and the evaporating flow moves upwards in the tube space [132]. Here, the former space is part of the condensation circuit and the latter one is part of the evaporation circuit.

Both circuits are flow-through systems, wherein energy exchange between them in the form of heat involves redistribution of substance between the components of the circulating flows. The latter results in occurrence of deformation interaction between the phases of each system, making it possible to treat the circulation circuits as heat engines ensuring a certain velocity of flows along the apparatus heat transfer surface.

This fact has to be emphasised rather clearly to be adequate to help resolve the issue of the heat transfer rate during phase transformations. With this in view, it is necessary to analyse this challenging physical situation and to comprehend, under a certain viewpoint, a multitude of outwardly isolated experimental results.

The experimentally observed hydrodynamic situation in a separately taken heat transfer tube is shown in Fig. 23. The next diagram shows the flow and wall temperature variation profiles in a heated tube [133]. Evidently, prior to boiling, the primary flow temperature rises by several degrees. This effect can be explained by secondary vapour pressure build-up in the solution boiling zone, which is required for overcoming channel resistance to a two-phase flow.

As the boiling flow advances inside the channel, the emulsion flow regime is replaced with a plug one, and subsequently, with a core flow regime.

At the same time, secondary vapour, in lifting the fluid to a certain height, creates a reserve of gravitational field energy. After vapour has been discharged, the gravitational field uses this reserve to lower the fluid.

The following hydrodynamic situation occurs in the tube space. Here primary vapour condenses to form a condensate film on the external surface of evaporation tubes, this again allowing to create a reserve of gravitational field energy. Using this reserve, the gravitational field makes the condensate film flow downwards in the heating chamber. In so doing, the thickness of the streaming down film increases in the tube downward direction as subsequent portions of primary vapour condensate. Moving in the same direction, the primary vapour flow accelerates the flow of the condensate film.

According to Reynolds' analogy, in establishing a definite dependence between channels' resistance to flows and heat transfer intensity, one expects to

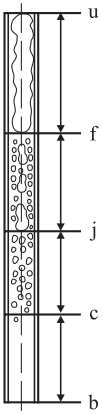

Flow sections:: bc — one-phase; cj — emulsion; jf — plug; fu — core.

Fig. 23. Flow structure during fluid boiling inside a vertical tube.

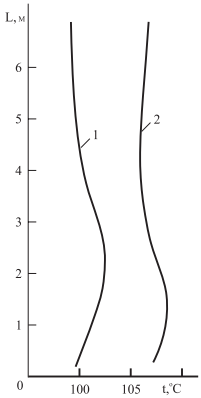

1 — flow; 2 — tube walls.

Fig. 24. Temperature vs. heat transfer tube height

find different values of heat transfer coefficients over the height of evaporation tubes.

To evaluate the local calorific efficiency values, we will represent the processes proceeding in the evaporator channels as a binary cycle in the *T-S* coordinate system (Fig. 25). In so doing, we will match the cycles so that the process of adiabatic expansion of primary vapour in the beginning of the tube space (line $m_e z_e$) would be above the point of termination of the process of adiabatic boiling of the solution in the exit zone of the heating tube (point z_i).

As a rule, the temperature of vapour arriving from the thermal plant exceeds that required for the evaporator. Due to this, primary vapour is moistened prior to being fed to the tube space. For this, a reduction-cooling installation (RCI) is mounted upstream the evaporator [134 and 135].

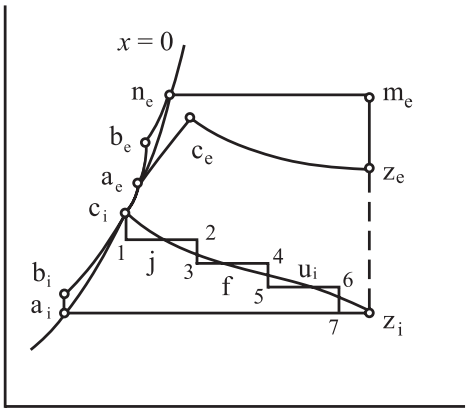

Fig. 25. Binary cycle of an evaporator installation in the T-S coordinate system

It follows that the previous condition, concerning arrangement of cycles, can be easily satisfied by selecting an adequate moisture content of primary vapour.

Nevertheless, the method of superimposing the evaporation and condensation cycles accepted here for visualisation purposes should obey the general principle — invariance of the values of the heat flux flowing through different media (see Eq. III.4).

Thus, the area of the upper stage of the binary cycle, limited by line $a_e b_e n_e m_e z_e c_e a_e$, corresponds to the amount of heat converted to work executed by primary vapour to accelerate the condensate film flow.

In turn, part of the heat energy, limited on the *T-S* diagram by the area of figure $a_i b_i c_i u_i z_i a_i$, is converted in the evaporator circuit to mechanical energy spent on circulating the boiling flow.

Comparing the forms of both figures, we note that the profile of line $b_i c_i u_i$, which reflects the boiling solution temperature profile over the height of the heating tube, approximately matches the profile of line $a_e c_e z_e$, which indicates the variation of the temperature of the condensate film streaming down outside the same tube.

The area within these lines is numerically equal to loss of system efficiency due to a temperature drop in the condensate film, tube wall and solution boundary layer.

The diagrams of the upper and lower stages designate work performed by elastic working media — primary and secondary water vapour when expanding in the longitudinal direction.

As regards the work of the gravitational field in the evaporator downtake channel and the tube space during downflow of the condensate film, fluid temperature variations in both cases will be negligible.

It is known that, if mass m decreases with distance L, at gravitational acceleration g, decrease in gravitational energy by mgL is equal to an increase in kinetic energy by $\frac{mV^2}{2}$, where V is velocity. If the height difference L is expressed in terms of meters (m), L will also be the available work, e.g. 1 kg of water in kgm. Suppose that, due to friction between flows and tubes of walls, the available work is converted completely to heat. Then, at $H = 10$ m, the temperature of 1 kg of water will increase by

$$\Delta t = \frac{10 \cdot 1}{427} = 0.0234 \ ^\circ\text{C}.$$

Let us split our further calculations into three consecutive stages. In the first stage, we will find the coefficients of heat transfer from stationary heating vapour to the solution; and in the second stage, we will account for condensate film acceleration by the vapour flow.

In the third, most involved stage, we will substantiate a new kind of analytic relationships.

First, we will use the technique of estimating the rate of natural circulation described in Part I of this book.

For this, we assume that the "operating" agent is but the temperature difference that acts in the longitudinal direction over the height of heat transfer tubes. In diagram T-S, the adiabatic process is shown by vertical line cd (Fig. 4 Part I). The flow velocity v found is in correspondence to a certain heat transfer intensity found from convective heat transfer relationships [131].

The flow velocity values found are used to determine the distribution of temperature differences between heating vapour and evaporating fluid.

The total temperature difference is

$$\Delta t = \Delta t_i + \Delta t_p + \Delta t_e. \qquad \text{(III.3)}$$

The values of partial temperature differences are found from the system of equations

$$q = \alpha_i \Delta t_i = q_e \frac{\Phi_e}{\Phi_i} = \alpha_e \Delta t_e \frac{\Phi_e}{\Phi_i} = \frac{1}{\varepsilon} \Delta t_p, \qquad \text{(III.4)}$$

where the thermal resistance is equal to:

$$\varepsilon = \varepsilon_i + \varepsilon_p + \varepsilon_e \frac{\Phi_i}{\Phi_e}; \qquad \text{(III.5)}$$

$$\varepsilon_p = 1.15 \frac{\Phi_i}{\lambda_p} \log \frac{\Phi_e}{\Phi_i}, \qquad \text{(III.6)}$$

whence

$$\Delta t_e = \frac{\alpha_i}{\alpha_e} \frac{\Phi_i}{\Phi_e} \Delta t_i; \qquad \text{(III.7)}$$

$$\Delta t_p = \alpha_i \varepsilon \Delta t_i. \qquad \text{(III.8)}$$

The heat transfer coefficients are found using the Nuselt formula (III.1):

$$\alpha_e = \frac{1.15 \left(\frac{r \rho^2 \lambda^3}{\mu L} \right)^{0.25}}{\Delta t_e^{0.25}}.$$

Here r are taken at t_e; ρ, μ and λ for a condensate film, and found for the condensation temperature t_{con}, which is specified initially by relationship $t_{con} = 0.15 t_i + 0.85 t_e$. The expression in the numerator is denoted as β. Substituting the value of α_e into formula (III.7), we obtain

$$\Delta t_e = \left(\frac{\alpha_i}{\beta} \frac{\Phi_i}{\Phi_e} \Delta t_i \right)^{4/3}. \qquad \text{(III.9)}$$

After substituting the values of partial temperature differences (III.8) and (III.9) into formula (III.3), we obtain

$$\Delta t - \left(1 + \alpha_i \varepsilon\right) \Delta t_i = \left(\frac{\alpha_i}{\beta} \frac{\Phi_i}{\Phi_e} \Delta t_i \right)^{4/3}. \qquad \text{(III.10)}$$

The values of α_i for the convective heat transfer zone are found from relationships

$$\mathrm{Nu} = 0.021 \mathrm{Re}^{0.8} \mathrm{Pr}^{0.43}, \qquad \text{(III.11)}$$

where, to calculate criterion Re, we used the values of circulation rates found from thermodynamics analysis. After substituting α_i into equation (III.10), we find value Δt_i, and then use relationships (III.8) and (III.9) in turn to determine the values Δt_p and Δt_e. Having found the value Δt_e, we can first calculate α_e, and then the heat transfer coefficient.

The second stage of analysis, consisting in finding the heat transfer coefficients during boiling, is implemented after the hydrodynamic situation arising in the boundary layer at an established Δt_i has been analysed.

In essence, circulation of boiling fluid in the boundary layer resembles natural flow circulation in the apparatus. Due to this, boiling calculations are also performed by using the diagrams given in Fig. 4, Part I. The fluid separating from the wall (see Fig. 4 Part I) starts boiling during process *cd* (*cn* is the actual process of flow expansion). After vapour has been separated in the centre of the tube (process *da*), the fluid affected by the gravitational field again drops to the wall (process *ab*), where it is heated to increase its temperature by Δt_i (process *bc*).

In stationary conditions, the pressure of the medium adjacent to the vertical heat transfer wall remains invariable. However, if the vapour that was formed during boiling separates from the heat transfer surface with a definite velocity, then, according to the momentum conservation law, the pressure at the surface has to increase. At the same time, the bubble reacts to the mass of overlying fluid layers, making it move along a path at an angle to the tube axis. Bubbling is a periodic process. At the instance the bubbles start rising, the pressure near the wall drops, making it possible for the fluid flow, which also has a velocity head, to advance from the tube central zone to its surface. For a longitudinal flow, delivery of vapour therein from the transverse flow is practically an isothermal process. This is shown in the *T*-*S* diagram by horizontal lines.

Having divided the heat transfer tube over the height into separate sections, as shown in Fig. 25, we will find the actual flow velocity by using in turn the longitudinal and transverse temperature differences. This velocity is used to refine the hydrodynamic flow regime and the value of α_i. Then, having calculated the steady-state temperature differences, we will find the final value of α_e. The calculation is finalised by estimating the heat transfer coefficient [50].

It has been found that, at drop condensation, α_e increases dramatically [136].

In this case, at rather low vapour velocities (v_v = 4.5–13.3 m/s), heat transfer coefficient α_e increases by 1.5–3.5 times as compared to its value for

stationary vapour. With increase in vapour flow velocity to $v_v = 19.5-67.2$ m/s, the heat transfer coefficient increases by 1.9 to 7.4 times.

In so doing, the heat transfer coefficient, at drop condensation and increasing vapour velocity, increases more significantly than it does at film condensation. Thus, at laminar film flow, an increase in vapour flow velocity from 19.4 to 44.7 m/s makes α_e increase only by 3.5 times as compared to stationary vapour. The *T-S* diagram (Fig. 25) is used to estimate the vapour velocity, and investigate the adiabatic expansion process.

For the conditions listed above, respective criteria relationships have been established for their implementation in practical calculations [137]. Before evaluating the heat transfer surface in the third approximation, it is necessary to discuss the physico-chemical basics of the boiling and condensation processes.

3.2. PHYSICO-CHEMICAL BASICS OF THE PROCESSES OF BOILING AND CONDENSATION

So far, we considered interaction of vapour and fluid as mutual influence of energy origin, and as a means for energy exchange in the pure form. Redistribution of substance between the components of both subsystems — the condensation and evaporation ones — was of concern only to the extent of deformation interaction occurring between them during transformations.

However, the share of mechanical energy is negligible in the total amount of energy contained in vapour. As known, heat of vaporisation is a sum of two quantities — the inner potential energy of the body (designated as ζ) and the external work of expansion (Ψ):

$$r = \zeta + \Psi. \qquad \text{(III.12)}$$

The external work and internal energy variation is found from formulas

$$\Psi = Ap(V'' - V') \qquad \text{(III.13)}$$

and

$$\zeta = r - \Psi = r - Ap(V'' - V'), \qquad \text{(III.14)}$$

where A is thermal equivalent of unit work;

p is vapour pressure;

V' is fluid volume; and

V'' is vapour volume.

Quantities Ψ and ζ are also known as external and internal vaporisation heat [138]. At all pressures, internal vaporisation heat ζ is significantly greater than external vaporisation heat Ψ. Thus, for example, at different pressure of water vapour (p, MPa), the values of ζ and Ψ (kJ/kg) are as follows:

$p = 0.01;$ $\zeta = 2247.1;$ $\Psi = 147.9;$
$p = 10;$ $\zeta = 1160.63;$ $\Psi = 169.7;$
$p = 20;$ $\zeta = 553.1;$ $\Psi = 75.84.$

In the previous section, we adequately addressed the problem of dependence of the heat transfer rate on external vaporisation heat Ψ. Now we have to clarify just as adequately the impact of quantity ζ on the process. This problem merits special attention, therefore we will address it in greater detail.

We know that ideas on such a physical quantity as energy are linked to the momentum of matter. In particular, heat is nothing else than the momentum of microworld particles (electrons, atoms, and molecules). Hence, heat transfer involves exchange of momentums between components involved in the process. A distinctive feature of this form of energy transfer is growth of entropy, which is assumed to indicate an increase in system disorder.

The evaporator uptake channel demonstrates a clear growth of entropy. To explain this, we will again use the notions of configuration and heat entropies that were suggested in Section I of our study. The point that puzzled us then in the analytical statement appeared self-evident in the geometrical interpretation.

In this case, we will assume that the variety of structures of the two-phase flow, which increases over the channel height, reflects the growth of configuration entropy, whereas increase in secondary vapour entropy with respect to the boiling fluid entropy reflects growth of heat entropy. Conventionally, external vaporisation heat can be assumed responsible for the growth of configuration entropy, and the internal one assumed responsible for the heat entropy.

The dynamics of total entropy change is one of the major coordinates of the system state. Temperature is the interaction potential linked to entropy [139].

Recall that entropy is the ratio of the heat increment obtained in the cycle and the absolute temperature. As we have just ascertained, the authors of formula (III.2) simply present the heat transfer coefficient during boiling as a function of the time-dependent heat increment. In so doing, they indirectly introduce into consideration the behaviour of entropy in time.

However, to take the value of entropy as a quantitative characteristic of the heat transfer rate, one should be positive that the temperature difference in-

deed defines the process dynamics. The situation in the evaporator uptake channel appears to confirm the firmness of our notions on temperature whose drop involves growth of entropy.

The situation in the condensation circuit, however, is different. Here, in spite of the temperature difference that acts in the direction from vapour to the wall, the system entropy during the process drops rather than grows because the molecules are arranged more orderly in the condensate film than in vapour.

Experiments have also shown that, at equal temperature differences, the intensity of heat transfer, for instance, in evaporators heated with vapours of high-temperature organic heat carriers (a diphenyl compound) is five to six times less than when heating with water vapour. This specifically involves the necessity to introduce strictly individual criteria relationships into design standards for evaporators with a streaming down film for each specific case of heat transfer [50, 140, and 141].

From the above it follows that, for open systems, the temperature cannot serve as a potential of interaction of components. Hence, entropy is not a quantitative characteristic of transient processes. Increase or decrease in disorder, reflected by entropy, results from development of dynamic processes in the system, but the effect cannot be the cause, and furthermore, quantitatively define the heat transfer rate. A chain of logical inferences makes us believe that thermodynamics should have a quantity that characterises the intensity of heat transfer in open systems more completely than temperature does.

Indeed, for systems wherein energy and substance interchange occurs, such a quantity is the chemical potential [142]. A change in the state of an open system caused by this kind of interaction is manifested as redistribution of its mass between separate phases. Obviously, it is the mass (designated by letter m), which is the physical quantity that represents the quantitative measure of change occurring in the system.

Thus, we arrive at the simple functional relationship

$$dGi = \mu dm. \qquad \text{(III.15)}$$

In our case, the chemical energy of the process dGi completely transforms to heat energy, therefore the mass change in time practically reflects the heat transfer rate.

It remains to specify the procedure of determining the value of μ.

Here we are considering the phase transitions of one substance — H_2O, therefore the values of the chemical potential per unit mass practically coincide with the values of free energy ΔGi.

In turn, the values of ΔGi^0_{vap} can be calculated by treating vaporisation as a chemical reaction [41]

$$\Delta Gi^0_{исп} = \Delta H^0_{исп} - T\Delta S^0_{исп}. \quad \text{(III.16)}$$

In contrast to ΔH^0_{vap} and ΔS^0_{vap}, which depend little on temperature, ΔGi^0_{vap} has a very strong dependence on temperature T, which appears explicitly in relationship (III.16). If, for the sake of simplicity, we assume that enthalpy and entropy changes are steady, then the dependence of ΔGi on ΔH and ΔS can be graphically presented as shown in Fig. 26 for H_2O. At high temperatures $T\Delta S^0$ is greater than ΔH^0; the free evaporation energy is negative, and water should evaporate spontaneously at the partial pressure of water vapour equal to 1 atm. At low temperatures, ΔH^0 is greater than $T\Delta S^0$, so ΔGi^0 is positive, and water vapours condensate spontaneously. In the boiling point at 373 K, ΔGi^0 is equal to zero, and the liquid and vaporous water are in equilibrium.

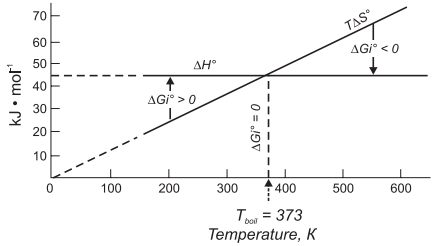

Fig. 26. Contributions of enthalpy and entropy to changes in the free energy of evaporation of liquid water

The molar evaporation heat can be found as the difference of the standard heat of formation of liquid and gaseous H_2O:

$$\Delta H^0_{vap} = \Delta H^0_{gas} - \Delta H^0_{liq}. \quad \text{(III.17)}$$

These formulas show that the values of ΔGi^0_{vap} differ significantly from ΔH^0_{vap}. Therefore, quantity ΔH^0_{vap} should not appear in the heat transfer equation as the motive force. However, looking at the boiling and condensation formulas being analysed, the case is exactly the opposite one.

Let us explain this statement. Thus, if we recalculate the values of the heat of vaporisation from kJ/mol units adopted in chemistry to kJ/kg units adopted in heat engineering, we will obtain the already known quantity r_{vap}, i.e. we have

$$\Delta H^0_{vap} \rightarrow r^0_{vap}. \quad \text{(III.18)}$$

After this, we find that the heat emission formula for film condensation (III.1) takes the following form:

$$\alpha_c = f(r^{0.25}), \quad \text{(III.19)}$$

for drop condensation:

$$\alpha_c = f(r^{0.7}), \qquad \text{(III.20)}$$

and, finally, for condensation of diphenyl compound vapours:

$$\alpha_c = f(r). \qquad \text{(III.21)}$$

Thus, it is clear that the authors of the formulas made an indirect attempt to apply thermodynamic formalism when describing the heat transfer process. But even in this variant, imperfect from the thermodynamics viewpoint, the formulas presented allow establishing a certain dependence of heat transfer intensity on the hydrodynamic situation on the surfaces of the tubes.

Therefore, besides substituting r for μ, in the following calculation stages it is necessary to introduce two more quantities, viz. surface tension s and the geometric parameters of a solid surface. Further, having calculated the values of Gibbs' surface energy ΔGi_σ, one can find the conditions of destruction of the condensate film.

The case is no better when calculating heat transfer during boiling. In the pseudo thermodynamic variant, formula (III.2) takes the form

$$\alpha_v = f(r^{0.7}). \qquad \text{(III.22)}$$

The exponent of r corresponds approximately to the value that can be obtained at the second stage of evaporator design by presenting a in explicit form as a function of r.

The dynamics of change of the exponent of r in the transient process can be tracked by using Yerofeev's formula. Recall that such an operation had been performed when the process of water evaporation in a mountain lake was investigated.

Thus, with increase in Δt, the number of vapour formation centres (and consequently, the exponent of r) increases to reach a maximum in the point of inflection of the S-shaped curve. This corresponds to the above relationship. Then, as secondary vapour forces the fluid away from the wall, the number of vapour formation centres decreases. Hence, variation of the exponent of r reflects the variations in the size of the phase's surface of contact in immediate proximity to the solid wall.

As a rule, when estimating the process rates, one attempts to introduce measurable quantities into the calculations, such as temperature, pressure, and concentration. For instance, Lewis and Randall suggested replacing the chemical potential with thermodynamic activity, which can be considered as a rectified concentration [143]. This method is quite acceptable for homogeneous systems. However, during phase transitions, as we have just ascer-

tained, there appears a variable such as the surface of contact of phases, which is difficult to calculate.

Moreover, in chemical reactions, which we shall start investigating now, the gas being produced is continuously withdrawn from the interaction zone. This fact prevents achieving equilibrium conditions, therefore, the gas pressure (or its concentration) cannot be calculated using Gibbs' energy. All this makes it impossible to use the recommendations given by Lewis and Randall.

Let us summarise this section of studies. Based on analysing the evaporation process, one can make several recommendations concerning the sequence of generalising experimental data, and analysing the reactions of interaction of alloys with water.

At low pressures, the rate of heat transfer between alloy samples and water can be estimated by evaluating the stepwise process of adiabatic boiling of water. Using the heat removal rate found, one can then simply determine the reaction rate. If the reaction surface value is unknown, experimental data should be generalised using Yerofeev's equation. Having found the optimal conditions that correspond to the points of inflection of *S*-shaped curves, where the reaction surface is approximately equal to the initial surface of the solid phase, it is necessary to present experimental data via their chemical potentials. Note that this stage of generalisation is especially necessary at high pressures when water cannot boil, and gas (hydrogen) liberated during the reaction creates the hydrodynamical situation in the system.

During the process, the values of Gibbs' energy change accordingly. Therefore, having taken the equilibrium values of Gibbs' energy to estimate the values of μ, we thereby turn the estimate performed into an approximate one. More accurate data can be obtained by performing several subsequent iterations.

3.3. REGULARITIES OF HETEROGENEOUS REACTIONS

In this section we will consider a fairly involved problem — estimate the rate of topochemical reactions. Several investigators assume that the role of concentration in these systems is performed by the reaction surface value. Hence, in their opinion, the reaction rate depends on how developed the reaction surface is. However, this is but one of the factors that affect the process.

The reaction rate is a result of the following factors: the available energy potential; the properties of alloys and water; the contact surface of phases and the gas-dynamic situation within the apparatus.

We will attempt to put in order our notions on the process by considering reactions of interaction of aluminium and silicon alloys with water.

3.3.1. Interaction of activated aluminium with water

Production of hydrogen in field conditions is most widespread in the hydro meteorological service.

According to data of the World Meteorological Organisation (WMO), in the majority of countries hydrogen is generated in situ at meteorological stations. The basic method of producing hydrogen is the reaction of interaction of alloys with an aqueous solution of caustic soda [144].

In the future, due to progressively increasing costs of hydrocarbon source materials, water will remain the key source of producing hydrogen. The high calorific value and absence of hazardous substances in the combustion products have defined the key advantages of hydrogen over other kinds of fuel. It is quite possible that the technology used currently at meteorological stations is a prototype of those large-scale hydrogen production facilities, which in the near future will occupy a fitting place in the economy of highly developed countries. Due to this, there is an unwavering interest in investigating the regularities of interaction of alloys with water. To describe this phenomenon in its entirety, it is necessary to resort to both thermodynamics methods and interdisciplinary sciences that treat the process from the kinetics angle. In this study, we will focus on identifying the role of heat-and-mass transfer during chemical and physical transformation of alloys to oxides.

As a subject for studies, we have selected the reaction of interaction of aluminium with water

$$2Al + 6H_2O \leftrightarrow 2Al(OH)_3 + 3H_2\uparrow. \qquad \text{(III.23)}$$

It is necessary to find the rate and completeness of this reaction.

The equilibrium characteristics of the process have been investigated in detail. It is known that, at the temperature of 363 K, Gibbs' energy is equal to $\Delta Gi = -927.2$ kJ, and the equilibrium constant takes the value $K = 2.66 \cdot 10^{133}$. Large negative values of ΔGi point to high probability of the reaction. The reaction completeness estimated by the equilibrium constant is practically close to unity. During an adiabatic course of the process, a temperature of 2,880 K develops in the reaction zone, whereas a 5-fold excess of water relative to the stoichiometric volume reduces the temperature to 760 K [145]. At present, ideas on the reaction rate are vague. At moderate temperatures, pure aluminium is covered with a dense oxide film, and practically fails to react with water [146]. At the same time, under the same conditions, several aluminium alloys demonstrate an exceptionally high activity. For instance, the rate of hydrogen displacement from water with alloy AG505I5 (mass %: Al —

85, Ga — 5, Sn — 5, and In — 5) exceeds the rate of displacement of hydrogen with alumina-silica alloys by more than two orders [147 and 148].

In the general case, the reaction rate is a function of the structure and composition of an alloy; the water properties and the oxide layer formed; temperature; pressure; form and dimensions of the reacting system, as well as the properties of the medium contacting therewith. Nevertheless, there are certain key factors that allow considering the possibility of estimating the process limit rate that can be achieved under other favourable conditions.

In particular, these factors include the local air speed that constrains the velocity of hydrogen outflow from the zone of formation of oxide nuclei. However, to evaluate the reactor capacity, the number of gas liberation zones and their cross-section areas per unit area of alloy surface should also be known. Determining the reaction surface area, which changes during the process, is a challenging problem, therefore it would be more practical to focus our attention on heat transfer.

Heat is capable of "spreading" in a solid. As a first approximation, this allows taking the area of the heat exchange surface to be equal to that of the alloy specimen surface.

Due to gas liberation, the volume of the reacting system increases by hundreds of times, involving the occurrence of natural circulation of water close to the reacting surface. The velocity of the uptake flow is also constrained by the local sound velocity.

Determining the values of the temperature difference and the velocity of the fluid that flows around the sample allows calculating heat transfer intensity using adopted criteria relationships. Having data on the specific heat flux, one can easily calculate its equivalent hydrogen mass flow. Thus, it is possible to perform a tentative estimate of the maximum achievable gas liberation rate. Such an approach is valid if one assumes that the chemical phase of the process offers minimal resistance. Hence, the resistance of the physical phase, resulting from feeding water and discharging reaction products and heat, defines the reaction rate.

Experiments in investigating heat-and-mass transfer were conducted in a glass Kipp generator and a metal reactor [50]. The intensity of heat transfer from cubes made of alloys AG505I5 and FSA to the circulating flow has been investigated.

A thermocouple is fitted in the centre of a cube with the side of (10 to 25) $\cdot 10^{-3}$ m. The hole for the thermocouple ($d_h = 3 \cdot 10^{-3}$ m) is filled with epoxy resin, having preliminarily isolated the thermocouple junction from the epoxy resin with a layer of cotton. Contact between the thermocouple and the cube

body is monitored with a multimetre. The secondary instruments used are potentiometer type KSP-4 and mirror potentiometer KP-59.

The temperature in the sample centre is registered simultaneously with recording the medium temperature. The temperature of the sample surface is measured with a thermocouple and probe when conducting the reaction in an open vessel.

The system response time is checked using a method accepted earlier [149].

The samples had the initial surface area of $(1.4 \text{ to } 1.8) \cdot 10^{-3}$ m^2. The pressure in the reactor was within 0.94 MPa. At this, the maximum hydrogen liberation rate was $W_{max} = 1.05 \cdot 10^{-3}$ m^3/(kg • s) or $W_{max} = 7.14 \cdot 10^{-3}$ m^3/(m^2 • s).

When investigating the reaction in an open vessel, it was found that the temperature of the outer surface of the hydroxide layer in gas liberation sites (t_m) was higher than that of the medium (t_d) by 1.6 to 2.4 °C. The temperature in the sample centre (t_c) exceeds that of the medium by 2.4 to 6.2 °C (Fig. 27).

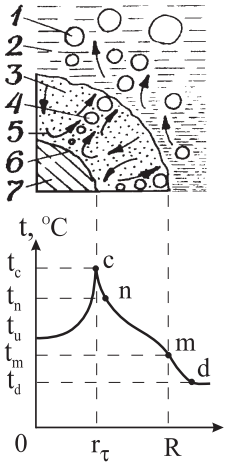

1 – gas bubbles in a fluid, 2 – fluid, 3 – layer of generated hydroxide, 4 – gas bubbles in hydroxide layers, 5 – direction of fluid circulation flows in hydroxide layer, 6 – particle reaction surface, 7 – non-reacted particle core.

Fig. 27. Diagram of alloy particle and its temperature change during interaction with water

The approach of the reaction front to the thermocouple junction in the centre of the sample makes the temperature jump by 5 to 9 °C during boiling and gas liberation (Kipp generator), and by 37 to 53 °C during gas liberation alone (closed reactor). A larger jump is observed at a higher temperature. The temperature surge time is 10 to 15 s. When the sample is extracted, the temperature of the outer surface (t_m) increases rapidly, and then drops. The reason of this is that the reaction continues for some time due to water remaining on the surface.

After the surge decays, the instrument indicates the medium temperature (measured additionally with a mercury thermometer). This suggests reaction termination due to complete destruction of the sample. The dynamics of temperature growth in the sample centre, when the cube falls into water in a kinetic reactor is shown in Fig. 28. At the initial phase, the temperature grows abruptly, then the rate of increase drops due to the influence of the oxide layer being formed. Destruction and disintegration of the sample during the reaction increases the temperature on the reactor bottom.

The temperature at the aluminium-glowing aluminium oxide interface indicates that water boils on the interfacing surface.

The experimental values of the temperature on the reaction surface (t_n), with account of the system response time accepted, were equal to the temperature of boiling liquid at a critical pressure of gas outflow. Thus, at the final reaction phase, the temperature increased from 102 °C to 114 °C in 15 s (Fig. 28).

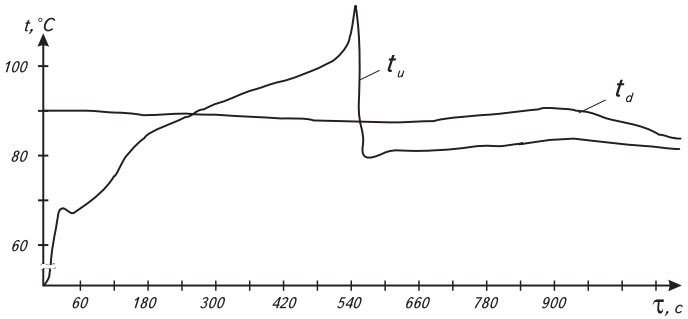

t_u is sample centre; t_d is reactor bottom; $m = 11.8 \cdot 10^{-3}$ kg.

Fig. 28. Temperature vs. time during reaction of alloy AG505I5 with water (kinematic stand), $t_н = 90$ °C

Due to short-time existence of the thin reacting layer and a significant time response of the measurement system, the actual temperature was 194°C. The actual jump was 92 °C. In terms of the reaction half-time ($\tau_{0,5} = 330$ s), the temperature grows from 90 °C to 173 °C, i.e. the jump equals 83 °C. The value 173 °C is the temperature of saturation at critical pressure of outflow registered at the point of time corresponding to $\tau_{0,5}$.

The temperatures of the reaction surface of alloy AG505I5 that have been found allow calculating the mean logarithmic temperature difference that ensures heat transfer. At this, $\Delta t_{max} = t_n - t_d$, and $\Delta t_{min} = 2$ to 3 °C (Fig. 28).

Natural circulation ensures layerwise interaction of particles with the surrounding fluid. The particle surrounding flow velocity is equal to the reduced fluid velocity in the uptake channel $v_{пр}$. To find $v_{пр}$, it is necessary to assess the hydrodynamics of the circulating flow. At low pressure, the flow in the uptake channel is determined by vapour, and when the pressure increases, hydrogen is responsible for this. At the initial point of time, the flow velocity is found by the change in enthalpy of the boiling fluid [50]. In the latter case, formulas are used to estimate the local sound velocity in a two-phase flow [150]. In so doing, account is taken of not only the stoichiometric amount of reaction products, but of the volume of water that has evaporated on the reaction surface and condensed in the uptake flow as well. The average flow velocity is 2/3 of the outflow one. The average velocity value found allows refining the amount of rising fluid by using gas lift relationships [151 and 152].

$$(1-\varphi)=\frac{0.01\mu_{f}^{0.3}+0.14}{d_{u.c.}^{0.34}\quad v_{g.r.}^{0.48}}, \qquad \text{(III.24)}$$

where φ is gas content; μ_f is fluid viscosity, mP•s; $d_{u.c.}$ is uptake channel diameter, m; and $v_{g.r}$ is reduced gas flow velocity, m/s.

Using the data in [151] made it possible to recognise that the r.h. part of the equation has to be multiplied by coefficient k_E that changes within 0.292 to 0.753. A drop in k_E was observed when the uptake flow diameter decreased, which is taken to be equal to the sum of the diameters of the particle and two bubbles [153]. For the conditions examined here, $k_E = 0.333$.

The value of the reduced fluid velocity found using the technique developed is within 1.81 to 2.1 m/s. The Reynolds numbers vary within 45,626 to 110,891. Since the drag factor k_d in this interval increases [154], one should expect an increase in the dimensionless heat transfer coefficient with increase in Reynolds number.

Experimental data were treated using known relationships. Calculations were performed at the point of time $t_{0.5}$. It turned out that Kuney's formula yields the least deviations, and the Katsnelson-Timofeeva formula yields the biggest ones [155]. In the works mentioned, the degree of influence of *Re* numbers is within 0.5 to 0.58. Flow around a reacting particle demonstrates a more significant influence of Reynolds criterion

$$Nu = 1.85 \cdot 10^{-6} Re^{1.6} Pr^{0.33}. \qquad \text{(III.25)}$$

The deviation of estimated values of the Nu criterion from experimental ones is within 13.5 %.

With increase in surrounding flow velocity, vaporising and gassing increases, resulting in turbulisation of the boundary layer. Close conditions of heat-and-mass transfer are observed when water evaporates to its own superheated vapours [157].

From the above it follows that, in heterogeneous system conditions, the maximum limit value of a chemical reaction rate is defined by the intensity of heat transfer during natural circulation [158]. The results obtained allow identifying two key factors that define the reaction rate.

First, when interfacing the basic exothermal reaction (hydrogen generation) with a concurrent endothermic one (water boiling), the process runs at small temperature differences, i.e. in conditions close to equilibrium of the second reaction.

Secondly, in a heterogeneous system, the interacting components react layerwise [159].

Both above factors ensure relatively low velocities of a 3-phase flow, i.e. resistance loss is negligible. The efficiency of a boiling system is known to be within 0.25 %, i.e. only a quarter of a per cent of the heat transferred through the system is converted to mechanical energy [50]. With increasing pressure, a hundredth part of a per cent of the chemical reaction converts to kinetic energy of a circulating flow (dissipative structure) [36]. This corresponds to minimal production of entropy due to friction [160].

Let us proceed with investigating the process of interaction of an aluminium alloy with water.

As an object of investigation, we will now take the reaction of interaction of a multitude of particles of activated aluminium (powder) with water. During this process, the temperature and hydrodynamic conditions occurring on the surface of a separate particle have a dramatic effect on the reaction of water with adjacent particles.

Here we again encounter collective phenomena considered briefly in Section 1. As we already know, the most convenient form of generalising experimental data in this case is Yerofeev's equation.

Let us review some works of authors that arrived at such a conclusion. First, we will mention some investigations that made a significant contribution to development of the theory of heterogeneous reactions.

Models of topochemical reactions were developed with account of geometric and energy characteristics of the system.

The key factors that define the sites of nucleation on surfaces of particles are the probability of capture and liberation of gaseous products. The expression for the fraction of the reacted substance accounts for both these factors, and it can be solved only approximately. However, for a random distribution,

Avrami [161] solved the equation using the concept of an extended volume of reacted substance. The assumption made was valid only for moderate transformations. Mampel [162] considered the process of formation of nuclei and their growth in systems consisting of spherical microcrystals. The model suggested had a minor affect on development of the theory of the process because of difficulties encountered when preparing a sample for validating the model. Prout and Tompkins [163] took account of the possibility of nuclei formation in the chain process, and suggested their own generalising equation. Boldyrev [164] explained the affect of impurities on the kinetics of the nucleation process, firstly, by the deformation action of the impurity lattice on the boundary layer of the primary substance, and secondly, by changes in the character of electron and ion processes occurring in the impurity-primary substance interface. Young [165] classified decomposition reactions into two subclasses. In one subclass, the branching-chain reaction occurs only on the surface of the crystal. In so doing, compact spatial nuclei are formed in the branching points. The second subclass is characterised by decrepitation caused by reaction penetration into the primary substance volume. Delmon [166] developed the approach suggested by Mampel, and considered the kinetic characteristics of interaction of a gas with a solid, including subsequent diffusion. Delmon suggested numerical solutions and gave tabular data for many important kinetic problems. Barret [167] offered a review of works in kinetics of heterogeneous reactions, paying special attention to the physical meaning of constants appearing in mathematical relationships. Rozovsky [168] built several theoretical models, and suggested numerical solutions applicable to specific reactions. Brown et al [169] recommended intervals of applicability and correctness for known kinetic equations of interaction and thermal decomposition reactions. The majority of relationships were found to give an unsatisfactory description of the final phase of the process. This is linked to the simultaneous influence of such factors as the sizes of particles, fragmentation of crystallites, chemical sorption of gaseous products on the solid residue, poisoning, etc.

Analysing the probability of interaction of molecules of the given system, Yerofeev [42] derived equation (I.1), which was considered earlier.

In works [159, 165, 169, and 170], an opinion is expressed that equation (I.1) reflects the formal kinetics of the process to the utmost.

Therefore, we will not be in big error if we generalise experimental data using Yerofeev's equation.

In $\alpha-\tau$ coordinates, the kinetics is described by typical sigmoids, which practically represent the variation of the reaction surface area in time (Fig. 7). Experimental data are presented in logarithmic coordinates in Fig. 29; and the estimated values of n and k are summarised in Table 1. With increase in tem-

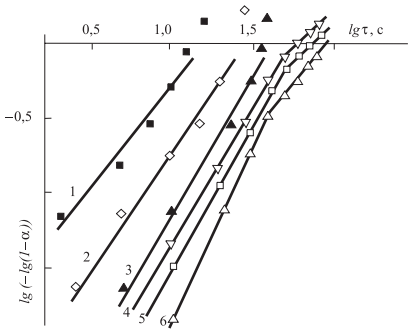

Fig. 29. Value lg [-lg(1-α)] vs. logarithm of time lgτ at different temperatures and dispersive compositions (size fractions) of the alloy Al — 85 %, Ga — 5 %, In — 5 %, and Sn — 5 %:

1 — 90°C, fr. (0.1÷0.16)•10⁻³ m;
2 — 75°C, fr. (0.2÷0.4)•10⁻³ m;
3 — 65°C, fr. (0.4÷0.63)•10⁻³ m;
4 — 50°C, fr. (0.01÷0.2)•10⁻³m;
5 — 40°C, fr. (0.63÷1.0)•10⁻³ m;
6 — 35°C, fr. (1.0÷1.6)•10⁻³ m.

Table 1

Degree of conversion (α_τ, %) and hydrogen liberation rate vs. temperature and size fractions of activated aluminium (5 % Ga, 5 % In, 5 % Sn)

Temperature, °C	Size fractions, mm	Specific surface, m^2/kg	Degree of conversion α_τ, %	Hydrogen liberation rate $W_1 \cdot 10^3$, $m^3/(kg \cdot s)$	Hydrogen liberation rate $W_2 \cdot 10^3$, $m^3/(m^2 \cdot s)$	$k \cdot 10^3$	n
35	1.0–1.6	50.7	64.71	1.51	29.78	0.0631 (5.01)	2.3 (1.42)
40	0.63–1.0	62.1	72.64	1.75	28.18	0.3548 (22.39)	1.94 (1.0)
50	0.01–0.2	184	83.96	2.0	10.87	0.7583 (37.15)	1.82 (0.93)
65	0.4–0.63	82.7	92.45	2.27	27.45	1.096	1.81
75	0.2–0.4	96.3	98.11	3.44	35.76	5.012	1.57
90	0.1–0.16	152	98.0	6.06	39.87	45.7	1.32

perature, the values of *k* grow, and those of *n* decrease. At high temperatures, scattering of experimental points increases, hence, Yerofeev's equation describes the process only approximately. At the end of the reaction, the rate constant increases by 49.2–79.5 times, and index *n* decreases by 1.6–2.0 times. This is caused by diffusive retarding of the process due to accumulation of solid reaction products on the alloy surface. Comparison with Lepin's data [43] shows that the character of the reaction of the alloy investigated with water over time (index *n*) retains the same features as those for pure aluminium. However, in the case of activated aluminium, the rate constant *k* is four times greater at the temperature of 40 °C, and greater by an order of two at 70 °C than

that for pure aluminium. This points to a different nature of substances considered. In particular, the fact is confirmed that development of the reaction surface in an activated aluminium sample with a fine-grain structure occurs due to its decrepitation.

Based on the investigations conducted, a more effective alloy was developed [171].

The kinetics of interaction of this alloy with water is presented in work [172].

3.3.2. Thermodynamics of hydrogen generation in reactions of aluminium, silicon and iron with water

In the following, tabular values of quantities [87] are used to calculate changes in Gibbs' energy of reactions of interaction of aluminium, silicon and iron with water and water vapour. The thermodynamics of the following reactions was investigated earlier [50, 145, and 173]

$$2Al + 3H_2O \leftrightarrow Al_2O_3 + 3H_2\uparrow,$$
$$2Al + 6H_2O \leftrightarrow 2Al(OH)_3 + 3H_2\uparrow,$$
$$Si + 2H_2O \leftrightarrow SiO_2 + 2H_2\uparrow,$$
$$3Fe + 4H_2O \leftrightarrow Fe_3O_4 + 4H_2\uparrow.$$

Rendering tribute to tradition, the authors of the above literature use the relationship

$$\Delta H^0(T_2) = \Delta H^0(T_1) + \int_{T_1}^{T_2} \Delta C_P^0(T)dT,$$

where C_P is heat capacity at P — const.

The presence of tabulated values of $H^0(T)-H^0(0)$ or $H^0(T)-H^0(298)$ in modern literature allows simplifying the calculation of reaction enthalpy variation.

The types of possible reactions, including those given above, are shown in Fig. 30. The calculated values of Gibbs' energy are given there. The averaged values of this energy were given in Fig. 19. The stoichiometric ratios of substances were found after the composition of reaction products had been assessed.

Interaction of aluminium or its oxide with a moist atmosphere yields several products: hydrargillite γ-$Al(OH)_3$, bayerite α-$Al(OH)_3$, boehmite γ-AlO(OH), and diaspore α-AlO(OH), γ- and α-Al_2O_3 [119, 124, and 175–177].

With rising temperature, the products undergo several changes. Thus, hydrargillite, when heated to 200–250 °C, changes to boehmite. Bayerite, when heated to 200–300 °C, changes to boehmite. Boehmite, when heated to

300–450 °C, changes to η- or γ-Al_2O_3; and diaspore, when heated to 450–500 °C, changes to α-Al_2O_3.

As to its chemical composition, a compound of hydrargillite and bayerite can be considered as betagibbsite $Al_2O_3 \cdot 3H_2O$, and a compound of boehmite and diaspore can be considered as metahydroxide $Al_2O_3 \cdot H_2O$ [119 and 145]. There also might be pseudoboehmite $Al_2O_3 \cdot 1{,}3H_2O$ [178]. The authors of work [178] note that, at the temperature of 20 to 90 °C, the oxide film is a three-layer one: directly on the aluminium surface there is an amorphous oxide or an hydroxide several nanometres thick; and further there is a layer of pseudoboehmite with an overlying layer of bayerite. The thicknesses of pseudoboehmite and bayerite amount to microns. In the range of temperatures 100 to 374 °C, the oxide film consists of boehmite, however, columnar crystals of diaspore have been found on its external surface. The external layer is separated from the metal surface with a thin layer of γ-Al_2O_3. At a temperature above 374 °C (critical point of water), the oxide film consists of γ-Al_2O_3 and α-Al_2O_3 (corundum).

Besides, it is noted that, at the temperature of 500 to 900 °C, molten aluminium and the products of its interaction might react with water vapour. At this, aluminium oxides turn in part to a gaseous form (reactions 5 and 6). In part, they dissolve in liquid aluminium and form complex compounds of the $(Al_2O_3)_xH$ or $(Al_2O_3 \cdot nH_2O)_yH$ type [119].

At low temperatures, silicon decomposes water according to equation 7 in Fig. 30. Should the temperature exceed 600 °C, the reaction proceeds according to equation 8 in Fig. 30 [116 and128].

During the iron-vapour process of generating hydrogen at 570 °C, the presence of components Fe_3O_4, FeO, and Fe is equally likely. Oxide Fe (II) and hydrogen are formed at temperatures above 570 °C. At lower temperatures, most stable is Fe_3O_4 (see equation 9 in Fig. 30) [173, and 178]. In expression 10 in Fig. 30, Fe_3O_4 is taken as the compound oxide, i.e. FeO and Fe_2O_3 [128, 173, and 179].

Gibbs' energy values obtained indicate a high probability of reactions of silicon and aluminium with water (except for reaction 11 in Fig. 30). Iron reactions are also likely, however, with increasing temperature the reaction completeness declines.

In gassing zones, the surfaces of aluminium and silicon are red-hot, which results in boiling of water entering the reaction [149].

Although equilibrium thermodynamics imposes certain constraints on the process kinetics, it fails to account for the time factor and the character of

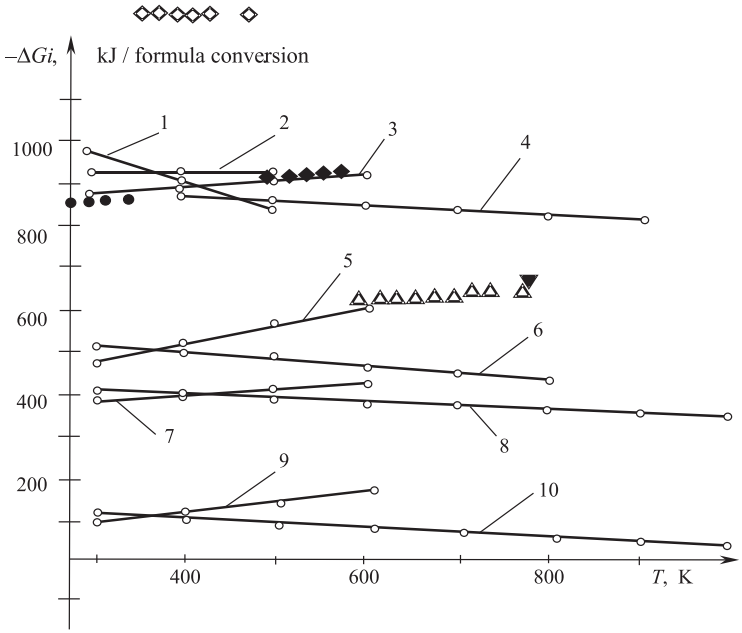

1 – $2Al + 6H_2O$ (vapour) $\leftrightarrow 2Al(OH)_3 + 3H_2\uparrow$,
2 – $2Al + 6H_2O \leftrightarrow 2Al(OH)_3 + 3H_2\uparrow$,
3 – $2Al + 3H_2O \leftrightarrow Al_2O_3 + 3H_2\uparrow$,
4 – $2Al + 3H_2O$ (vapour) $\leftrightarrow Al_2O_3 + 3H_2\uparrow$,
5 – $2Al + 6H_2O \leftrightarrow 2Al(OH)_3$ (gas) $+ 3H_2\uparrow$,
6 – $2Al + 6H_2O$ (vapour) $\leftrightarrow 2Al(OH)_3$ (gas) $+ 3H_2\uparrow$,
7 – $Si + 2H_2O \leftrightarrow SiO_2 + 2H_2\uparrow$,
8 – $Si + 2H_2O$ (vapour) $\leftrightarrow SiO_2 + 2H_2\uparrow$,
9 – $3Fe + 4H_2O \leftrightarrow Fe_3O_4 + 4H_2\uparrow$,
10 – $3Fe + 4H_2O$ (vapour) $\leftrightarrow Fe_3O_4 + 4H_2\uparrow$,

● – *IPMash data for reaction 2,* ($Al(OH)_3$ *— amorphous structure);*
◇ – *IPMash data for reaction 2,* (α, γ-$Al(OH)_3$ *);*
◆ – *IPMash data for reaction 3,* ($Al_2O_3 \cdot H_2O$ *— boehmite);*
△ – *IPMash data for reaction 4;*
▼ – *H. Kostron's data for reaction 4 [145].*

Fig. 30. Gibbs' energy vs. temperature

transient processes. Thus, fulfilment of stoichiometric relationships between reagents and reaction products implies that, for each reaction, there is one and only one independent kinetic equation. Gas is one of the components of the systems investigated, making it possible to use information of a non-thermodynamic character when determining equilibrium. Specifically, appearance of the equilibrium constant and partial pressures in the structure of the fundamental equations of thermodynamics results from applying the ideal gas state equation. There is a relation between the equilibrium constant and the rate constants of the direct and reverse reactions, making it possible to use two quantities to find a third one [174]. Thus, according to Vant-Hoff, the isotherm equation of the reaction linking the equilibrium constant value to the variation of the thermodynamic potential has the form

$$K = e^{-\left(\Delta Gi/RT\right)},$$

where ΔGi is Gibbs' energy variation; R is gas constant; and T is temperature.

On the other hand, according to the law of acting masses, the equilibrium constant of reactions is found from expression

$$K = \frac{P_{H_2}^{\upsilon_i}}{P_{H_2O}^{\upsilon_j}},$$

where P is gas pressure; and

υ_i and υ_j are stoichiometric coefficients of components.

Having calculated the equilibrium constant, and knowing the hydrogen pressure in the reactor, one can find the water vapour elasticity. Thereby the pureness of hydrogen obtained is estimated.

Using known techniques [41], reaction completeness α or degree of substance decomposition is found by using the equilibrium constant.

The completeness of reaction of aluminium with water vapour is related to the equilibrium constant by equation

$$\alpha_{\text{theor.}}\left(2 - \alpha_{\text{theor.}}\right) = \frac{4\sqrt[3]{K}}{1+4\sqrt[3]{K}}.$$

For the reaction of silicon with water vapour, the equation for determining the constant has the form

$$\alpha_{\text{theor.}} = \frac{\sqrt{K}}{1+\sqrt{K}}.$$

By substituting the value of constant K, one can ascertain that, at any temperature, the values of $\alpha_{theor.}$ are close to unity, i. e. the reactions proceed practically to the end.

The completeness of the process of interaction of iron with vapour obeys equation

$$\alpha_{theor.} = \frac{\sqrt[4]{K}}{1+\sqrt[4]{K}}.$$

For this case, the estimated value of $\alpha_{theor.}$ changes from unity at low temperatures to $\alpha_{theor.} = 0.72$ at the temperature of 1,000 K.

A pressure increase has no affect on the value of the constant, but shifts equilibrium to decrease the number of moles of gases involved. This calls for additional analysis of iron and water reaction conditions. The equilibrium constant of the reaction considered is related to hydrogen pressure as follows

$$K = P^4.$$

At the temperature of 600 K, a hydrogen pressure increase to 269.5 MPa yields an equilibrium state. Hence, the pressure of 15 MPa built up in stand-alone reactors cannot shift reaction equilibrium.

Reactions of interaction of alloys with water vapour are more informative than reactions with water are. Having experimentally found the total pressure, and taken the water vapour pressure to be equal to the saturation pressure (at the given temperature), one can determine the partial pressure of hydrogen. The latter allows to assess to what extent the given reaction regime differs from the equilibrium one. The challenge consists in determining the elasticity of water vapour immediately above the reaction surface because it has an oxide layer.

For the reaction of aluminium with water vapour, we have

$$K = \frac{P_{H_2}^3}{P_{H_2O}^6}.$$

Taking the hydrogen pressure to be 15 MPa at the temperature, for instance, of 500 K, we find the equilibrium pressure of vapour $P_{vap} = 7.7 \cdot 10^{-15}$ MPa. The small pressure value indicates the possibility of obtaining high-purity hydrogen. The same calculation shows that ultrahigh hydrogen pressure corresponds to insignificant elasticity of water vapour. At the same time, in a closed system, equilibrium pressure can build up only when the system's volume decreases by a value equal to the difference of volumes of condensed source and final products. Otherwise, the hydrogen pressure fails to achieve the equilibrium value. Thus, for reaction 1 in Fig. 30, the pressure in the closed volume of

the reactor cannot exceed 119.3 MPa. Since the reactor has an excess amount of water relative to its stoichiometric quantity, hydrogen is saturated with water vapour. The moisture content of the vapour-gas mixture is found from relationship [180]

$$x = \frac{M_v}{M_g} \cdot \frac{\varphi \cdot P_{sat}}{P_{total} - \varphi \cdot P_{sat}} \quad \left[\frac{\text{kg } vapour}{\text{kg } dry\ gas} \right],$$

where M_v and M_g are molecular masses of vapour and gas;

φ is relative gas moisture content;

P_{total} and P_{sat} are total pressure of the vapour-gas mixture and pressure of saturated vapour, respectively, at the given temperature, MPa.

If we take the reactor temperature to be 200 °C and the pressure to be 15 MPa, then, at complete hydrogen saturation ($\varphi = 1$) and $P_{sat} = 1.58$ MPa, the value of x will be 0.89 kg of vapour per 1 kg of dry hydrogen.

Using tabulated values of thermodynamic quantities allowed increasing the accuracy of calculating Gibbs' energy by 5 to 9 % as compared to those found earlier.

Hence, in thermodynamic investigations, we have extended the range of analysed aluminium and silicon reactions, and introduced reactions with iron into consideration.

It has been shown that the probability of reactions increases with dropping temperature. The reactions of aluminium and silicon with water in the range of temperatures 200 to 600 K, and with water vapour at 300 to 1000 K, proceed to the end. In the range of temperatures 300 to 600 K, iron reacts with water at reaction completeness $\alpha_{theor.} = 1$. When iron interacts with water vapour in the range of temperatures 300 to 1000 K, $\alpha_{theor.}$ changes from unity to 0.72. An increase in pressure up to 15 MPa has practically no affect on hydrogen output.

Estimates have demonstrated the possibility of producing high-purity hydrogen. This was also proved experimentally [181].

3.3.3. Testing high-pressure hydrogen reactors

As mentioned earlier, the open systems considered herein are relatively far from the state of equilibrium. In spite of the high values of chemical potentials, the affect of topochemical factors constrains the gassing rate, making it possible, in the first approximation, to describe the process by a linear relationship

$$dGi/d\tau = Ad\alpha/d\tau, \qquad \text{(III.26)}$$

where $A = \sum \nu_i \mu_i$ is chemical affinity;

$\mu_i = (\partial Gi/\partial n_i)p,T,(n_i)$ is chemical potential;

p, T, n_i are indices denoting constancy of pressure, temperature, and mass concentrations of components except for the concentration of the i-th component.

Here special attention is drawn to the fact that interaction of a multitude of particles with water presents a challenge to determining the size of the reaction surface. More or less definite values of $d\alpha/d\tau$ can be found but for a narrow range of maximal rates of hydrogen liberation when the reaction surface is approximately equal to the external surface of the granulated alloy mass. As we already know, the maximum rates correspond to the inflection points of S-shaped curves built in $\alpha-\tau$ coordinates.

Evaporators' test data allow to introduce, with certain assumptions, an additional equation into consideration

$$\frac{d\alpha}{d\tau} = L\sum \nu_i \mu_i, \qquad \text{(III.27)}$$

where L is a coefficient found experimentally.

The relevancy of applying both equations results from the provisions of thermodynamics of irreversible processes.

The key stages of formation of models of processes accounting for the energy factor are described below.

Onsager first stated the general principle, namely, the principle of least dissipation of energy. In addition, Onsager advanced a partial principle, according to which irreversible processes, at small deviations from thermodynamic equilibrium, can be described by linear differential equations with constant coefficients [182 and 183]. De Donder [184] introduced the notion of the degree of proceeding, or chemical variable, and also demonstrated the possibility of using affinity functions for analysing equilibrium shifts in heterogeneous systems. Prigogine [36] suggested a new general principle — the principle of least generation of entropy, which turned out to be more convenient for solving practical problems than Onsager's principle was. Zubarev [185] treated the statistical theory of chemical reactions, in terms of thermodynamic forces, both in the linear and nonlinear approximation. Gyarmati [186] established a relationship between Onsager's and Prigogine's principles, and the forms of equations of subsequent approximations since Onsager's equations are linear approximations. From the variational principle of least dissipation of energy, presented in terms of forces, Gyarmati derived the equations of heat transfer, diffusion and viscous flows. Information on thermodynamics of irreversible processes is presented in greater detail in works [187–192].

It should be noted that the mathematical apparatus developed by the above investigators gives no way of computing the phase trajectory of a specific chemical system or the parameters of the cycle suggested. To solve this problem, we need dynamic equations that govern the changes of coefficient L.

Hence, the thermodynamic methods developed, jointly with kinetic ones, allow for rather complete investigation of equilibrium and non-equilibrium conditions of heterogeneous systems.

Let us review the published data [193]. The maximum rates of displacement of hydrogen by aluminium and silicon alloys as well as sodium borohydride are summarised in Table 2. The experimental values of coefficient L are also given there.

Table 2

Thermodynamic and kinetic data of the reactions of sodium borohydride and aluminium and silicon alloys with water and a caustic soda solution at t = 90 °C

Substance name	Reaction Gibbs' energy ΔGi, kJ	Specific Gibbs' energy Δμ, kJ/kg*	Maximum hydrogen liberation rate, $W \cdot 10^3$, $m^3/(m^2 \cdot s)$	Coefficient $-L \cdot 10^8$, $m^3/(m^2 \cdot s \cdot kJ)$
AG505I5	−925	−17130	32	188
$NaBH_4$, $CoCl_2$	−344	−9053	0.68	7.5
$NaBH_4$	−344	−9053	0.377	4.2
FSA 25	(see Al and Si)	−14115	0.318	2.25
FS 75	−362.4	−12943	0.08	0.6

Evidently, the values of L follow the changes of values A, though not in direct relation. The latter fact is linked to different values of activation energy defined to a large extent by the character of wash-off of reaction products from the surface of interacting substances.

The results analysed were obtained at moderate pressures. We are interested, however, in reactions proceeding in Earth's interior at high pressures.

Investigations were carried out on an installation with a standard cylinder single-neck gas generator type AVG-45 with the capacity of 45 litres and working pressure of 15 MPa. The installation with the gas generator AVG-45 is similar to the automated reactor installation shown in Fig. 31, except for systems of preparing and feeding alkali and sludge.

* The values of Δμ refer to 1 kg of the alloy's active part.

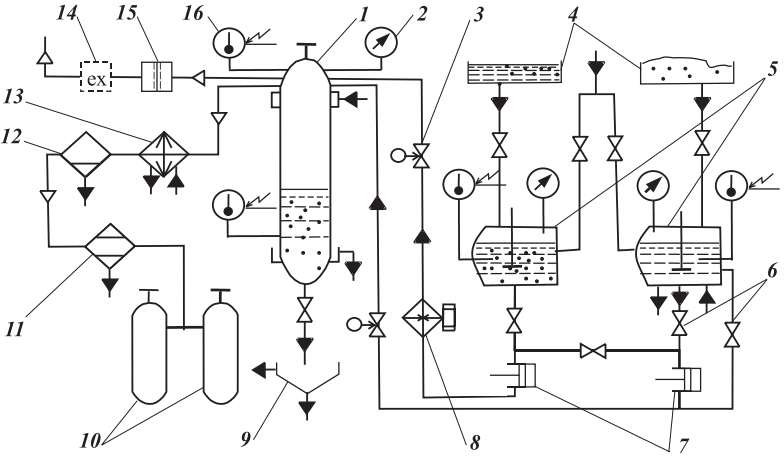

1 – reactor, 2 – pressure gauge, 3 – pneumatically-controlled valve, 4 – vessels for reagents, 5 – mixers for preparing reagents, 6 – valves, 7 – piston pumps, 8 – heat exchanger with electric heating, 9 – vessel for reaction products, 10 – cylinders for hydrogen, 11 – silica gel dessicator, 12 – separator,13 – condenser, 14 – fire extinguisher,15 – safety diaphragm,16 – electric-contact thermometer (thermocouple).

Fig. 31a. Diagram of automated reactor installation (UVR)

Fig. 31b.
Reactor unit (on the left) and reagents preparation unit (on the right)

Experiment procedure

During experiments, the alloy powder and the granulated alkali are filled into the reactor, followed by priming the required amount of water.

The reactor is cooled after the process has been completed. The amount of hydrogen generated is determined by the pressure in and the volume of the free part of the cylinder. Gas is discharged to the atmosphere via a condenser, separator, and flow meter GSB-400. The volume of sludge drained is measured with a volumetric vessel.

Appropriate instrumentation is used for monitoring the process in the apparatus.

Since the medium in the reactor is a corrosive one, the thermocouples are mounted in stainless steel tubes with a diameter of $8 \cdot 10^{-3}$ m. The tubes are inserted into the gas generator through a custom-design head to the heights of 0.02 m and 1.17 m from the cylinder bottom. The temperature of the cylinder external wall is monitored at the same time.

Alloys of the following chemical composition, mass %, were used: FSA 11 (Fe-18.15, Si-61.9, Al-11.13, Ti-0.68, Mg-0.15, Ca-4.0, P-0.059, S-0.04); FSA 16 (Fe-17.5, Si-60.4, Al-15.8, Ti-0.84, Mg-0.22, Ca-3.6, P-0.088, S-0.040; FSA 18 (Fe-7.2, Si-74.8, Al-18); FSA 25 (Fe-10, Si-65, Al-25); FS 75 (Fe-20 to 25, Si-74 to 80, Al-0.6, Cr-0.5, P-0.05, S-0.03); C — pure metallic silicon; CAC — 1 (Si-25 to 30, Al-62 to 68, Ni-5 to 7, Fe-0.5).

The experimental results are presented in Tables 3 and 4, and Figs. 32 and 33. The tables contain data published earlier [194]. The figures in parentheses indicate the pressure after reactor cooling and the induction time interval.

The reference numbers of experiments in Table 3 correspond to the reference numbers of curves in Fig. 32. The same holds for Table 4 in this section and Fig. 33.

Discussion of results

The first series of experiments conducted in the summer period have shown that the reactor's capacity is greatest when working with metallic silicon. During reactor cooling, however, liquid glass solidifies in the lower part of the cylinder. In the event of hydrogen discharge from the hot reactor the solution boils, and solid reaction products are ejected to the gas line. Due to this, the problem of discharging sludge from AVG-45, when working with pure silicon, requires further investigation.

Alloy CAC-1 interacts instantaneously with water, however, the hydroxide being formed starts absorbing water at some point in time [195]. As water disappears, the reaction decays (experiment 4). The required process completeness is ensured by increasing the volume of supplied water by about two-fold (experiment 5).

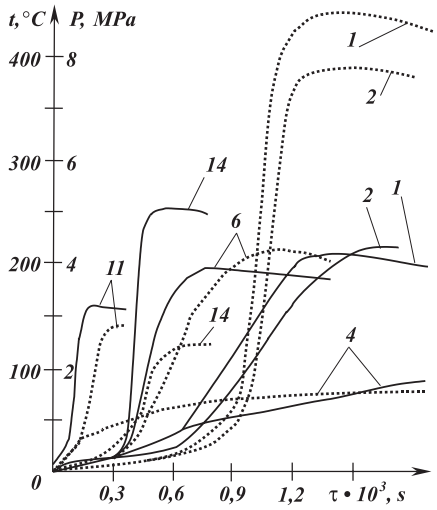

1, 2 – Si; 4 – CAC-1; 6 – FS 75; 11, 14 – FSA 25.

Fig. 32. External wall temperature and pressure in gas generator AVG-45 during reaction

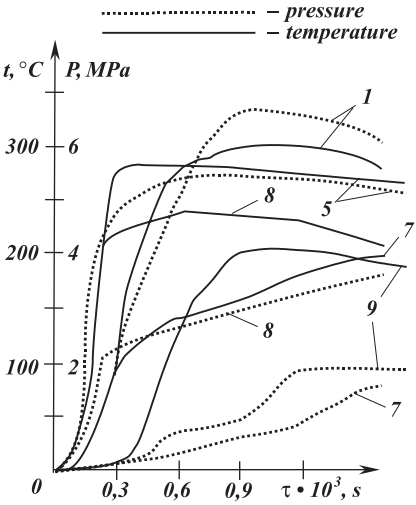

1 – FS 75; 5, 7 – FSA 18; 8, 9 – FSA 11.

Fig. 33. Temperature and pressure in gas generator AVG-45 during reaction

Table 3

Results of testing gas generator AVG-45 working with pure silicon, standard alloys (CAC-1 and FS 75), and synthetic alloys (FSA 18 and FSA 25) (1st series of experiments)*

Ref. No.	Ratio of charged components, kg	Alkali concentration, %	Maximum temperature in reaction zone, °C	Pressure in reactor, MPa	Total reaction time, min	Amount of hydrogen obtained, m^3
	Si : Al : NaOH : H_2O					
1	1.2 : 0.05 : 0.8 : 6.0	13.3	385	8.8 (6.0)	22	1.835
2	1.2 : 0.05 : 0.8 : 6.0	13.3	380	7.8 (5.2)	25	1.64
	CAC-1 : NaOH : H_2O					
3	1.25 : 0.9 : 6.0	15	350	2.5	5	0.73
4	1.25 : 0.65 : 6.5	10	190	1.5	30	0.56
5	0.65 : 0.9 : 6.0	15	330	2.5	19	0.8
	FS75 : Al : NaOH : H_2O					
6	1.25 : 0.05 : 0.9 : 6.0	15	320	4.0	30	1.485
	FSA18 : Al : NaOH : H_2O					
7	1.25 : 0.05 : 1.0 : 6.0**	16.6	310	3.5	20 (6)	1.3
	FSA25 : Al : NaOH : H_2O					
8	1.2 : 0.3 : 1.0 : 6.0	16.6	320	4.0	35	1.45
9	1.2 : 0.3 : 0.8 : 6.0**	13.3	310	3.8	39 (4)	1.36
10	1.0 : 0.2 : 1.0 : 6.5	15.4	300	3.0	25 (4)	1.2
11	1.0 : 0.2 : 0.5 : 2.5	20	295	2.8	4	1.12
	FSA25 : NaOH : H_2O					
12	1.5 : 0.2 : 3.0	6.66	275	2.0 (2.0)	20 (12)	0.8
13	1.2 : 0.4 : 2.5	16	360	(3.0)	6	1.15
14	1.3 : 0.5 : 3.0	16.6	350	(2.6)	13 (3)	1.05
15	1.25 : 0.5 : 2.5	20	370	2.8	5	1.25

* Granular composition of alloys: C(Si) — $(0.05 \div 3.0) \cdot 10^{-3}$ m, CAC-1 — $(0.005 \div 0.63) \cdot 10^{-3}$ m, FS 75 — $(0.05 \div 3.0) \cdot 10^{-3}$ m, FSA 18 and FSA 25 — $(0.05 \div 4.0) \cdot 10^{-3}$ m;

** Alloy CAC-1 is used instead of aluminium to heat up the reactor.

Table 4

Results of testing gas generator AVG-45 working with standard alloy (FS 75), synthetic alloy (FSA 18), and alloys (FSA 11 and FSA 16) obtained from coal (2nd series of experiments)*

Ref. No.	Ratio of charged components, kg	Alkali concentration, %	Maximum temperature in reaction zone, °C	Pressure in reactor, MPa	Total reaction time, min	Amount of hydrogen obtained, m^3
	FS75 : Al : NaOH : H_2O					
1	1.2 : 0.05 : 0.9 : 6.0	15	290	6.5	22	1.38
	FSA18 : Al : NaOH : H_2O					
2	1.2 : 0.3 : 0.8 : 6.0	13.3	255	5.0 (4.8)	32	1.3**
	FSA18 : NaOH : H_2O					
3	1.25 : 0.5 : 2.5	20	275	5.0 (4.8)	10	1.1**
4	1.25 : 0.5 : 2.5	20	280	4.6 (3.4)	13	1.14**
5	1.25 : 0.6 : 2.5	24	285	5.3 (3.7)	8	1.25**
6	1.25 : 0.6 : 3.0	20	280	4.5 (3.3)	12	1.2**
7	1.25 : 0.3 : 3.0	10	200	(1.25)	25 (5)	0.59**
	FSA11 : NaOH : H_2O					
8	1.25 : 0.5 : 3.0	16.6	240	3.7 (3.3)	37 (1.5)	1.22
9	1.25 : 0.466 : 3.5	13.3	205	(1.8)	18 (6)	0.8
	FSA16 : NaOH : H_2O					
10	1.25 : 0.5 : 3.0	16.6	245	3.5	30 (2)	1.18

It has been found that the volume of hydrogen liberated during interaction of FSA 25 with water differs slightly from that obtained during a similar reaction with FS 75. Generating hydrogen during the winter season requires adding aluminium powder for heating up the reactor (experiments 6 and 7).

Aluminium can be excluded by reducing the volume of filled water. In so doing, the amount of alkali used can be reduced by one-half as compared to the standard consumption (experiments 10—12).

The temperature in the gas generator, at a standard charge of FS 75, alkali and water, is close to that indicated in instructions [196]. During interaction of FSA 25 and CAC-1 the temperature rises slightly. By reducing the amount of supplied water the temperature of reaction of FSA 25 with a caustic soda solu-

* Granular composition of alloys: FS 75 — $(0.16 \div 2.0) \cdot 10^{-3}$ m; FSA 18 — $(0.16 \div 2.0) \cdot 10^{-3}$ m — in experiments Nos. 2-4, $(0.1 \div 2.0) \cdot 10^{-3}$ m — in experiment No. 5 and $(0.315 \div 2.0) \cdot 10^{-3}$ m — in experiments Nos. 8 and 9; FSA 11, FSA 16 — $(0.1 \div 3.0) \cdot 10^{-3}$ m.

** Discharge of reaction products is hindered.

tion increases to 370 °C. Maximum temperatures were recorded in experiments with pure silicon.

In the winter season (the temperature in the operator's room is 0–7 °C) the temperature changes as follows. For the reaction with FS 75, the maximum temperature of the external wall in the lower part of the cylinder was 160–170 °C; for silicon it was 185–220 °C; for FSA 25 it was 145–165 °C (when the amount of supplied water was reduced by one-half, the temperature increased to 220 °C).

The gas temperature in the upper part of the cylinder during the reaction varied within 90–110 °C, and after the reaction was completed it was no more than 50 °C.

As seen in the graphs, the growth of reacting composition temperature, as a rule, leads over pressure build-up. Hence, in the initial period, water boils partially.

In the summer season (the temperature in the operator's room is 18–25 °C), when using FSA 75, the external wall in the lower part of the cylinder is heated to 180–200 °C; when using FSA 25, it heats up to 165–185 °C (when the volume of supplied water is reduced by one-half it heats up to 260 °C).

As data [197] indicate, at high pressure, the surface temperature of the alloy particles significantly exceeds that of the solution temperature. Based on this, the high temperatures recorded by the author of work [198] at the beginning of the process result apparently from contact of the thermocouple junction with the surface of reacting particles.

The heat liberated during the reaction is used for heating the interaction products, the metal in the lower part of the reactor, and for partial evaporation of water. The estimated temperature determined for experiments with FS 75 from the heat balance corresponds to the temperature found experimentally (290 °C in the winter season, and 320 °C in the summer one).

The second series of experiments was focused to searching for regimes of discharging reaction products in the winter season at reduced water supply. In the cold season, the water supplied to the reaction is heated to 50–60 °C because adding cold water (10–15 °C) fails to initiate the reaction.

Discharging the products of interaction of alloy FSA 18 from the reactor (experiments 2–7) was found to be impossible. Apparently, this is partially due to the drop in the process temperature. The products of reaction of alloys FSA 11 and FSA 16 obtained by reduction of the inorganic part of coal are removed readily from AVG-45 (experiments 8–10).

Experimental data treatment procedure

The hydrogen generation rate in the reaction space is:

$$W = \Delta V/(m \cdot \Delta\tau) \text{ and } W = \Delta V/(f_s \cdot \Delta\tau) \qquad \text{(III.28)}$$

Experimental data were generalised using equation (III.27)
Combining equations (III.27) and (III.28), we obtain

$$W = d\alpha/d\tau = LA, \qquad \text{(III.29)}$$

$$L = \Delta V/(f_s \cdot \Delta\tau \cdot \Delta\mu). \qquad \text{(III.30)}$$

The values of coefficient L for gas generator AVG-45 and the kinetic stand are summarised in Tables 5 and 6.

With temperature increase from 363 K to 500 K, the reaction rate increases dramatically for silicon and FS 75, but drops slightly for aluminium alloys and synthetic FSA alloys. Apparently, rate reduction is associated with the regime of erosion of hydroxide aluminium formed on the surface of particles.

Table 5

Thermodynamic and kinetic data for reactions of interaction of alloys with water and aqueous solutions of alkali in AVG-45

Alloy	Specific Gibbs' energy*, $-\Delta Gi$, kJ/kg	Maximum hydrogen liberation rate,		Coefficient, $-L \cdot 10^8$, $m^3/(m^2 \cdot s \cdot kJ)$
		$W \cdot 10^3$, $m^3/(kg \cdot s)$	$W \cdot 10^5$, $m^3/(m^2 \cdot s)$	
t ≈ 100°C (373 K), P ≈ 0.1 MPa				
FSA 18	14598	1.38	2.77	0.19
FSA 11	14465,2	5.93	11.85	0.82
FS 75	14002,6	4.52	9.04	0.646
t = 227°C (500 K), P ≤ 5 MPa				
CAC-1	15225.7 (16212.5)	3.12	2.61	0.171 (0.161)
FSA 25	14400.34 (15197.1)	1.74	3.04	0.211 (0.2)
FSA 18	14237.5 (14996.8)	2.23	7.19	0.505 (0.48)
FSA 16	14263.5 (15028.8)	2.76	6.91	0.33 (0.46)
FSA 11	14156.73 (14897.4)	2.93	7.33	0.36 (0.491)
FS 75	13875.65 (14551.6)	3.01	6.02	0.361 (0.414)
C (Si)	13860.6 (14533.1)	2.55	4.28	0.309 (0.295)

* The values in parentheses are given for gas-lift conditions (without fluid boiling, P > 2.6 MPa).

Table 6

Thermodynamic and kinetic data for reactions of interaction of alloys with water and an aqueous solution of alkali in the kinetic stand reactor (reactor volume $1.13 \cdot 10^{-3}$ m^3)

Alloy	Specific Gibbs' energy*, $-\Delta Gi$, kJ/kg	Maximum hydrogen liberation rate,		Coefficient, $-L \cdot 10^8$, $m^3/(m^2 \cdot s \cdot kJ)$
		$W \cdot 10^3$, $m^3/(kg \cdot s)$	$W \cdot 10^5$, $m^3/(m^2 \cdot s)$	
t ≈ 100°C (373 K), P ≈ 0.1 MPa				
FSA 18	14598	6.95	13.9	0.952
FSA 11	14465.2	21.6	43.2	2.987
FS 75	14002.6	10.65	21.3	1.52
t = 227°C (500 K), P ≤ 5 MPa				
FSA 18	14237.5	2.44	9.76	0.686
FSA 16	14263.5	8.81	29.4	2.06
FSA 11	14156.73	5.7	19	1.34
FS 75	13875.65	12.2	48.8	3.52
C (Si)	13860.6	8.25	33	2.38

With increase in apparatus dimensions, one should expect intensification of irregularity of flow circulation, affecting the intensity of gassing. In this case, it is appropriate to represent coefficient L as a function of criterion Re of the ascending flow fluid:

$$L = k \cdot \mathrm{Re}^n. \qquad \text{(III.31)}$$

In the first approximation, the values of criterion Re are found using the method developed for evaporators [50]; and in the second approximation these values are found for gaslifts [152]. The dependences of coefficient L on the Re number for the cylinder gas generator AVG-45 and the kinetic stand are shown in Fig. 34 (including IPMash data on testing reactors 0.08 m^3 and 0.2 m^3 [50 and 199]). The characteristics of the reactors are shown in Table 7.

Table 7

Characteristics of reactors

Volume, $V \cdot 10^3$, m^3	Diameter, d, m	Length, l, m	Mass, m, kg	Working pressure, P, MPa	Liquid level height, h, m
1.13	0.072	0.25	51	50	0.12
45	0.205	1.54	64	15	0.3
80	0.304	1.38	135	15	0.9

* The values in parentheses are given for gas-lift conditions (without fluid boiling, P > 2.6 MPa).

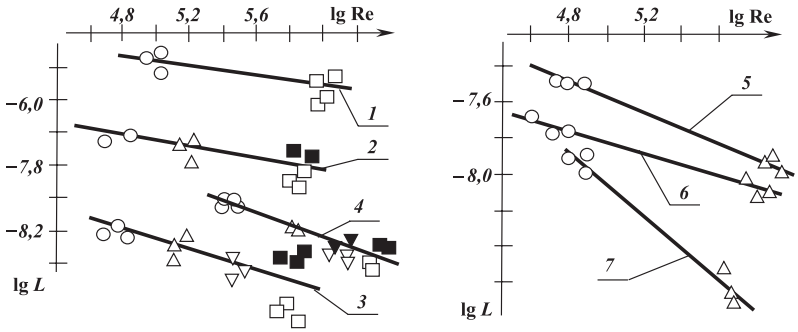

Fig. 34. Coefficient L vs. Re number of ascending flow fluid for reactions

1 – AG5O5I5 with water; 2 – FSA 25 with 10 % NaOH; 3 – FS 75 with 25 % NaOH; 4 – FS 75 with 15 % NaOH; 5 – FSA 11 with 16.6 % NaOH; 6 – FS 75 with 15 % NaOH; 7 – FSA 18 with 20 % NaOH.

Lines 1–3 and 5–7 are found for conditions t = 100 °C , P ≤ 0.1 MPa; Line 4 is for t = 227 °C, P ≤ 1 MPa.

Lines1–3 are IPMash data; lines 4–7are data of this work.

Reactors: ○ — kinetic stand — 1.13•10⁻³ m³; △ — standard AVG-45 — 0.045 m³; ▽ — included in UVR — 0.08 m³, stationary regime; ▼ — included in UVR — 0.08 m³, pulsating regime; □ — pilot-industrial — 0.2 m³, stationary regime; ■ — pilot-industrial — 0.2 m³, pulsating regime.

Works published earlier give relations for the following alloys:
AG5O5I5 (activated aluminium) with water (Fig. 34 a, line 1)

$$L = 5.61 \cdot 10^{-6}\ \mathrm{Re}^{-0.11}. \qquad \text{(III.32)}$$

FSA 25 with 10 % NaOH (Fig. 34 a, line 2)

$$L = 0.153 \cdot 10^{-6}\ \mathrm{Re}^{-0.17}. \qquad \text{(III.33)}$$

FS 75 with 25 % NaOH (Fig. 34 a, line 3)

$$L = 0.245 \cdot 10^{-6}\ \mathrm{Re}^{-0.33}. \qquad \text{(III.34)}$$

In this work, relations for the following alloys have been established:
FSA 11 with 16.6 % NaOH (Fig. 34 b, line 5)

$$L = 1.5 \cdot 10^{-5}\ \mathrm{Re}^{-0.55}. \qquad \text{(III.35)}$$

FS 75 with 15 % NaOH (Fig. 34 b, line 6)

$$L = 6{,}24 \cdot 10^{-7}\ \mathrm{Re}^{-0{,}32}. \qquad \text{(III.36)}$$

FSA 18 with 20 % NaOH (Fig. 34 b, line 7)

$$L = 2.82 \cdot 10^{-5}\,\mathrm{Re}^{-0.82}. \qquad \text{(III.37)}$$

FS 75 with 15 % NaOH (Fig. 34 a, line 4)

$$L = 4 \cdot 10^{-6}\,\mathrm{Re}^{-0.48}. \qquad \text{(III.38)}$$

Equation (III.32) is designated for conditions $t = 100$ °C (373K) and $P \le 0.1$ MPa that hold for $4 \cdot 10^4 < \mathrm{Re} < 8 \cdot 10^5$; equation (III.38) is designated for $t = 227$ °C (500K), $P \le 1$ MPa, and for Reynolds numbers $3 \cdot 10^5 < \mathrm{Re} < 2 \cdot 10^6$.

The fact that coefficient L decreases with increasing apparatus dimensions has been confirmed for each type of reaction. Irregularity of flow circulations increases with growth of density of alloy particles. Reactor capacity can be increased by pressure pulsation. An increase in reactor pressure is associated with growth of composition temperature. During an abrupt pressure drop the fluid boils, causing an intensive mixing of phases.

As seen in the graph, a reactor with the volume of 0.08 m^3 is most optimal with regard to capacity and ensuring process stability.

For apparatus design, heat transfer relationships were found. Experimental data on investigating heat transfer in reactor AVG45 are shown in Fig. 35. For alloy FS 75, heat transfer follows relationship

$$\mathrm{Nu} = 1.5 \cdot 10^{-17}\,\mathrm{Re}^{3.7}\,Pr^{0.33}. \qquad \text{(III.39)}$$

Equation (III.39) is designated for the reaction half-time ($\alpha_r = 0.5$) and holds for the range of $7 \cdot 10^3 < \mathrm{Re} < 2 \cdot 10^4$ ($t \cong 227$ °C (500K); $P > 2.6$ MPa).

Here number Re is found with account of phase slippage using the technique described in para. 3.3.1.

In this case, the volume of gases formed depended on the type of reagents, and partly, on varying the charge.

Fig. 35 shows the values of the Nuselt criterion for pure silicon and alloys FSA 11, FSA 18, FSA 25, and FS 75. The straight line in Fig. 35 corresponds to equation (III.39). The high values of the Re exponent point to significant turbulisation of the boundary layer, which contacts the reaction surface, by a flow of generated hydgogen bubbles. Specific mathematical relationships that govern the heat transfer intensity for other alloys can be recommended as statistical data are further accumulated.

The experimental and theoretical data obtained are used for designing the automated reactor installation shown in Fig. 31 [200]. The equations of chemical reactions involving alkali are given in work [200].

Comparing the results of this research with those of the previous one, where an opposite influence of Reynolds number was found, we can once more

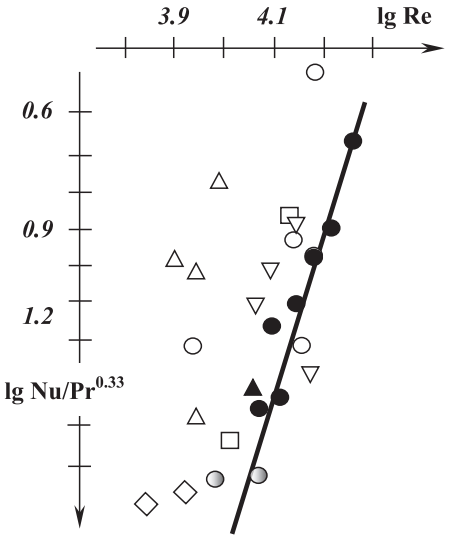

□ – *FSA 11;* ▲ – *FSA 18; 20 % NaOH;* ○ – *FS 75; 15 % NaOH;* ◇ – *C (Si); 13,3 % NaOH;* ▽ – *FSA 25 — acc. to data of this work;* ● – *FS 75 – acc. to [198];*
□, ○, △, ▽ – *the reagents charge differs significantly from the standard one.*

Fig. 35. Calorific efficiency of powders of various alloys in standard gas generator AVG-45 vs. ascending flow Reynolds number

make sure that the laws of friction in three-phase flows are invariant relative to variations in the spatial scale of systems, or, in other words, to similarity transforms.

At especially high pressures, the values of Gibbs' energy should be refined using formula

$$\Delta Gi = \Delta Gi \; ln \; (P_2/P_1), \qquad \text{(III.40)}$$

where P_2 and P_1 is the final and initial pressure in the apparatus, respectively.

Thus, the investigation conducted allows to state that, within the range of temperatures 0–400 °C, there is no strict proportionality between the driving force of the process and the rate of hydrogen displacement from water by aluminium, silicon, and iron alloys.

Heat-and-mass transfer deteriorates with increase in apparatus diameter.

The data obtained can serve as baseline ones when estimating the rate of underground reactions.

3.4. RATE OF UNDERGROUND REACTIONS

In this section, we will use our knowledge on physico-chemical transformations to disclose the regularities of underground reactions.

First, let us select a reference point against which the possible rates of underground reactions will be compared. A good analog can be the rate of aluminium alloy-induced displacement of hydrogen from water. For instance, at the temperature of 90 °C, the rate of hydrogen generation during interaction of activated aluminium with water is

$$W_{H_2} \approx 0.04 \text{ m}^3/(\text{m}^2 \cdot \text{s}).$$

Assume that the conditions in Earth's interior allow interaction of silicon alloys with water with the rate of W_{H_2}. Let us estimate how long the water in the World Ocean will last.

The volume of water in the World Ocean is known to be $1{,}370 \cdot 10^9$ km^3, and the ocean surface area is $361.1 \cdot 10^6$ km^2 [83].

Further, we assume that the area of the ocean bottom is equal to that of the ocean surface, and corresponds to the reaction surface. After simple arithmetic calculations, we find that the World Ocean should disappear from Earth's surface in 30 years.

The reaction rate achieved in high-pressure reactors, when FSA alloys and silicon interact with water, is lower than the value taken as an analog by two orders. Taking this rate as a reference, we will but little affect the ocean's destiny — it will vanish in three thousand years. However, during hundreds of millions of years of its existence, the ocean has yielded negligibly [95].

Let us investigate the causes of such behaviour of the ocean. To do this, we will analyse the key factors affecting the rate of underground reactions. Temperature and pressure are known to grow with depth. At the same time, the layer of oxides between the ocean and the stratum of silicon alloys continues to increase.

Let us investigate the affect of temperature on the reaction rate. In the previous section, we have seen rather high values of the energy of activation of the aluminium-water interaction process [114]. The same regularity has been noticed in reactions of silicon with water and water vapour [116, 201, and 202]. Both phenomena relate to comparatively low temperatures of interacting media.

The situation undergoes a radical change at high temperatures. In this case, the reaction rate drops with increase in temperature [203 and 204]. This suggests that the reaction rate values follow the changes in Gibbs' energy val-

ues, which drop with increase in temperature. Hence, with increasing temperature, the chemical stage of the process cannot offer high resistance to the reaction flow. Note that high temperatures can result in transition of crystalline substances in the reaction zone to a molten state.

Further, we will define the influence of heat sink on the reaction rate. The thermal conductance of the FSA alloy and of silicon-magnesium alloys, which comprise the base of Earth's interior layers, exceeds that of steel by about twice [116 and 205]. Therefore, heat is redistributed relatively freely in Earth's substance. Hence, the fixed heat flow from the interior to the surface has an approximately equal value in different parts of the planet.

The temperature differences in effect are linked to the reaction zone and Earth's core.

The maximum temperature occurs in the zone of contact of water or water vapour with alloys of silicon and magnesium or aluminium. The temperature rise from Earth's surface to this layer occurs similar to that observed in the currently investigated case of a reacting lump of activated aluminium. Below the reaction front, in the direction to the planet's centre, a less significant temperature drop should be observed than that recorded in our experiments. The point is that Earth's core stores the heat that was generated by gravitational compression. Besides, it is quite possible that it acquired part of the heat from the Protosun. Obviously, the heat sinks to the poles from both the silicon alloy-water reaction zone and Earth's core.

To all appearances, heat liberation from the reaction zone cannot limit the reaction rate otherwise.

Monographs [206 and 207] give a detailed presentation of the heat propagation process by heat conductance.

Let us consider the affect of pressure on the process considered.

As estimates show, the pressure corresponding to the equilibrium constant found can reach many billions of atmospheres. This implies that hydrogen can overcome any obstacles to its flow from the reaction zone to Earth's surface.

Hence, one can infer that pressure increase with depth cannot stop the reaction or change its rate substantially.

Thus, we have approached the key factor of resistance to the process, namely, the obstacle created by the lithosphere's oxide layer to penetration of water and water vapour to the reaction surface. In addition, it is necessary to account for the rate of water evaporation when approaching this surface, and its partial condensation in the uptake channels.

Let us evaluate the forces affecting detachment of the oxide layer.

First, note that, for the terrestrial globe with a radius of 6,371 km, the lithosphere layer of several dozens of kilometres is but a thin "film". Let us trace the transformation of this "film" during Earth's development.

As known, Earth's shape is a geoid. Due to its rotation, its shape is close to an ellipsoidal one, being oblate at the poles and extended in the equatorial zone. When Earth was in a liquid state, it rotated more rapidly and was more oblate than it is presently.

As the planet cooled, it generated less energy, and the rotational speed decreased to make the Earth progressively acquire a spherical shape. This resulted in occurrence of latitudinal faults in the yet weak terrestrial crust. During the same period, prior to emergence of mountains on Earth's surface, the cracks formed were filled with heavy compounds, including alloys of iron, magnesium, nickel and other metals. Incidentally, this phenomenon demonstrates the extreme irregularity of crystallisation front advancement into Earth's interior. This irregularity resulted in formation of local zones of liquid metals in the common layer of the crystalline mass.

As the World Ocean formed and the reaction zones advanced to Earth's centre, meridional faults started developing. As mentioned earlier, Earth crystallised in the form of meridional fibres whose separation displacement due to interior forces was the most likely process. The terrestrial crust as a whole had to be covered initially with a grid of meridional and latitudinal faults.

Further, it is common knowledge that Earth's solid substance experiences lunar-solar tidal effects. The lithosphere heaves by dozens of centimetres, and the swelling wave circles the planet every day. Similar to sea tidal effects, the greatest heave of Earth's solid mantle occurs under the combined action of lunar and solar gravitational forces [208].

Shot operations performed on Earth's surface as well as continuous wars racking our planet have no less affect on separation of the oxide layer. Perhaps this influence is commensurable with the affect of earthquakes on underground reactions.

Annually, the globe experiences, on the average, one violent earthquake; 10 to 100 moderate ones, and over 10,000 slight earthquakes [82].

Actually, underground reactions belong to the class of autocatalytic ones because earthquakes accelerate their flow. This issue merits a separate discussion; therefore, we will consider it in greater detail.

However, before starting to discuss the next global issue we will enlarge on a series of local data obtained, specifically, in the Kola ultradeep borehole [115].

The Kola Peninsula was selected because during hundreds of millions of years the Baltic Shield experienced erosion, viz. 5 to 15 kilometres of the upper

granite layer were destructed, and ablated by water and glaciers. Hence, the geological section of the Kola borehole actually corresponds to the depths of 15 to 25 km. The age of the Baltic Shield rock is 1.5 billion years. At the depth of 12 km, it is 3 billion years, and Earth's age is 4.5–5 billion years. The "length" of the borehole — 1.5 billion years — comprises an essential period of our planet's life.

Direct data were first obtained in the Kola borehole from depths below 10 km. Let us highlight the most significant results.

V.I. Vernadsky's hypothesis on existence of life in the Precambrian epoch was confirmed. Over 17 kinds of microorganisms were discovered — direct witnesses of what occurred on our planet 1.6–1.9 billion years ago.

Permeability of strata at the depth of 6–8 km was higher in some locations than closer to Earth's surface. It was there that porous, fissured, water-saturated strata were detected. This is linked to a unique phenomenon known as a wave guide. This is a zone with reduced seismic velocities resulting from reduced rock density.

For a long while it was assumed that the so-called Mohorovicic discontinuity, at which the seismic-wave velocity rapidly changes, is linked to the boundary between the granite and basalt strata. The Kola borehole has traversed the discontinuity boundary, however, no basalt was found. The rapid velocity increase proved to be linked to a decrease in rock density.

It has been ascertained that, in principle, even at depths below 9.5 km there can be deposits of copper, lead-zinc, and nickel ore.

First in world practice, the Kola ultradeep borehole made it possible to obtain data on the deep "breathing" of Earth, viz. the gas flow (nitrogen, methane, noble gases, mercury vapours, etc.) from the mantle. It was assumed that the temperature in the Baltic Shield increases slightly with depth — about 8–10 °C per each kilometre. However, at the depth of 10 km it reaches 180 °C. These data demonstrate the proximity of the zone of reaction of oxygen-free compounds with water. However, it is likely that there is an increased content of radioactive elements.

Future ultradeep drilling will also allow assessing the oil-and-gas bearing capacity of deep horizons. At present, oil and gas in commercial quantities have been discovered at rather great depths (to 4.5–5 km). Recently it has been proved that, at depths exceeding 7–8 km and at temperatures above 200 °C, both gas and oil can be found.

In the terrestrial deep, there is one more non-conventional kind of natural material — methane dissolved in stratum water. Its reserves exceed those of conventional gas raw stock many-fold, and are practically inexhaustible,

though they have not been utilised yet. The reason of this is that each borehole taken separately yields too little gas. It is likely that the gas content will increase with depth.

It is clear that the data from the Kola borehole confirm the necessity of introducing water percolation in porous media into the gamut of processes considered. Here we can rely on the data presented in numerous monographs, in particular, in works [209–212]. The dynamic situation in underground water collectors can analysed only by being based on the specific characteristics of porous media in specific areas being investigated. In this case, it is impossible to do without ultradeep drilling.

Oscillation of continents due to Earth's rotation and seasonal winds [213] causes increased percolation of water in zones shown in Fig. 20. Siting geothermal plants specifically in zones of intense volcanism would yield the greatest effect.

To gain an insight into the laws of deformation of the terrestrial crust and its evolution, it remains to consider the specific features of orogeny and earthquakes.

3.5. OROGENY AND OCCURRENCE OF EARTHQUAKES

Now we will discuss the irreversible processes occurring in Earth's interior.

First let us focus on the character of the terrain relief. Formation of ordered structures represented by mountain ranges indicates the presence of an intense energy flux from Earth's interior to outer space.

Here it would be appropriate to introduce a geometric scale of mountain structures, i.e. to consider both the location, accounted for by the configuration entropy, and the dimensions and shape of mountains. In addition, it is necessary to take note of the time scale reduced to the periodicity of specific phenomena during orogeny.

In our quest for elements of symmetry in tectonic heaves, we will start by considering processes occurring in individual circulation cells. The functional purpose of these cells is to supply water to deep strata and remove reaction products therefrom.

Our prime interest is in flows of heat, hydrogen and dislocations moving from reaction zones to Earth's surface. The dislocation flow ensures dissipation of potential and kinetic energy in Earth's interior similar to heat. This flow is manifested in the form of earthquakes. The case in point is periodic release of mechanical energy to the surface layers.

Hence, we are dealing with one of the types of creational-dissipative structures that act, in this case, in solid terrestrial masses. The principle of

emergence of these structures differs little from that investigated in fluid media. But certainly there are specific features worth discussing now.

As we have found, the possibility of oxidation of metals and metalloids by the oxygen in water is determined by the properties of their external oxide films. This is especially evident in underground conditions where the capillary forces practically proportion water supply to the reaction surface.

According to the principle of Pilling and Bedworth [214–216], if the volume of oxide formed is less than the volume of the metal or metalloid replaced thereby, the oxide film has a loose cellular structure, and cannot protect the metal or metalloid safely from further oxidation.

But if the ratio of the oxide volume and metal (or metalloid) volume is greater than unity, the oxide film formed has a compact continuous structure. It safely isolates the metal or metalloid from the affect of water vapour or oxygen and, hence, prevents their further oxidation.

The Pilling and Bedworth ratio ε is found from the formula

$$\varepsilon = \frac{M_{ox} \cdot \rho_{me}}{\rho_{ox} \cdot A_{me} \cdot n},$$

where M_{ox} is oxide molecular weight;

ρ_{ox} is oxide density;

ρ_{me} is metal or metalloid density;

A_{me} is atomic weight of metal or metalloid; and

n is the number of metal or metalloid atoms in the oxide formula.

Table 8 summarises the values of e for different metals and silicon. As Table 8 shows, $\varepsilon < 1$ for light metals: alkaline, alkali-earth and magnesium; and $\varepsilon > 1$ for heavy metals and aluminium. As Pilling and Bedworth state, the values of ε determine metal behaviour during corrosion: if $\varepsilon < 1$, the metal readily corrodes. At $1.31 < \varepsilon < 1.7$, the oxide film protects the metal safely from corrosion. This is why aluminium powder can be kept in water, though thermodynamic calculations indicate that this system should explode.

At $2.04 < \varepsilon < 3.92$, the oxide film experiences significant stresses, which can lead to its destruction.

In underground conditions, an aluminium alloy contains many impurities that contribute to formation of a loose oxide film.

Judging by Pilling and Bedworth ratios, the volume of oxides significantly exceeds the volume of the source alloy of silicon and iron, and aluminium. Therefore, the mass of oxides being accumulated should squeeze out overlying layers, resulting in orogeny.

Table 8

Ratio of oxide volume and metal or metalloid volume (ε) according to Pilling and Bedworth

Na	0.55	Al	1.45	Cu	1.70
K	0.45	Pb	1.31	Ti	1.73
Li	0.58	Cd	1.32	Fe	2.06
Sr	0.69	Sn	1.33	Mn	2.07
Ba	0.78	Zr	1.45	Co	2.10
Ca	0.64	Zn	1.59	Cr	3.92
Mg	0.81	Ni	168	Si	2.04

The rate of orogeny varies in different locations of the world. For example, the mountains in Altai grow at a rate of one meter annually, though, on the average, the annual rate is within 1 mm.

With account of the amount of water in the World Ocean, one could suggest that the mountains on our planet should grow rapidly. This opinion is supported by comparing the heights of mountains on Earth and Mars, where their height reaches 25 km.

Presently, there is evidence that specifically underground processes forced Africa away from Asia.

Orogeny is not a smooth process, and, as a rule, it involves earthquakes.

The majority of earthquakes originate at the depth of 60 km, i.e. within Earth's crust. In some regions, however, there is a large share of earthquakes with seismic centres at the depths of 200 to 700 km.

Presently, earthquake and volcano science is, in essence, descriptive [217–219]. However, with data on the rate of underground reactions and depth percolation of water becoming available, the periods of earthquakes can be estimated.

Earth's crust is known to be inhomogeneous and separated into blocks of various volume and shape, which can move independently to a certain extent. Affected by interior stresses, rock fractures in certain sites or displaces rapidly to originate, in essence, seismic waves and oscillations. Of course, it is necessary to know the strength properties of rock in a certain region to assess these phenomena.

At present, there are many options for strength testing of materials. Among these, one can distinguish investigations that establish a relationship between thermodynamics and the theory of elasticity [220]. Since elastic strain is reversible, the free energy of an elasto-strained body F is a function of state.

This serves as a basis for constructing thermodynamic formalism with regard to calculating the strength of elastic bodies [11].

Dislocation flows occur where the strength of rock is disturbed. These flows are estimated using well-known techniques [221].

The velocity of dislocation propagation to the surface depends on local conditions. For example, let us take the Tashkent earthquake in 1966. The magnitude of the first shock was 5.5 points; the hypocentre was at the depth of only 8 km, and the epicentre was in the downtown sector of the city. There was a total of 750 shocks of progressively diminishing magnitude. At this, the depth of seismic centres decreased on the whole from 8 to 2 km, though in separate cases there were also deep-focus shocks [122].

Hence, statistical data on earthquakes, combined with data on local terrestrial crust profiles and rates of depth reactions, allow forecasting natural disasters.

CONCLUSIONS

In conclusion, let us highlight the distinctive features of phase and chemical transformations, which have been presented above.

Thus, evaporation and condensation processes running in conditions close to equilibrium depend largely on the chemical potential value.

Due to this, the accepted methods of estimating heat-and-mass transfer intensity should be supplemented with computations based on thermodynamic formalism.

The evaporation process limits the temperature of reaction of alloys with water. The thermodynamics of reactions of interaction of aluminium, silicon and iron with water in the range of temperatures 300 K < T < 1,000 K has been investigated. The reactions considered have an extremely high probability.

The statement that reactions involving gassing proceed to the end has been confirmed. Thus, during interaction of aluminium and silicon with water, the reaction completeness equals unity. At low temperatures, the reaction of iron with water has the same value, but with increase in temperature the completeness of this reaction drops to 0.72.

The kinetics of interaction of aluminium, silicon and iron alloys with water has been investigated at temperatures within 0 °C to 400 °C, and pressure up to 15.0 MPa.

Comparison of selected systems has shown that, at equal temperature conditions, the rate of reactions is cymbate with variation of Gibbs' energy values. However, within the limits of each system, with increasing t, the values of W increase, irrespective of a certain decrease in value $\sum \nu_i \mu_i$.

As data published earlier have shown, at temperatures of flaring of alloys in oxygen or water vapour, the reaction rate values follow the variations in Gibbs' energy.

In the temperature range investigated, the rate of interaction of activated aluminium with water is higher by about two orders than that during interaction of water and iron-aluminium-silicon alloys. Evidently, alloys with a fine crystalline structure are highly active.

Detachment of reaction products is another critical factor that affects the kinetics of the gassing process. This is shown by the dependence of the reaction and heat-and-mass transfer rate on the hydrodynamic situation that occurs in high-pressure reactors.

The reactions investigated can serve as an analog of reactions occurring in Earth's interior.

The rate of underground reactions becomes limited at the stage of water percolation to the zone of contact with silicon alloys, followed by its concurrent evaporation, as well as at the stage of removal of solid products from the reaction zone.

The following factors have a critical affect on detachment of reaction products (oxides) being formed: tidal waves occurring in Earth's crust due to lunar and solar gravitation; and earthquakes and explosions on the terrain as well as irregular rotation of the Earth.

If the conditions of progress of deep reactions approach those observed in high-pressure vessels, the World Ocean should vanish from Earth in 3,000 years.

More accurate values for underground reactions can be obtained only by investigating the filtration capacities of deep water collectors, as this was done at the Kola ultradeep borehole.

Data on the rate of underground reactions in specific locations of Earth's crust, combined with statistical data on earthquakes, allow predicting the periods of occurrence of transient processes in Earth's interior.

CHAPTER 4

GEOTHERMAL POWER PLANTS

In this section, we will study the problem of practical conversion of the heat flow from Earth's interior. The problem can be traced as far back as the last century when Italy pioneered the construction of the first geothermal power plants, but so far this issue has not been duly treated.

As we will see, by studying the state of affairs in this area, there are critical and unsolved yet problems. The issue, however, cannot be considered hopeless.

4.1. THE ENERGY CAPACITY OF UNDERGROUND HEAT SOURCES

The thermal condition and the thermal history of Earth's interior is determined by the combined affect of interplanetary and cosmic processes.

The Sun, stars and galaxies affect Earth's thermal regime externally. The planet receives their radiation and different kinds of emission continuously. By example of processes occurring in the atmosphere and ocean, we found that solar radiation affects only a thin terrestrial surface layer.

With increasing depth, however, the temperature rises, as this has been established during mine development and borehole drilling. This proves the existence of energy sources in Earth's interior.

Large-scale heat evolution is caused by the following processes: decay of radioactive elements; chemical and phase conversions involving the origination of creational-dissipative structures, and finally, tidal effects.

Radioactive generation of heat energy is caused mainly by decay of uranium, thorium and potassium, which are concentrated in Earth's upper strata. The total amount of heat liberated by radioactive decay is estimated to be within $(0.6-2.0) \cdot 10^{31}$ J [222].

Approximately $1.2 \cdot 10^{31}$ J of heat could have been liberated in Earth's interior due to chemical and phase transitions [223].

Tectonic processes, as we have found from previous thermodynamic calculations, convert less than one percent of the chemical energy of interacting substances to mechanical energy, and subsequently, to heat.

The Earth experiences deformation effects due to solar and lunar gravitation. The energy being thereby evolved is expended on heating the planetary substance. The total amount of heat that evolved due to tidal effects during Earth's existence equals about 30 % of the radioactivity-generated heat [78].

The energy of the total heat flow from Earth's interior amounts to 25 TW, this being about eight times more than the capacity of all power plants worldwide [10, 12, and 78].

Nevertheless, this heat flow is four thousand times less than that received from the Sun.

The heat flow density differs widely in various regions of the planet. Its least value has been found in regions of development of ancient crystalline shields; increased values have been found, as a rule, in relatively young folding regions related to current volcano activity. For tectonically active regions, the heat flow density amounts to 0.1 W/m^2. As mentioned earlier, more accurate values of heat flow can be found by estimating the rate of chemical and phase transitions.

The superior drivers of tectonic processes are reactions of silicon alloys with water that penetrates into Earth's deep through terrestrial faults.

Indeed, it is extremely difficult to believe that the bulk of radioactive substances could be concentrated specifically in zones of orogenic displacements. This is also manifested by the low radioactivity of magma that gushes out during volcano eruptions.

Based on experimental data, it can be stated that radioactive substances, in decaying, increase the temperature in Earth's interior, thereby promoting chemical reactions.

Water circulating at great depths is heated to very high temperatures, and can be piped to the surface from wells. In regions of active volcanism, geothermal water, which rises to the surface via cracks in Earth's crust, has the highest temperature. On some occasions, hydrothermal sources yield steam-and-liquid flows with a temperature of 200–300 °C (the Pauzhetka field in Kamchatka, The Geysers in the U.S.A., Wairakei in New Zealand, Lardarello in Italy, and others) [82].

Natural circulation of flows carries to the terrestrial surface but a slight part of heat evolving during reactions. The bulk of this heat, however, is distributed within Earth's interior by heat transfer.

Many experts pin their hope on underground thermonuclear explosions to develop petrothermal occurrences. They believe that in this way the hot dry rock can be fissured. Then water will be pumped through a multitude of cracks, and the steam thus generated will be piped to power units located on the surface [224 and 225].

From the standpoint of the theory of lithosphere processes developed here, implementing thermonuclear explosions will lead to grave consequences. It is quite possible that underground explosions will intensify reactions in the deep underground, which will ultimately result in orogeny. Formation of mountain ranges in unpredictable places will change the wind rose. We have already considered the following scenario: the compression effect will retard Earth's rotation, and the ocean, moving by inertia, will wipe out cities in Europe, the Middle East and Western Africa. The water will gush through many canyons in the Cordilleras to America's flatlands, and will flood its inhabited locations. No better will be the case for Australia. The only safe place will be the Antarctica.

Such a prospect can hardly favour underground thermonuclear explosions. The sole alternative to underground explosions is deep drilling. In so doing, experts should develop techniques of telescopic drilling that would provide for connecting separate wells in the interior with small-section collectors. It is likely that geothermal wells could be stimulated by low-intensity chemical explosions.

Significant amounts of heat could be extracted by pumping water through a network of collectors with porous walls.

In conclusion of this section, we will estimate the energy potential of Earth's interior. The key zones of volcanic activity and geothermal fields are as follows: the Pacific Ocean Belt extending along the Pacific Ocean coastline; the group of islands located in the region of the Mid-Atlantic Ridge; the rift zone in Eastern Africa and the Middle East as well as the orogeny belt extending from the Mediterranean Basin of Europe through Asia to the Pacific Ocean (Fig. 20). Significant areas with geothermal fields are found on the coast of the Gulf of Mexico in the U.S.A.; in extensive regions in Western Siberia; in the Northern Alps and the Carpathian region, and in the Crimea Peninsula.

As the above figures show, active tectonic zones occupy about 10 % of Earth's surface, and hence, one can talk about long-term harnessing of a heat flow with an energy of 2.5–3 TW. With account of the efficiency of underground heat generators and surface power equipment, the installed capacity of geothermal power plants can amount to 1.0–1.2 TW.

Zones that would be promising for geothermal power plant development are being explored intensively. For example, the heat energy capacity of six regions in Kamchatka with active volcanism would suffice for constructing geothermal power plants with a capacity up to 365 MW; and, in developing fields to the depth of 3 km, the capacity reserves would increase to 400–800 MW [224 and 226].

Similar projects are being considered for Siberia and the Far East. Here the explored reserves of thermal water are 3.35 mln. m^3/day. Utilising these resources would allow saving 8.5 mln. t of valuable fossil fuel annually [227]. Several promising projects have been suggested for Crimea and the Carpathian region [228].

4.2. ANALYSING LIMIT CYCLES OF GEOTHERMAL POWER PLANTS

First we will trace the dynamics of electric power generation utilising underground heat.

In 1972, the capacity of Italian power plants in Lardarello amounted to 390 MW. After being commissioned, The Geysers power plant in the U.S.A. started generating 300 MW of geothermal power.

A 160 MW power plant was put into operation in Wairakei (New Zealand).

Iceland built a 3.4 MW geothermal power plant. Japan completed the construction of two power plants with the total capacity of 40 MW.

The construction of a 5 MW power plant near Pauzhetka in South Kamchatka was launched in 1964, and completed in 1967.

In early 1973, a 75 MW power plant had to be commissioned in Cerro-Prieto in Baja California (Mexico) [224]. In those times, power engineering based on low-potential heat could not compete yet with conventional power facilities. The situation changed dramatically in twenty years (Tables 9 and 10). As we can see, the capacity of power plants increased significantly, and the number of countries developing geothermal fields has grown. The same growth rate is also being observed presently.

GeoTPPs have a straightforward design, as seen in the schematic diagram in Fig. 36. It shows a power plant located in the valley of the Pauzhetka River in southern Kamchatka in the vicinity of the Koshelev and Kambalny volcanoes. The water-steam mixture with the calorific capacity of up to 840 kJ/kg is piped via wells to the surface and delivered to separators, which separate the steam from water under the pressure of 0.23 MN/m^2. The separated steam is delivered to turbines, and the hot water with a temperature of 120 °C is utilised for direct heating of houses in inhabited locations.

The first unit of the Pauzhetka GeoTPP has two 2.5 MW turbines. The surface condensers of the turbines are replaced with mixing ones, and the steam ejectors are replaced with water-jet ones. The process water supply is a direct-flow one, from the Pauzhetka River.

Table 9

Geothermal power plants worldwide

(data from Survey of Energy Resources, World Energy conference, 1993, 578 pp)

Country	Number of operated fields	Operating GeoTPPs		GeoTPPs being constructed		Total capacity of operating and being constructed GeoTPPs, MW	Capacity of GeoTPPs scheduled for construction, MW
		Number of units	Capacity, MW	Number of units	Capacity, MW		
U.S.A.	17	91	2756	10	601.8	3357.8	3331
The Philippines	4	26	1041	–	–	1041	2266
Mexico	2	16	700	15	325	1025	1290
Italy	4	39	548	14	298	846	1400
New Zealand	3	10	260	4	116	376	317
Japan	9	9	215	4	138	353	353
Indonesia	2	3	140	5	223	363	1272
El Salvador	1	3	95	5	75	170	175
Kenya	1	3	45	–	–	45	90
Iceland	3	5	41	1	30	71	71
Nicaragua	1	2	70	–	–	70	180
Turkey	1	1	21	1	5	26	130
China	11	19	18	5	14	32	32
Russia	1	1	11	1	200	211	–
France (Guadalupe)	1	1	4	–	–	4	4

Table 9 cont'd

Portugal (Azores)	1	1	3	–	–	3	13
Greece	1	1	2	1	0.8	2.8	3
Argentina	1	1	0.6	–	–	0.6	50
Romania	1	1	0.6	–	–	0.6	1
Zambia	1	1	0.2	–	–	0.2	0.2
Costa Rica	–	–	–	1	55	55	55
Guatemala	–	–	–	1	15	15	30
Ethiopia	–	–	–	1	3.5	3.5	3.5
Saint Lucia	–	–	–	1	0.9	0.9	5
Thailand	–	–	–	1	0.3	0.3	1
India	–	–	–	–	1	1	4
Other countries	–	–	0.6	–	0.5	1.1	160
TOTAL	66	234	5972	72	2102	8074.8	11236.7

Table 10

Utilisation of thermal water with temperatures of 60-90 °C

(data from Survey of Energy Resources, World Energy conference, 1993, 578 pp)

Country	Heating, heat pumps, hot water supply, MW	Greenhouses, husbandry, agriculture, MW	Oil producing industry, MW	Balneology, MW	Multi-purpose usage, MW	Total utilised		Annual energy savings, TNE×10^3
						Including balneology, MW	Excluding balneology, MW	
1. Bulgaria	No data	–	–	No data	135	135	–	50
2. China								
3. France	660	16	–	No data	–	676	–	266
4. Hungary	75	565	70	581	289	1580	999	630
5. Iceland	945	77	75	209	–	1306	1097	650
6. Italy	131	94	30	76	–	631	55	240
7. Japan	49	50	38	4475	152	4764	289	1675
8. New Zealand	42	2	105	26	1	176	150	111
9. Romania	30	85	No data	136	22	273	137	95
10. Russia	429	395	220	360	–	1404	1044	640
11. Turkey	34	4	–	97	65	200	103	75
12. U.S.A.	936	129	427	284	–	1776	1492	642
13. Yugoslavia	14	111	–	2	–	127	125	45
14. Other countries	68	55	4	103	59	289	186	111
TOTAL	3546	1729	1060	6674	723	13732	7058	5446

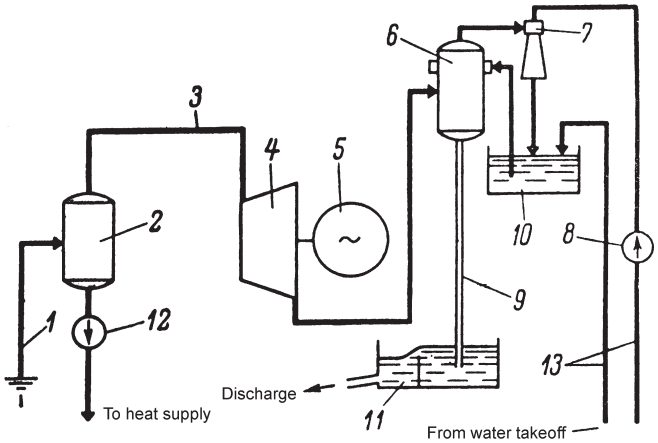

1 — well; 2 — separator; 3 — steam pipe; 4 — turbine; 5 — generator; 6 — mixing condenser; 7 — water-jet ejector; 8 — ejector pump; 9 — pressure gauge pipe; 10 — cooling water tank; 11 — drain well; 12 — hot water pump; 13 — cold water pipe.

Fig. 36. Schematic diagram of Pauzhetka geothermal power plant

The GeoTPP has no boiler room, fuel feed systems, ash collectors, and many other devices/equipment that are components of conventional fossil-fuel plants. The cost of power generation at this plant is several times less than at local diesel power plants [229 and 230].

In 1998-1999, Russia commissioned the Verkhne-Mutnovskaya GeoTPP with a capacity of 12 MW. Based on the performance indicators of this facility, a cascade of GeoTPPs are scheduled for development at the Mutnovsky hydrothermal field [231].

Several power plants in Italy utilise steam converters, this being explained by the high content of metal-corrosive gases in the underground steam. These gases are as follows: carbon dioxide, hydrogen sulphide, boracic acid, and ammonia.

In the infancy stage of geothermal power engineering, developers were challenged by the issues of both corrosion protection and removal of non-condensing gases from the condenser.

Utilising natural steam in steam converters, which generated pure steam for turbines, was a successful solution to both these problems (Fig. 37). The installation shown operates as follows.

Steam from well 1 is delivered to steam converter 2 where it transfers its heat to a secondary heat carrier circulating in a closed circuit: turbine — con-

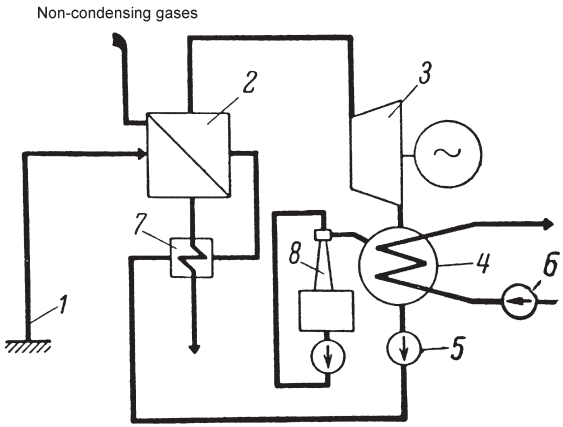

1 — well; 2 — steam converter; 3 — condensing turbine;4 — surface-type condenser; 5 — condensate feed pump; 6 — cooling water pump; 7 — water-water heat exchanger; 8 — ejector assembly.

Fig. 37. Schematic diagram of a geothermal power plant with a steam converter

denser — steam converter — turbine. The underground steam is condensed in the steam converter, and the non-condensed gases are discharged under excess pressure to the atmosphere or delivered to chemical production facilities. Pure secondary steam expands to drive turbine 3, and then flows to condenser 4. The condensate in apparatus 4 is discharged by pump 5 and delivered to stream converter 2 via heat exchanger 7. In heat exchanger 7, the turbine condensate is heated by the cooling underground steam condensate. Water-jet ejector 8 serves for removing air that leaks into the condenser through non-tight seals [229].

Further refinement of GeoTPPs is focused to developing binary cycles and utilising corrosion-resistant materials. This approach stems from the fact that a major share of explored geothermal fields comprises low-temperature sources where the water temperature is within 80-100 °C. In this case, developers suggest employing two-circuit schemes and utilising Freon as the working medium.

Utilising the hydro-steam cycle instead of the Freon one will not only exclude thermodynamic losses inherent to the two-circuit scheme, but will also allow excluding all kinds of heat exchange apparatus. This fact could be of critical importance because in conditions of low temperature differentials the surface of heat exchangers related to efficient capacity can increase dramatically and comprise the major share of capital investment required [232].

Analysis of limit cycles of power plants with steam and hydro-steam turbines has shown that electric power output in the latter case is 2.4 times higher than that in the former one [10].

It is worth mentioning that the Kaluga Turbine Plant and NPVP "Turbokon" have launched pilot production of hydro-steam turbines [228].

4.3. ENVIRONMENTAL ISSUES OF EXPLOITATION OF UNDERGROUND ENERGY RESERVES

To operate specific GeoTPPs, a developed infrastructure of wells, pipelines, electric transmission lines, and roads should be provided. Drilling wells involves supply and storage of diesel fuel, lubricants, and spare parts. Certainly, the entire gamut of above activities should be executed in strict compliance with environmental regulations.

As mentioned earlier, underground water carries to Earth's surface hydrogen sulphide, ammonia, mercury compounds and other substances having an adverse environmental impact.

Each hydrothermal field should have its own system of reclaiming and neutralising hazardous substances.

Intensification of natural circulation of flows in the vicinity of a GeoTPP can possibly result in an increased rate of underground reactions associated with earthquakes. In this case, it is necessary to erect earthquake-resistant buildings and drilling rigs.

Meeting environmental control and labour safety requirements will involve an increase in power generation cost. As a rule, this increase is not so substantial as compared to that incurred at coal-fired TPPs.

Let us highlight one more issue related to operating GeoTPPs. Underground well collectors get clogged with rock and deposition in time. On the one hand, this phenomenon is caused by the presence of salts in underground water, and on the other hand, it results from pressing out of upper terrestrial strata by solid products of underground reactions. In estimating the forces arising in underground conditions, we can draw on the valuable experience gained in mine development [233-235].

In any case, employing maintenance drilling to restore the performance of geothermal fields is an option to be considered.

CONCLUSIONS

Developing the second-ranking energy source — underground heat — will allow generating within 1.0 to 1.2 TW of electric power.

The dynamics of development of geothermal power plants indicates that the majority of countries are interested in utilising underground energy.

The most promising method of geothermal field development is deep drilling.

The optimal heat engine for a GeoTPP is a hydro-steam turbine.

Since GeoTPPs are located, as a rule, in regions of active volcanism, the buildings, drilling rigs and equipment should comply with regulations set forth for earthquake-hazardous areas.

AFTERWORD TO PART II

Here, as in Part I of the book, we will discuss the activities required for utilising renewable energy sources.

Thus, having examined the most likely cosmic processes and transient phenomena during the period of Earth's formation, we have gained some insight into Earth's structure and the processes occurring in its interior.

Clearly, the key to interpreting underground processes can be found only by discovering the regularities of natural circulation of flows in the deep. It was natural circulation of water in underground conditions, involving its partial interaction with silicon alloys that made the World Ocean share its hydrogen with oil and gas fields. Evidently, besides utilising heat flows, in the immediate future it is necessary to start utilising hydrogen and methane flows from Earth's interior.

Within the topical framework of this book, it is impossible to consider in detail such an extensive and exciting issue. However, we will give a brief presentation of activities being conducted in this area.

One of the paths of oil formation could have been the processes of high-temperature high-pressure action on the organic substrate that emerged due to the vital activities of hydrogen-oxidising bacteria. This was considered in Part I of the book.

One of the first steps aimed at validating this assumption was conducting experiments on growing bacteria based on hydrogen obtained by interaction of activated aluminium and silicon alloys with water.

It was found that microbes develop well by consuming hydrogen from the first reaction, but reproduce somewhat slower in the second case. There is nothing strange about this because bacteria are very sensitive to different impurities in aqueous solutions. For example, a deficiency of but 1 ppm of germanium in the composition of nutritive substances cancels growth of these bacteria.

One can also wonder at the rate of protein growth: in favourable conditions the mass of bacteria doubles every four hours. For comparison, trees in the midlatitudes of our country increase their mass 4-fold annually. So creating fields with billions of tons of oil was no challenge for bacteria.

To implement the program of utilising hydrogen flows, it is necessary first to revert to the earlier suggested project of drilling the terrestrial crust in the Tunkin depression adjacent to the Lake Baikal trough. Here, at the depths of only six to eight kilometres, extraordinarily high electric conductivity of the terrestrial crust has been recorded. It was assumed that this is the result of rising of hydrogen-saturated anoxic substances from Earth's interior [236].

It is also necessary to investigate the behaviour of several volcanoes and find a method of utilising the hydrogen they eject. The same investigations will seemingly allow to estimate the intensity of methane flow from Earth's interior.

Similar to space programs, ultradeep drilling can be effected by the joint efforts of developed countries. It will reveal the picture of the underground world and make it possible to estimate more accurately the local flows of underground heat. At the same time, this will allow estimating the stresses and compressions of the terrestrial crust in rifting zones, which is imperative for understanding the regularities of earthquakes.

The memory of those many people who perished in earthquakes insistently demands studying the mechanism of this extremely disastrous natural phenomenon. We have to learn to not only predict the occurrence of earthquakes, but, if possible, control them. In anticipation of this, it is necessary to adopt an international agreement on limiting the number of small and medium-scale explosions, and impose a total ban on nuclear and thermonuclear tests. Presently, there is no guarantee that, at the site of the next thermonuclear explosion, a mountain range towering to dozens of kilometres will appear; and whose formation will consume the bulk of the World Ocean water.

Here we once again stress the necessity of expanding the expertise of the scientific community in thermal processes. This will pave the way to resolving many critical issues.

For example, when building models of cosmic processes based on thermodynamics, many imaginary projects will be no longer relevant.

As is well known, in one of the statements of the second law of thermodynamics suggested by Thompson, the law of entropy growth was suggested to be considered as the law of dissipation of radiant energy.

According to this statement, the heat of heated bodies dissipates in the Universe, and there are no processes that could concentrate in one place and initiate its active functioning [237].

Anyway, we are unaware of conditions resulting in concentration of radiant energy. Hence, growth of entropy of the Universe is an indisputable fact. In this connection, it is worth stressing once again that, in constructing models of cosmic processes, one cannot depart from the laws of thermodynamics. This pertains equally to the process of formation of planets and, in particular, of Earth. The key role in formation of planets belongs to creational-dissipative structures that ensure redistribution of energy in their mantles.

Mastering the methods of thermodynamics in all respects would allow engineers to develop highly efficient installations for utilising low-potential heat.

The Earth is our native home, though unfortunately not so big as one would like it to be — the international space station orbits the planet in just an hour. It would be naive to believe that such a small planet possesses inexhaustible reserves of coal, oil and gas. Most likely, these reserves will be depleted far before the coming of the catastrophic global warming which is alarming the majority of countries.

The alternative to this situation is but one — to learn to utilise renewable energy sources.

REFERENCES

1. Ambartsumian V.A. Scientific Works. 2 volumes. — Yerevan: Publ. AS Armenian SSR, 1950. — v. 2. — 362 pp.

2. Baranov V.I. Age and Evolution of Earth's Substance. — M.: Nauka Publishers, 1971. — 20 pp.

3. Vinogradov A.P. Origin of Earth's Mantles // Vesn. AS USSR, 1962. — № 9 — p. 16–29.

4. Hawking S. A Brief History of Time: From the Big Bang to Black Holes. — M.: Mir Publishers, 1990. — 168 pp. (Translated to Russian).

5. Pannekuk A. History of Astronomy. — M.: Nauka Publishers, 1966. — 592 pp.

6. Vorontsov-Veliaminov B.A. Laplace. — M.: Nauka Publishers, 1985. — 288 pp.

7. Alfven H. and Arrhenius G. Structure and Evolutionary History of the Solar System. — K.: Nauk. Dumka Publishers, 1981. — 332 pp. (Translated to Russian)

8. Novikov I.D. Evolution of the Universe. — M.: Nauka Publishers, 1990. — 192 pp.

9. Gurevich L.E. and Chernin A.D. Origin of Galaxies and Stars. — M.: Nauka Publishers, 1988. — 190 pp.

10. Troshenkin B.A. Renewable Energy. In 2 Parts. — Part I. — Thermodynamics of the Ocean and the Atmosphere. Ocean Thermal Energy Conversion Plants. — Kharkov: Fort Publishers, 2003. — 104 pp. (www.library.ulstu.ru/news/bulet/03_2004.doc; www.iitd.ernet.in/acad/library/services/recent/july04.html)

11. Physical Encyclopaedic Reference: 5 volumes. — M.: Sov. Encycl. Publishers, 1960–1966. — v. 1. — pp. 367–370; v. 4. — pp. 569–578.

12. Comprehensive Soviet Encyclopaedia: 30 volumes. — M.: Sov. Encycl. Publishers, 1970–1978. — v. 6. — pp. 51–54; v. 24. — pp. 150–154.

13. Bakulin P.I., Kononovich E.V., and Moroz V.I. Course of General Astronomy. — M.: Nauka Publishers, 1974. — 512 pp.

14. Agekian T.A. Stars, Galaxies and Metagalaxies. — M.: Nauka Publishers, 1982. — 416 pp.

15. Gorbatsky V.G. Introduction to Physics of Galaxies and Galaxy Clusters. — M.: Nauka Publishers, 1986. — 256 pp.

16. Stratonov V.V. The Sun. An Astronomical Popular Monograph. — Tiflis: "Lieberman and Co." Publ., 1910. — 248 pp.

17. Waldmeier M. Ergebnisse und Probleme der Sonnenforschung. — M.: Inostr. Lit. Publishers, 1950. — 240 pp. (Translated to Russian)

18. Frank-Kamenetsky D.A. Physical Processes Inside Stars. — M.: State Publ. Phys.-Math. Liter., 1959. — 544 pp.

19. Schwarschild M. Structure and Evolution of the Stars. — M.: Inostr. Liter. Publishers, 1961. — 192 pp. (Translated to Russian)

20. Zeldovich Ya.B. and Novikov I.D. Structure and Evolution of the Universe. — M.: Nauka Publishers, 1975. — 736 pp.

21. Tayler R.J. The Stars: Their Structure and Evolution. — M.: Mir Publishers, 1973. — 280 pp. (Translated to Russian)

22. Golitsyn G.S. Introduction to Dynamics of Planetary Atmospheres. — L.: Gidrometeoizdat Publishers, 1973. — 104 pp.

23. Discovery. Diploma № 274 (USSR). The Pulsating Property of the Sun / V.A. Kotov, A.B. Severny, and T.T. Tsap. — Publ. in Bull. Discov. and Inventions., 1963. — № 48. — p. 3.

24. Kotov V.A., Severny A.B., and Tsap T.T. Investigating the Global Oscillations of the Sun // Izv. Crimean Astrophysical Observatory, 1983. — v. 66. — p. 3.

25. Shklovsky I.S. Stars: Their Birth, Life and Death. — M.: Nauka Publishers, 1984. — 384 pp.

26. Physics of the Cosmos: Concise Encyclopaedia. — M.: Sov. Encycl. Publishers, 1986. — 783 pp.

27. Weyl H. Symmetry. — M.: Nauka Publishers, 1968. — 192 pp. (Translated to Russian)

28. Wigner E. Symmetries and Reflections. — M.: Mir Publishers, 1971. — 320 pp. (Translated to Russian)

29. Sirotin Yu.I. and Shaskolskaya M.P. Fundamentals of Crystal Physics. — M.: Nauka Publishers, 1979. — 640 pp.

30. Zheludev I.S. Symmetry and its Applications. — M.: Energoatomizdat Publishers, 1983. — 304 pp.

31. Elliott J. and Dawber P. Symmetry in Physics. 2 vols.. — M.: Mir Publishers, 1983. — v. 1. — 366 pp.; v. 2. — 412 pp. (Translated to Russian)

32. Astrofisica e Cosmologia Gravitazione Quanti e Relativita. — M.: Mir Publishers, 1982. — 560 pp. (Translated to Russian)

33. Hargittai I. and Hargittai M. Symmetry through the Eyes of a Chemist. — M.: Mir Publishers, 1989. — 496 pp. (Translated to Russian)

34. Functional Materials for Science and Engineering. — Kharkov: Institute for Monocrystals, 2001. — 624 pp.

35. Bader R. Atoms in Molecules: A Quantum Theory. — M.: Mir Publishers, 2001. — 534 pp. (Translated to Russian)

36. Glansdorff P. and Prigogine I. Thermodynamic Theory of Structure, Stability and Fluctuations. — M.: Mir Publishers, 1973. — 280 pp. (Translated to Russian)

37. Careri G. Ordine e Disordine Nella Materia. — M.: Mir Publishers, 1985. — 230 pp. (Translated to Russian)

38. Klimontovich Yu.L. Turbulent Motion and Structure of Chaos. — M.: Nauka Publishers, 1990. — 320 pp.

39. Kondepudi D. and Prigogine I. Modern Thermodynamics: From Heat Engines to Dissipative Structures. — M.: Mir Publishers, 2002. — 462 pp. (Translated to Russian)

40. An Album of Fluid Motion / Assembled by M. van Dyke. — M.: Mir Publishers, 1986. — 184 pp. (Translated to Russian)

41. Dickerson R., Gray H., and Haight G. Jr. Chemical Principles. 2 vols. — M.: Mir Publishers, 1982. — v. 1. — 652 pp; — v. 2. — 620 pp. (Translated to Russian)

42. Yerofeev B.A. Generalised Equation of Chemical Kinetics and its Application to Reactions Involving Solids. — Dokl. AN SSSR, — 1946. — 12. — № 6. — pp. 515–518.

43. Lepin L.K., Tetere A., and Schmidt A. On Interaction of Aluminium with Water. — Dokl. AN SSSR, 1953. — 88. — № 5. — pp. 871–874.

44. Troshenkin B.A. and Dolgikh T.N. Thermodynamics and Kinetics of Interaction of Aluminium Alloys with Water. — Vopr. atom. nauki i tekhniki. Ser. Atomno-vodorod. energetika, 1982. — Issue. 3. — pp. 51–52.

45. Villat H. Lecons sur la Theorie des Tourbillons. — L. — M.: ONTI NKTP, 1936. — 200 pp. (Translated to Russian)

46. Modern Hydrodynamics. — M.: Mir Publishers, 1984. — 502 pp.

47. History of Mechanics. — M.: Nauka Publishers, 1972. — 414 pp.

48. Taylor G.I. Diffusion by Continuous Movements. — Proc. Lond. Math. Soc., 1921. — v. 20. — p. 196.

49. Kolmogorov A.N. Local Structure of Turbulence in a Non-Compressible Fluid at Very Large Reynolds Numbers. — Dokl. AN SSSR, 1941. — v. 30. — pp. 299–303.

50. Troshenkin B.A. Circulation and Film Evaporators, and Hydrogen Reactors. — Kiev: Nauk. Dumka Publishers, 1984. — 174 pp. (www.eugene980.narod.ru/lit.htm)

51. Inv. Cert. 435,6625 (U.S.S.R.). Film Evaporator/ B.A. Troshenkin, Yu.N. Piskunov, V.G. Ponomarenko et al.. — Publ. In Bull. Inv., 1974, № 133.

52. Pat. 367,132 Sweden, IPC B01D1/22. Film Evaporator/ B.A. Troshenkin, G.I. Soloviova , Yu.N. Piskunov et al. (U.S.S.R.). — Publ. 29.08.74.

53. Pat. 388,0702 U.S.A., IPC B01D1/22. Film Evaporator/ B.A. Troshenkin, G.I. Soloviova , Yu.N. Piskunov et al. (U.S.S.R.). — Publ. 29.04.75.

54. Pat. 1,415,441 Great Britain, IPC B01D1/22. Film Evaporator/ B.A. Troshenkin, G.I. Soloviova, Yu.N. Piskunov et al. (U.S.S.R.). — Publ. 26.11.75.

55. Pat. 994,227 Canada, IPC B01D1/22. Film Evaporator/ B.A. Troshenkin, G.I. Soloviova , Yu.N. Piskunov et al. (U.S.S.R.). — Publ. 03.08.76.

56. Pat. 7,326,211 France, IPC B01D1/22. Film Evaporator/ B.A. Troshenkin, G.I. Soloviova , Yu.N. Piskunov et al. (U.S.S.R.). — Publ. 09.09.77.

57. Pat. 54,232 Finland, IPC B01D1/22. Film Evaporator/ B.A. Troshenkin, G.I. Soloviova , Yu.N. Piskunov et al. (U.S.S.R.). — Publ. 31.07.78.

58. Pat. 2,333,885 FRG, IPC B01D1/22. Film Evaporator/ B.A. Troshenkin, G.I. Soloviova , Yu.N. Piskunov et al. (U.S.S.R.). — Publ. 18.01.79.

59. Pat. 12,282 Japan, IPC B01D1/22. Film Evaporator/ B.A. Troshenkin, G.I. Soloviova , Yu.N. Piskunov et al. (U.S.S.R.). — Publ. 21.10.80.

60. Inv. Cert. 324,038 (U.S.S.R.). Distribution Device / B.A. Troshenkin. — Publ. Bull. Inv., 1972, № 35.

61. Inv. Cert. 636,003 (U.S.S.R.). IPC B01D1/22. Film Evaporator/ B.A. Troshenkin and G.I. Soloviova . — Publ. Bull. Inv., 1978, № 45.

62. Inv. Cert. 247,248 (U.S.S.R.). Pneumatic Pulsator / S.M. Korpacheva, V.M. Muratov, L.S. Rachinsky et al. — Publ. Bull. Inv., 1970, № 35.

63. Golubentsov A.A. Thermodynamics of Industrial Processes. — Kiev: Tekhnika Publishers, 1969. — 160 pp.

64. Troshenkin B.A. and Zolotov G.L. Selecting Apparatus for Evaporating Soda-Potash Solutions. — M.: TsINTIKhimneftemash, 1969. — Data sheet. — Ser. XM-1, № 9. — 4 pp.

65. Chirva V.I. and Golovchenko O.A. Investigating the Hydraulic Circuit of an Evaporator // Khim. Tekhnologia (Chemical Technology), 1973. — Issue 2. — pp. 32–33.

66. Mathematical Encyclopaedia: 5 vols. — M.: Sov. Encycl. Publishers, 1977–1985. — v. 2. — p. 466.

67. Butusov K.P. The Golden Section in the Solar System. // Coll. "Astrometry and Celestial Mechanics". — M.-L., 1978. — pp. 475–500.

68. Siegel F.Ju. Astronomical Mosaic. — M.: Nauka Publishers, 1987. — 176 pp.

69. Idlis G.M. Revolutions in Astronomy, Physics and Cosmology. — M.: Nauka Publishers, 1985. — 232 pp.

70. Campbell J.A. Chemical Systems: Energetics. Dynamics. Structure. 3 vols. — M.: Mir Publishers, 1975. v. 1. — 552 pp. (Translated to Russian)

71. Riemann B. Collected Mathematical Works. — M.- L.: Gos. Izdat. Tekhniko-Teoret. Lit. Publishers, 1948. — 279 pp. (Translated to Russian)

72. Mathematics in the Modern World. — M.: Mir Publishers, 1967. — 206 pp. (Translated to Russian)

73. Liapunov A.M. General Problem on Motion Stability. — M.-L.: Gos. Izdat. Tekhniko-Teoret. Lit. Publishers, 1950. — 472 pp.

74. Chetayev N.G. Motion Stability. — M.: Nauka Publishers, 1990. — 176 pp.

75. Langweilwer H. Zur Frage der mit den heutigen Treibpulvern Maximal Erreichbaren Geschogeschwindigkeiten // Zeitschrift fur technische Physik, 1938. — 11. — S. 416–421. (Translated to Russian)

76. Ballistic Installations and their Application in Experiments / ed. N.A. Zlatin and G.I. Mishin. — M.: Nauka Publishers, 1974. — 344 pp.

77. Schternfeld A.A. Paradoxes in Cosmonautics. — M.: Nauka Publishers, 1991. — 160 pp.

78. Bott M. The Interior of the Earth. — M.: Mir Publishers, 1974. — 374 pp. (Translated to Russian)

79. Bolt B. Inside the Earth: Evidence from Earthquakes. — M.: Mir Publishers, 1984. — 189 pp. (Translated to Russian)

80. Hallam A. Great Geological Controversies. — M.: Mir Publishers, 1985. — 216 pp. (Translated to Russian)

81. Holland H. The Chemical Evolution of the Atmosphere and Oceans. — M.: Mir Publishers, 1989. — 552 pp. (Translated to Russian)

82. Mining Encyclopaedia: 5 vols. — M.: Sov. Encycl. Publishers, 1984–1991. — v. 1. — pp. 452–454; v. 2. — pp. 371–386.

83. Physical Encyclopaedia: 3 vols. — M.: Sov. Encycl. Publishers, 1989–1991. v. 2. — pp. 78–80.

84. Fourmarier P. Le Probleme de la Derive des Continents. — M.: Nedra Publishers, 1971. — 83 pp. (Translated to Russian)

85. Sholpo V.N. Earth's Structure: Orderliness or Disorder? — M.: Nauka Publishers, 1986. — 160 pp. (Translated to Russian)

86. Troshenkin V.B. Improving the Process of and Reactor for Producing Hydrogen from Water by Means of Alloys Obtained from the Inorganic part of Coal: Abstract. Thesis Cand. Sci. (Eng.). — Kharkov: Kharkov State Polytechnic University, 1999. — 16 pp.

87. Thermodynamic Properties of Individual Substances. Reference Edition 4 vols. — M.: Nauka Publishers, 1978. — v. 1. — Book 2. — 328 pp.; v. 2. — Book 2. — 344 pp.; v. 3. — Book 2. — 400 pp.; v. 4. — Book 2. — 560 pp.

88. Marov M.Ya. Planets of the Solar System. — M.: Nauka Publishers, 1981. — 256 pp.

89. Zharkov V.N. Inner Structure of the Earth and Planets. — M.: Nauka Publishers, 1983. — 416 pp.

90. Physicochemical Properties of Oxides. Reference Guide. — M.: Metallurgia Publishers, 1978. — 472 pp.

91. Pelikan A. Molten Rock. — M.: Metallurgizdat Publishers, 1959. — 288 pp.

92. Yershov G.S. and Cherniakov V.A. Structure and Properties of Liquid and Solid Metals: — M.: Metallurgia Publishers, 1978. — 248 pp.

93. Beliaev A.N., Rappoport M.B., and Firsanova L.A. Electric Metallurgy of Aluminium. — M.: Metallurgizdat Publishers, 1953. — 720 pp.

94. Reference Book on Non-Ferrous Metals for Metallurgists. — M.: Metallurgia Publishers, 1971. — 560 pp.

95. Tugarinov A.I. General Geochemistry. — M.: Atomizdat Publishers, 1973. — 288 pp.

96. Markhinin Ye.K. Volcanoes and Life. — M.: Mysl' Publishers, 1980. — 198 pp.

97. Vernadsky V.I. and Kurbatov S.M. Terrestrial Silicates, Aluminium Silicates and Their Analogs. — L., M.: ONTI NKTP, Chief Editorial Board for Geological Survey and Geodesy Lit., 1937. — 376 pp.

98. Druianov V.A. Mysterious Biography of the Earth. — M.: Nedra Publishers, 1989. — 160 pp.

99. The Geological Systems: The Precambrian. Vol. 2, ed. K. Rankama — M.: Mir Publishers, 1968. — 384 pp. (Translated to Russian)

100. Combustion Fuel in the U.S.S.R.. Reference Book. — M.: Energia Publishers, 1979. — 128 pp.

101. Shpirt M.Ya., Kler V.R., and Pertsikov I.Z. Inorganic Components of Solid Fuels. — M.: Khimia Publishers, 1990. — 240 pp.

102. Reference Book on the Content of Rare Elements in Commercial Products of Coal-Mining and Coal-Concentrating Enterprises in the Donets Basin. — Dnepropetrovsk: Ukrainian State Inst. For Mineral Resources DO, 1994. — 188 pp.

103. Litvinenko A.I., Gromov V.A., Yanko S.V., Kabanov A.I., and Troshenkin B.A. Requirements to Coal Waste used for Melting Ferro-Silica-Aluminium // Metallurgy. Proc. Zaporozhye State Engineering Academy, 2003. — Issue 7. — pp. 38–40.

104. Litvinenko O.I., Gromov V.A., Yanko S.V., Chuprina Ye.S., and Troshenkin B.A. Melting Ferro-Silica-Aluminium from Coal Concentration

Waste // Metallurgy. Proc. Zaporozhye State Engineering Academy, 2004. — Issue. 10. — pp. 33–37.

105. Baisanov S.O., Tolymbekov M.Zh., Takenov T.D. et al. Developing the Technology of Electric Thermal Melting of Ferro-Silica-Aluminum from Coal Waste at OJSC "Ispat-Karmet" // Steel. — 2000. — № 7. — pp. 28–30.

106. Baisanov S.O., Tolymbekov M.Zh., Akhmetov A.B. et al. Obtaining Ferro-Silica-Aluminum from High Ash-Content Carbonaceous Rock // Modern Problems in Metallurgy (Proc. Inst. Ferrous Metallurgy). — Dnepropetrovsk: IChM NAS Ukraine, 2001. — v. 2. — pp. 248–251.

107. Zakharov M.V. and Zakharov A.M. High-Temperature Alloys. — M.: Metallurgia, 1972. — 384 pp.

108. Investigations at High Temperatures. — M.: Inostr. Lit. Publishers, 1962. — 480 pp. (Translated to Russian)

109. Kulikov I.S. Thermodynamics of Carbides and Nitrides. Reference Guide. — Cheliabinsk: Metallurgia Publishers, 1988. — 320 pp.

110. Petrov V.P. Magma and Genesis of Magmatic Rock. — M.: Nedra Publishers, 1972. — 136 pp.

111. Problems in Nuclear Science and Engineering. — Kharkov: National Scientific Centre "Kharkov Physical Engineering Institute", 1999. — 140 pp.

112. Concise Handbook for Geochemistry. — M.: Nedra Publishers, 1977. — 184 pp.

113. Chemistry and Technology of Rare and Disseminated Elements. 3 Parts: — M.: Vysshaya Shkola Publishers, 1976. — Part 1. — 368 pp.; — Part 2. — 360 pp.; — Part 3. — 320 pp.

114. Kozin L.V. and Volkov S.V. Chemistry and Technology of High-Purity Metals and Metalloids. 2 vols. — Kyiv: Nauk. Dumka Publishers, 2002. — v. 1. — 542 pp.; v. 2. — 352 pp.

115. Kol'skaya Ultradeep. — M.: Nedra Publishers, 1984. — 490 pp.

116. Silicon. Collection of articles. — M.: Inostr. Lit. Publishers, 1960. — 436 pp. (Translated to Russian)

117. Gold P.V. and Riabov R.A. Hydrogen in Metals and Alloys. — M.: Metallurgia Publishers, 1974. — 272 c.

118. Hydrides of Transition Metals. — M.: Mir Publishers, 1975. — 312 pp.

119. Gases and Oxides in Aluminium Alloys. — M.: Metallurgia Publishers, 1975. — 264 pp.

120. Constants of Interaction of Metals with Gas. Reference Guide. — M.: Metallurgia Publishers, 1987. — 368 pp.

121. Basteev A.V., Obolensky M.A., and Solovey V.V. Activation of Hydrogen and Hydrogen-Containing Energy Carriers. — Kyiv: Nauk. Dumka Publishers, 1993. — 164 pp.

122. Derpgolts V.F. Water in the Universe. — L.: Nedra Publishers, 1971. — 224 pp.

123. Garrels R.M. Circulation of Carbon, Oxygen and Sulphur During Geological Time. — M.: Nauka Publishers, 1975. — 48 pp. (Translated to Russian)

124. Latimer W.M. The Oxidation States of the Elements and Their Potentials in Aqueous Solutions. — M.: Inostr. Lit. Publishers., 1954. — 400 pp. (Translated to Russian)

125. Garrels R.M. and Christ C.L. Solutions, Minerals and Equilibria. — M.: Mir Publishers, 1968. — 368 pp. (Translated to Russian)

126. Geology and Geochemistry of Mineral Deposits. International Geological congress. Report of the 23 Session. Czechoslovakia, 1968. — M.: Mir Publishers, 1971. — 272 pp. (Translated to Russian)

127. Kirillin V.A., Sheindlin A.Ye., and Shpilrein E.E. Thermodynamics of Solutions. — M.: Energia Publishers, 1980. — 288 pp.

128. Nekrasov B.V. Fundamentals of General Chemistry. 2 volumes. — M.: Khimia Publishers, 1974. — v. 1. — 656 pp.; — v. 2. — 688 pp.

129. Nusselt W. Die Overflachenkondensation der Wasserdampfes — Z. Ver. Dtsh. Ing., 1916, 60, № 27, S. 541–546; № 28, S. 569–573.

130. Ten-Bosch. Heat Transfer. — M.: Petr. Publishers, 1930. — 220 pp.

131. Mikheev M.A. and Mikheeva I.M. Fundamentals of Heat Transfer. — M.: Energia Publishers, 1973. — 320 pp.

132. General-Purpose Vertical Tubular Evaporators. Reference Catalogue. — M.: TsINTIKhIMNEFTEMASH, 1965. — 52 pp.

133. Troshenkin B.A. and Gerasimenko A.V. Intensification of the Process of Evaporation of Black Sulphate Alkali in an Ascending Film. — In book: Chemical Machine-Building. K.: Tekhnika Publishers, 1969. — pp. 72–74.

134. Reduction-Cooling Installations. Reference Catalog — M.: NIIINFORMTIAZHMASH, 1964. — 14 pp.

135. Ilyin A.K. and Skachkov A.M. Injection Steam Coolers in Marine Power Plants. — L.: Sudostroenie Publishers, 1968. — 112 pp.

136. Isachenko V.P., Osipova V.A., and Sukomel A.S. Heat Transfer. — M.: Energoizdat Publishers, 1981. — 418 pp.

137. Isachenko V.P., Salomzoda F., and Shalakhov A.A. Investigating Heat Transfer at Droplet Condensation of Water Vapour in a Vertical Tube // Teploenergetika (Heat Engineering), — 1980. — № 4. — pp. 13–16.

138. Yastrzhembsky A.S. Engineering Heat Dynamics. — M.; L.: Gosenergoizdat Publishers, 1960. — 495 pp.

139. Gukhman A.A. On the Fundamentals of Thermodynamics. — M.: Energoatomizdat Publishers, 1986. — 384 pp.

140. RTM 26-01-71-75. Evaporators with a Streaming Down Film: Procedure for Thermal and Hydromechanical Design / B.A. Troshenkin. — M.: Minkhimmash, 1975. — 58 pp.

141. Troshenkin B.A. RTM 26-01-71-75. Evaporators with a Streaming Down Film: Procedure for Thermal and Hydromechanical Design. — Chemical and Oil-Refining Industry Machine-Building, 1975. — № 5. — pp. 4–5.

142. J.W. Gibbs. Scientific Writings in Thermodynamics. — M.; L.: Gosizdat. Tekhniko-Teoret. Lit. Publishers, 1950. — 492 pp. (Translated to Russian)

143. Lewis G.N. and Randall M. Thermodynamics and the Free Energy of Chemical Substances. — L.: ONTI KHIMTEORET, 1936. — 532 pp. (Translated to Russian).

144. Summary Analysis of the Questionnaire on the Use of Hydrogen for Meteo-rological Purposes. CIMO-VIII/Doc. 33, Appendix, 1982. — 12 p.

145. Kostron H. Aluminium und Gas//Z. Metallk., 1952. — 43. — № 8. — S. 269–284.

146. Zhuravlev V.A. and Zakharov A.P. Oxidation of Aluminium in Water at Different Temperatures // Dokl. AN SSSR, 1980. v. 252. — № 5. — pp. 1162–1166.

147. Inv. Cert. 535,364 U.S.S.R., IPC C22C21/00. Alloy Based on Aluminium for Producing Hydrogen / Sokolsky D.V., Kozin L.F., Barmin V.P. et al. — Publ. Bull. Inv., 1976, № 42.

148. Troshenkin B.A. Heat Transfer during Hydrogen Liberation in Reactions of Aluminium-Silicon Alloys With Water // Heat-and-Mass Transfer MMF-92: Proc. Minsk Int. Forum on Heat-and-Mass Transfer (Minsk, 1992) Minsk: ANK ITMO ANB, v. 3. — pp. 89–92.

149. Troshenkin B.A., Troshenkin V.B. Heat Transfer During Liberation of Hydrogen in Reactions of Amorphous-Crystalline Alloys With Water // Inzh.-Fiz. Zhurnal. — 1996. — v. 69, № 6. — pp. 1006–1008.

150. Sokolov Ye.A. and Singer A.M. Spray Apparatus. — M.: Energoatomizdat Publishers, 1989. — 351 pp.

151. Poroliu L.V. Air-Gas Fluid Lifters (Air-Gas Lifts). — M.: Mashinostroenie, 1969. — 160 pp.

152. Akopian B.A. Developing a Procedure for Designing the Operational Regimes of a Cyclic Gas Lift: Abstract. Thesis. ... Cand. Sci. (Eng.). — M.: Moscow Inst. Oil and Gas, 1989. — 24 pp.

153. Kumotos, Moysis, and Spiridonos. Investigating Detachment of Bubbles in Boiling Liquid During Forced Convection // Teploperedacha (Heat Transfer), 1968. — 80. — № 2. — pp. 44–52.

154. Idelchik I.Ye. Certain Interesting Effects and Paradoxes in Aerodynamics and Hydraulics. — M.: Mashinostroenie Publishers, 1982. — 96 pp.

155. Kutateladze S.S. Fundamentals of the Theory of Heat Transfer. — Novosibirsk: Nauka Publishers, 1970. — 660 pp.

156. Troshenkin V.B. Heat-and-Mass Transfer during Interaction of Activated Aluminium with Water. — Trans.: Vestnik Kharkov Polytechnic Univ., 1999. — Issue 49. — pp. 14–18.

157. Lykov A.V. Theory of Drying. — M.: Energia Publishers, 1968. — 472 pp.

158. Troshenkin V.B. Method for Designing Reactors for Producing Hydrogen from Water Using Alloys of Silicon and Aluminium // Ecology of Chemical Engineering and Biotechnology. Anniv. Coll. Works Chair Chem. Technology and Industr. Ecology. — Trans. Kharkov Polytechnic Univ., 1996. — v. 1. — pp. 107–111.

159. Eyring H., Lin S.H., and Lin S.M. Basic Chemical Kinetics / Transl. from English to Russian by Ye.L. Rosenberg; ed. A..M. Brodsky. — M.: Mir Publishers, 1983. — 528 pp.

160. Troshenkin B.A., Troshenkin V.B. Heat Transfer During Liberation of Hydrogen in Reactions of Activated Aluminium With Water // Heat-and-Mass Transfer MMF-2000: Proc. Minsk Int. Forum Heat-and-Mass Transfer (Minsk, 2000) Minsk: ANK ITMO ANB, v. 4. — pp. 246–254. (www.relay.itmo.by/jepter/mif4/volume 4/246. pdf)

161. Avrami M. Kinetics of Phase Change // J. Chem. Phys. — 1939. — 7. № 12. — pp. 1103–1112.

162. Mampel K.L. Zeitumsatzformeln fur heterogene Reaktionen an Phasengrenzen fester Korper // Z. Phys. Chem. — 1940. — 187. — 4. — s. 235–249.

163. Prout E.G. and Tompkins F.G. The Thermal Decomposition of Potassium Permanganate // Trans. Faraday Soc. — 1944. — 40. — № 274. — pp. 488–498.

164. Boldyrev V.V. Influence of Flaws in Crystals on the Rate of Thermal Decomposition of Solid Substances. — Tomsk: Tomsk Univ. Publishers, 1963. — 246 pp.

165. Young D. Decomposition of Solids. — M.: Mir Publishers, 1969. — 264 pp. (Translated to Russian)

166. Delmon B. Introduction a la Cinetique Heterogene. — M.: Mir Publishers, 1972. — 556 c. (Translated to Russian)

167. Barret P. Cinetique Heterogene. — M.: Mir Publishers, 1976. — 400 pp. (Translated to Russian)

168. Rozovsky A.Ya. Heterogeneous Chemical Reactions. — M.: Nauka Publishers, 1980. — 324 pp.

169. Brown M., Dollimore D., and Galwey A. Reactions in the Solid State. — M.: Mir Publishers, 1983. — 360 pp. (Translated to Russian)

170. Bretschneider S., Kavetsky V., Leiko Ya. Et al. General Fundamentals of Chemical Technology. — L.: Khimia Publishers, 1977. — 504 pp.

171. Inv. Cert. 1,108,773 (U.S.S.R.). Aluminium-Based Alloy for producing Hydrogen / L.F. Kozin, V.A. Sakharenko, B.A. Troshenkin. — Publ. Bull. Inv., 1984, № 30.

172. Kozin L.F. and Volkov S.V. Hydrogen Power Engineering and Ecology. — K.: Nauk. Dumka Publishers, 2002. — 336 pp.

173. Lebedev V.V. Physico-Chemical Basics of Processes of Generating Hydrogen from Water. — M.: Nauka Publishers, 1969. — 135 pp.

174. Benson S. Thermochemical Kinetics. — M.: Mir Publishers, 1971. — 308 pp. (Translated to Russian)

175. Dzis'ko V.A., Karnaukhova A.P., and Tarasova D.V. Physico-Chemical Basics of Synthesis of Oxide Catalysts. — Novosibirsk: Nauka Publishers, 1978. — 384 pp.

176. Torkar K. and Krischner H. Untersuchungen uber Aluminium — hydroxide und oxide. Das Zustands — Diagram Al_2O_3/H_2O//Monatshefte Chem., — 1960. — 91, — № 4. — S. 764–773.

177. Abramov V.Ya., Stel'makhova G.D., and Nikolaev I.V. Physico-Chemical Basics of Integrated Processing of Aluminium Stock (Alkaline Methods). — M.: Metallurgia Publishers, 1985. — 288 pp.

178. Structure and Corrosion of Metals and Alloys: Atlas. Reference Edition. / Sokol I.Ya., Ulianin Ye.A., and Feldgandler E.G. — M.: Metallurgia Publishers, 1989. — 400 pp.

179. Reference Book on Elementary Chemistry / Gen. ed. A.T. Pilipenko. — Kiev: Nauk. Dumka Publishers, 1978. — 544 pp.

180. Pavlov K.F., Romankov P.G., and Noskov A.A. Examples and Exercises for the Course of Processes and Apparatus in Chemical Technologies. — L.: Khimia Publishers, 1970. — 624 pp.

181. Troshenkin V.B. Investigating the Process of Generating Hydrogen in Gas Generator AVG-45/Heat-and-Mass Transfer in Chemical Technology Devices: Abstr. Reports. and Comm. V Minsk. Int. Forum Heat-and-Mass

Transfer. — A.V. Lykov Inst. Heat-and-Mass Transfer NANB, — Minsk, — 2004. — X. — v. 2. — pp. 451–452. (http://www.itmo.by/forum/mif5/S10/10-27.PDF).

182. Onsager L. Reciprocal relations in irreversible processes // Phys. Rev. 1931. — 37. — P. 405–407; — 38. — P. 2265–2267.

183. Onsager L., Fuoss J. Reciprocal relations in irreversible processes // Phys. Chem. 1932. — 36. — P. 2289–2293.

184. De Donder Th. and Van Rysselberghe P. Thermodynamic Theory of Affinity (A Book of Principles). — M.: Metallurgia Publishers, 1984. — 136 pp. (Translated to Russian)

185. Zubarev D.N. Non-equilibrium Statistical Thermodynamics. — M.: Nauka Publishers, 1971. — 416 pp.

186. Gyarmati I. Non-Equilibrium Thermodynamics (Field Theory and Variational Principles). — M.: Mir Publishers, 1974. — 304 pp. (Translated to Russian)

187. Folmer M. Kinetics of Formation of a New Phase- M.: Nauka Publishers, 1986. — 208 pp. (Translated to Russian)

188. Arnold von Munster. Chemische Thermodynamik. — M.: Mir Publishers, 1971. — 296 pp. (Translated to Russian)

189. Lykov A.V. and Mikhailov Yu.A. Theory of Heat-and-Mass Transfer. — M.; L.: Gosenergoizdat Publishers, 1963. — 536 pp.

190. Bulatov N.K. and Lundin A.B. Thermodynamics of Irreversible Physico-Chemical Processes. — M.: Khimia Publishers, 1984. — 336 pp.

191. Johnson D.A. Some Thermodynamic Aspects of Inorganic Chemistry. — M.: Mir Publishers, 1985. — 328 pp. (Translated to Russian)

192. Bazarov I.P., Gevorkian E.V., and Nikolaev P.N. Non-equilibrium Thermodynamics and Physical Kinetics. — M.: Moscow Univ. Publishing House, 1989. — 240 pp.

193. Troshenkin B.A., Dolgikh T.N., and Oleinik T.B. Heat-and-Mass Transfer During Liberation of Hydrogen in Reactions of Boron Sodium Hydride and Aluminium Alloys with Water // Heat and Mass Transfer in Chemically Reacting Systems: Selected Reports Minsk. Int. Forum Heat-and-Mass Transfer. -Inst. Heat-and-Mass Transfer NANB, — Minsk, 1989. — v. 3, — pp. 153–160.

194. Troshenkin V.B., Tkach G.A., and Troshenkin B.A Heat Transfer in Alloys with Water when Generating Hydrogen in Cylinder Reactors // Heat-and-Mass Transfer in Chemically Reacting Systems: Selected Reports. III Minsk Int. Forum: — Inst. Heat-and-Mass Transfer ANB, 1996. — XI. — pp. 237–240.

195. Troshenkin V.B. Influence of Temperature on the Rate of Displacement of Hydrogen from Water by Silicon and Aluminium Alloys // Information Technologies: Science, Engineering, Technology, Education, and Health: Proc. Int.. Sci.-Eng. Conf., – Kharkov: Kharkov State Polytechnic Univ. 1997. — Part 4. — pp. 430–432.

196. Instructions on Safe Operation of Cylinder Gas Generators AVG- 45 and Cylinders with Hydrogen. — M.: Hydrometeoizdat Publishers, 1978. — 32 pp.

197. Troshenkin V.B., Tkach G.A., Troshenkin B.A., and Zubarev B.N. Producing Hydrogen from Water by Employing an FSA alloy. — Kharkov, 1996. — 28 pp/ (Preprint AN UkrSSR, Inst. Problems in Mech. Eng., No. 396)

198. Rybakov Ye.T. Measuring Temperature Inside Gas Generator AVG-45 // Proc. Main Geophys. Observatory, 1961. — Issue 106. — pp. 69–74.

199. Varshavsky I.L., Troshenkin B.A., and Red'ko V.V. Experience in Operating a Periodic-Action Reactor for Generating Hydrogen from Water Using Ferrosilicon // Probl. Mashinostroenia. — 1981. — Issue 11. — pp. 106–111. (http://www.thesa.ru/chemprom/2003/09-03/pro-3.pdf).

200. Jurmanov V.A. and Troshenkin B.A. Automatic Facility for Generation of Hydrogen from Water Using Aluminium/Silicic Fusion // WMO Techn. Conf. on Instrum. and Methods of Observ. (TECO-92). — Vienna, Austria, 1992, No. 462, Rep. 49.

201. Kolobov N.A. and Staritsyn V.K. Kinetics of Accelerated Hydrothermal Oxidation of Silicon // Elektronnaya Promyshlenost (Electronics Industry). — 1982. — Issue. 7 (113). — pp. 44–47.

202. Maslov V.P., Danilov V.G., and Volosov K.A. Mathematical Simulation of Heat-and-Mass Transfer Processes. Evolution of Dissipative Structures. — M.: Nauka Publishers, 1987. — 352 pp.

203. Dushin Yu.A. Performance of Thermal Protection Materials in Hot Gas Flows. — L.: Khimia Publishers, 1968. — 224 pp.

204. Pankratov B.M., Polezhaev Yu.V., and Rud'ko A.K. Interaction of Materials with Gas Flows. — M.: Mashinostroenie, 1976. — 224 pp.

205. Zubov V.L. and Gasik M.I. Electric Metallurgy for Ferrosilica. Dnepropetrovsk: System Technologies, 2002. — 704 pp.

206. Carslaw H.S. Introduction to the Mathematical Theory of the Conduction of Heat in Solids. — M., L: OGIZ, 1947. — 286 pp. (Translated to Russian)

207. Matsevity Yu.M. Inverse Problems in Heat-and-Mass Transfer. 2 Parts. — K.: Nauk. Dumka Publishers, 2002. — v. 1. — 408 pp.; v. 2. — 392 pp.

208. Altshuler V. And Gurvich V. Lunar Rhythms. — L: Hydrometeoizdat Publishers, 1981. — 128 pp.

209. Gattenberger. Hydrogeology and Hydromechanics of Ground Water. — M.: Nedra Publishers, 1971. — 184 pp.

210. Gavrilenko Ye.S. et al. Deep Hydrosphere of Earth. — K.: Nauk. Dumka Publishers, 1971. — 272 pp.

211. Gavich N.K. Hydro Geodynamics. — M.: Nedra Publishers, 1988. — 350 pp.

212. Liashko I.I., Demchenko L.I., and Mistetsky G.Ye. Numerical Solution of Problems in Heat-and-Mass Transfer in Porous Media. — K.: Nauk. Dumka Publishers, 1991. — 264 pp.

213. Pavlov N.N. Changes in Earth's Rotational Speed; Deformation of Terrestrial Crust, and Solar Activity // Trans. Main Astronomical Observatory in Pulkovo. — 1968. — № 183. — pp. 1–23.

214. Shidlovsky A.A. Fundamentals of Pyrotechnics. — M.: Mashinostroenie Publishers, 1964. — 338 pp.

215. Pilling H.B. and Bedworth R.E. Oxidation of Metals at High Temperatures / J. Inst. Metals, 1923. — 29. — P. 529–591.

216. Brzustowski T.A. Combustion of Metal Additives in Solid-Fuel Rocket Engines. / Canad. Aeron. and Space Journal, 1963. — 9. — No 5. — pp. 141–149.

217. Kropotkin P.N. and Trapeznikov P.A. Variation of the Earth's Angular Rotational Speed, Polar Oscillations and Rate of Drift of the Geomagnetic Field, and their Possible Relation to Geotectonic Processes // Trans. AS U.S.S.R.. Geological Series. — 1963. — № 11. — pp. 32–51.

218. Tazieff H. Quand la Terre Tremble. — M.: Mir Publishers, 1968. — 252 pp. (Translated to Russian)

219. Eiby G.A. Earthquakes. — M.: Nedra Publishers, 1982. — 264 pp. (Translated to Russian)

220. Yastrzhembsky A.S. Thermodynamics and the History of its Development. — M.; L: Energia Publishers, 1966. — 668 pp.

221. The History of the Theory of the Chemical Process. General History of Chemistry. — M.: Nauka Publishers, 1981. — 448 pp.

222. Vinogradov L.P. Chemical Evolution of Earth. — M.: AS U.S.S.R. Publishers, 1959. — pp. 17–24.

223. Mangushev K.I. Issues in Development of World Geoenergetics. — M.: Nauka Publishers, 1981. — 184 pp.

224. Geothermal Energy. Resources, Development and Utilisation. — M.: Mir Publishers, 1975. — 356 pp.

225. Kapitsa P.L. Experiment, Theory, and Practice. — M.: Nauka Publishers, 1981. — 496 pp.

226. Zabarny G.N., Pashkevich R.I., and Gaidarov G.M. Mathematical Models of Heat-and-Mass Transfer During Filtration in Heat-Insulated Permeable Media. — Petropavlovsk-Kamchatsky, 1992. — 57 pp.

227. Vasen N., Blinov Yu.P., Vissarionov V.I. et al. Utilising Energy Sources in Siberia and the Far East to Improve Environment Quality // Renewable Energy, 2003 — July — pp. 14–16.

228. Nonconventional Power Engineering in the XXI century: Reports III Int. Conf. Crimea, Sudak, 9-15 Sept. — Kiev: Inst. Techn. Heat Physics, 2002. — 232 pp.

229. Vymorkov B.M. Geothermal Power Plants. — M.; L.: Energia Publishers, 1966. — 112 pp.

230. Dvorov I.M. Heat in Earth's Interior. — M.: Nauka Publishers, 1972. — 206 pp.

231. Povarov O.A., Luzin V.Ye., Nikolsky A.I. et al. Experience in Developing and Operating the Verkhne-Mutnovskaya GeoTPP (Kamchatka) // Nonconventional Power Engineering in the XXI century: Reports II Int. Conf. Crimea, Yalta, 17–22 Sept. — Kiev: Inst. Techn. Heat Physics, 2001. — pp. 16–17.

232. Flashing Adiabatic Flows / Ed. by V.A. Zysin. — M.: Atomizdat Publishers, 1976. — 152 pp.

233. Alekseev A.D., Revva V.N., and Riazantsev N.A. Destruction of Rock in the Volumetric Field of Compressing Stress. — K.: Nauk. Dumka Publishers, 1989. — 142 pp.

234. Kalfakchian A.P., Aleksandrov V.N., Vorobiev Ye.A. et al. Improving Means and Methods of Maintaining Development Headings in Mines in Central Donbass. — Dnepropetrovsk: Sich Publishers, 1994. — 208 pp.

235. Lozovsky S.P. Investigating the Process of Soil Swelling at the Mine "Komsomolets Donbassa" // Proc. National Mining Univ. — Dnepropetrovsk. 2003. — v. 2. — № 17. — pp. 70–74.

236. Yefremova N. Earth, Heat Us // Rabochaya Tribuna, 1990. — 1 Jan. — p. 4.

237. Trincher K.S. Biology and Information. Elements of Biological Thermodynamics. — M.: Nauka Publishers, 1965. — 140 pp.

CONTENTS

Please send your comments and requests to the following address:

A.N. Podgorny IPMash NAS of Ukraine
2/10 Dm. Pozharsky St.
61046, Kharkiv
Ukraine

Additional copies of the book can be ordered at the same address.
Books are delivered on a prepayment basis.

When designing the book the following photos from Internet sites were used:
Front cover — http://nature.espot.ru/vulcans/2/img1.jpg;
Back cover — http://images.myweb.ru/1152x864.jpg.

Наукове видання

Б.О. Трошенькін
Термодинаміка літосфери. Геотермічні електростанції
(англійською мовою)

Відповідальний за випуск *Г.Є. Лискова*

Підписано до друку 10.12.2004 р.
Формат 60x84/16. Папір офсетний. Друк різографічний. Гарнітура Літературна.
Ум.друк.арк. 8,6. Обл.-вид.арк. 7,4. Тираж 1000 прим. Зам. №

ТОВ "Видавництво "Форт".
Свідоцтво про внесення до Державного реєстру видавців
ДК № 333 від 09.02.2001 р.
61023, м. Харків, а/с 10325. Тел. (057) 714-09-08